Proceedings

International Conference on Nuclear Science and Technology

Nuclear Society Of Iran | Atomic Energy Organization of Iran | Nuclear Sciences and Technologies Research Institute

Papers on:

Radiation Safety & Security

*In this booklet, you will find the selected papers presented at the **First International Conference on Nuclear Science and Technology**, held from May 6-8, 2024, in Isfahan, Iran.*
We hope you find it informative and enjoyable!

ICNST 2024

Contact and Accessibility

icnst2024.com
registration@icnst2024.com


بسم الله الرحمن الرحيم

The Conference President's Message
ICNST 2024

Attendees, guests, and colleagues

I would like to warmly welcome you to the first International Conference on Nuclear Science and Technology (ICNST 2024). It has been a real honor and privilege to serve as the president of this conference. The conference this year has brought together an incredible diversity of authors and speakers from universities, government, and industry to share ideas and new perspectives on a wide range of radiation applications, nuclear reactors, particle accelerators, radiation measurements, fusion and plasma, stable and radioactive isotopes, radiation safety and security, nuclear agriculture, fuel cycle, lasers, education and training and nuclear governance.

Climate change, a new topic which has been added to this year's agenda as an important worldwide issue. a matter that has been brought up as a critical concern at the majority of IAEA conferences and nuclear scientific assemblies in recent years.

Panel discussions and exhibitions are being introduced as side activities in an attempt to keep this scientific meeting from becoming one-dimensional and increase its effectiveness.

More than 520 complete papers have been approved for this conference; when combined with the additional panels, get-togethers, and side activities, it is anticipated that over 1000 people will attend in person in the historical and touristic city of Isfahan. We look forward to welcoming participants to share their practical ideas and to enjoy an academical and cultural three days in Isfahan.

I'll close by wishing you everyone an incredible, instructive, and transformative experience during ICNST2024 and I hope that this conference can pave the route for academic materials to be used in industry and everyday life.

Prof. Javad Karimi-Sabet
President of ICNST2024
Javad Karimi-Sabet

welcome statment of scientific secretary ICNST 2024

"In the name of God, the Merciful,

Prior to giving the stage to address this distinguished forum, let me take this opportunity to express our deep gratitude, on behalf of all attendees, for His Excellency Mr. Islami's scientific, educational, and motivational remarks, as well as for his excellent organization of this conference.

I would also like to express our appreciation to His Excellency Dr. Mortazavi, Governor-General of Isfahan Province, for his constructive and useful support in enabling this meeting to take place.

This is a great pleasure and honor to extend a warm greeting to each and every one of you for the International Conference on Nuclear Science and Technology, scheduled from May 6th to May 8th, 2024, in the historic city of Isfahan, Iran.

With the aim of advancing our knowledge of nuclear science and technology, this conference is a major global convergence of experts, researchers, and practitioners. It is a platform for the sharing of creative concepts, the presentation of state-of-the-art research, and the formation of cooperative alliances.

As the scientific secretary of this prestigious event, I am particularly excited about the diverse array of participants expected to grace us with their presence. From the esteemed scientists and engineers of Russian universities and research centers to representatives from Islamic countries, friendly nations, and beyond, this conference promises to be a melting pot of perspectives, experiences, and expertise.

The extensive coverage of this conference is another aspect of its uniqueness. We have nearly 900 participants representing 22 countries around the world. Of the 900 participants, 620 are authors covering 13 major topics. There are 421 papers for oral and poster presentations, with additional documents for publication in ISC journals. There will be 3 plenary sessions, 16 panel discussions, 20 parallel oral presentation sessions, and 3 poster sessions.

Prof. Hosein Afarideh
Scientific Secretariat of ICNST2024

Organizers

Nuclear Society Of Iran (NSI)

Atomic Energy Organization of Iran (AEOI)

Nuclear Science and Technology Research Institute (NSTRI)

Scientific Partnership

International Atomic Energy Agency (IAEA)

Isfahan University

Sharif University

Kurchatov Institute

Amirkabir University of Technology (Tehran Polytechnique)

Shahid Beheshti University

Isfahan University of Technology

Shiraz University

Islamic Azad University

K. N. Toosi University of Technology

Ferdowsi University of Mashhad

Kerman Graduate University of Technology

Sahand University of Technology

University of Tabriz

Islamic World Scieence Citation Center

Journal of Nuclear Science and Technology (JonSat)

Radiation Physics and Engineering journal

Nuclear Watch

Cooperative Organization

Isfahan Governorate

Isfahan Municipality

Abbasi Hotel

Iran Atomic Energy Production & Development Co.

Iran's Nuclear Raw Materials & Fuel Production Co.

Radiation Application Development Co.

Ofogh Consulting Engineers Co.

Nuclear Power Plant Safety Development & Promotion Co.

Nuclear Power Plant Engineering & Construction Co.

Engineering & Design of Industrial Simulator Co.

Energy Industry Development Engineering Co

Atomic Power Plant Pepair & support

Nuclear Reactors Fuel Co.

Iran Radioactive Waste Management Co.

Mesbah Energy Co.

Iran Gharb Industrial, Mining and Energy Co.

Pars Isotope Co.

Center for Laser Science & Technology of Iran

Centrifuge Production of Iran Co.

Plasma Technology Development Co.

Rasa Technology and Innovation Center

Behyaar Sanaat Sepahan Co.

Nuclear Data Base of Iran (NDB)

Parto think tank (strategic studies of nuclear industry development)

International Conference Alerts

Local Scientific Board

RAW	NAME	ROLE	AFFILIATION
1	**Prof. Hossein Afarideh**	**Chairman of Local Scientific Board**	**Amirkabir University of Technology (Tehran Polytechnique)(AUT)**
2	**Prof. Mohammad Ghanadi Maragheh**	**Member of The Local Scientific Board**	**Nuclear Science and Technology Research Institute of Iran (NSTRI)**
3	**Prof. Mohammad Lamei Rashti**	**Member of The Local Scientific Board**	**Nuclear Science and Technology Research Institute of Iran (NSTRI)**
4	**Prof. Mohammad Bagher Ghofrani**	**Member of The Local Scientific Board**	**Sharif University of Technology (SUT)**
5	**Prof. Hosein Faghihian**	**Member of The Local Scientific Board**	**University of Isfahan (UI)**
6	**Prof. Javad Rahighi**	**Member of The Local Scientific Board**	**Institute for Research in Fundamental Sciences (IPM)**
7	**Prof. Seyed Amirhossein Feghhi**	**Member of The Local Scientific Board**	**Shahid Beheshti University (SBU)**

Scientific Committee

RAW	NAME	ROLE	AFFILIATION
1	**Prof. Ali Akbar Salehi**	**Member of The Scientific Committe**	**Sharif University of Technology (SUT)**
2	**Prof. Seyyed Javad Ahmadi**	**Member of The Scientific Committe**	**Nuclear Science and Technology Research Institute of Iran (NSTRI)**
3	**Prof. Farhoud Ziaee**	**Member of The Scientific Committe**	**Nuclear Science and Technology Research Institute of Iran (NSTRI)**
4	**Prof. Saeed Hamidi**	**Member of The Scientific Committe**	**University of Arak**
5	**Prof. Seyedzafarollah Kalantari**	**Member of The Scientific Committe**	**Isfahan University of Technology (IUT)**
6	**Prof. Naser Bagheri Moghaddam**	**Member of The Scientific Committe**	**National Research Institute for Science Policy (NRISP)**
7	**Prof. Naser Vosoghi**	**Member of The Scientific Committe**	**Sharif University of Technology (SUT)**
8	**Prof. Seied Rabi Mahdavi**	**Member of The Scientific Committe**	**Iran University of Medical Sciences**
9	**Prof. Meisam Torab Mostaedi**	**Member of The Scientific Committe**	**Nuclear Science and Technology Research Institute of Iran (NSTRI)**
10	**Prof. Fereydoun Abbasi Davani**	**Member of The Scientific Committe**	**Shahid Beheshti University (SBU)**
11	**Prof. Seyed Farhad Masoudi**	**Member of The Scientific Committe**	**K.N.Toosi University of Technology**
12	**Prof. Rasool Ruknizadeh**	**Member of The Scientific Committe**	**University of Isfahan (UI)**
13	**Prof. Gholamreza Raeesali**	**Member of The Scientific Committe**	**Nuclear Science and Technology Research Institute of Iran (NSTRI)**
14	**Prof. Asghar Sedighzadeh**	**Member of The Scientific Committe**	
15	**Prof. Hossein Kazeminejad**	**Member of The Scientific Committe**	**Nuclear Science and Technology Research Institute of Iran (NSTRI)**
16	**Prof. Seyyed Jaber Safdari**	**Member of The Scientific Committe**	**Nuclear Science and Technology Research Institute of Iran (NSTRI)**

17	**Prof. Omid Reza Kakuee**	**Member of The Scientific Committe**	**Nuclear Science and Technology Research Institute of Iran (NSTRI)**
18	**Prof. Alireza Keshtkar**	**Member of The Scientific Committe**	**Nuclear Science and Technology Research Institute of Iran (NSTRI)**
19	**Prof. Fereshte Haj esmail Beigi**	**Member of The Scientific Committe**	**Nuclear Science and Technology Research Institute of Iran (NSTRI)**
20	**Prof. Masoud Mahjour-shafiei**	**Member of The Scientific Committe**	**Nuclear Science and Technology Research Institute of Iran (NSTRI)**
21	**Prof. Mahmoud Payami Shabestar**	**Member of The Scientific Committe**	**Nuclear Science and Technology Research Institute of Iran (NSTRI)**
22	**Prof. Ali Bahrami Samani**	**Member of The Scientific Committe**	**Nuclear Science and Technology Research Institute of Iran (NSTRI)**
23	**Dr. Farhanaz Motamedi**	**Member of The Scientific Committe**	**Nuclear Science and Technology Research Institute of Iran (NSTRI)**
24	**Dr. Faezeh Rahmani**	**Member of The Scientific Committe**	**K.N.Toosi University of Technology**
25	**Dr. Ebrahim Moghiseh**	**Member of The Scientific Committe**	**Nuclear Science and Technology Research Institute of Iran (NSTRI)**
26	**Dr. Iraj Jabari**	**Member of The Scientific Committe**	**University of Isfahan (UI)**
27	**Dr. Nima Ghal-Eh**	**Member of The Scientific Committe**	**Ferdowsi University of Mashhad**
28	**Dr. Mitra Athari Alaf**	**Member of The Scientific Committe**	**Islamic Azad University Science and Research Branch**
29	**Dr. Gholamreza Etaati**	**Member of The Scientific Committe**	
30	**Dr. Amir Movafeghi**	**Member of The Scientific Committe**	**Nuclear Science and Technology Research Institute of Iran (NSTRI)**

Executive Committee

RAW	NAME	ROLE
1	Dr. Farshad Ghasemi	Chairman of the Executive Committee
2	Dr. Ehsan Molazadeh	Member of The Executive Committee
3	Dr. Seyyed Ghasem Biniaz	Member of The Executive Committee
4	Mr. Aliakbar Aminidoust	Member of The Executive Committee
5	Mr. Mohammad Hosein Arkannia	Member of The Executive Committee
6	Ms. Fatemeh Zamani	Member of The Executive Committee
7	Ms. Mahya Pazoki	Member of The Executive Committee
8	Mr. Hosein Maleki	Member of The Executive Committee
9	Mr. Maziar Dalili	Member of The Executive Committee
10	Mr. Shojaei	Member of The Executive Committee
11	Ms. Fatemeh Rezaei	Member of The Executive Committee
12	Mr. Reza Rafiei	Member of The Executive Committee
13	Ms. Seyyedeh Elham Ebrahimi	Member of The Executive Committee

Radiation Safety & Security Papers

ICNST 2024
International Conference on Nuclear Science and Technology
6- 8 MAY 2024 | Isfahan, Iran

Radiation Safety & Security

ICNST 2024
International Conference on Nuclear Science and Technology
6- 8 MAY 2024 | Isfahan, Iran

Forecasting the spread and dispersion of radioactive materials in effect of accident at the Barakah nuclear power plant using Hysplit4 software (Paper ID: 1021)

Valizadeh B[1]*, Rezaie M[2]
[1] Nuclear Science and Technology Research Institute, Atomic Energy Organization, Tehran, Iran
[2] Department of Nuclear Engineering, Faculty of Sciences and Modern Technologies, Graduate University of Advanced Technology, Kerman, Iran

Abstract

In this article, using Hysplit4 software, an attempt has been made to estimate the risk of leaking ionizing radiation due to a hypothetical accident on April 2023, at the Barakah nuclear power plant (BNPP). The leakage of radioactive ^{131}I was investigated in the neighboring places of this BNPP, such as Abu Dhabi. The result shows that the ^{131}I concentration rate is 6. 7E+02Bq/m^3. A week later, the radioactive material reached Abu Dhabi city and contaminated that area by spreading in the atmosphere and carrying it through the wind with a 10mSv/h dose rat. BNPP is near the Persian Gulf, and some of this element produced in this possible accident enters the Persian Gulf and pollutes the ecosystem. Based on the results of this research, the countries of the Persian Gulf should have the necessary preparation and equipment to prevent environmental and human disasters.

Keywords: Hysplit4, Barakah, Dose, Pollutant, Reactor, Persian Gulf

Introduction

Today, the need for energy production and consumption is continually increasing. Greenhouse gases caused by fossil fuels cause climate change and global warming [1]. Therefore, we are looking for alternative and clean solutions for energy supply [2]. One of the valuable solutions is the use of nuclear energy. Nuclear energy is one of the non-renewable [3] and clean sources that can meet the need for electricity at the global level [4]. Nuclear energy produces a lot of heat, rotates the turbines, and finally produces electricity [5]. The United Arab Emirates (UAE) is one of the countries [6] that needs new sources of electricity generation due to population growth and industrial development. This Barakah Nuclear Power Plant (BNPP) is located on the west coast of Abu Dhabi, 53 km from Al Ruwais City, and has four nuclear reactors with a capacity of 5600 MW [7]. This nuclear power plant can supply 25% of the electricity needed in the UAE and reduces greenhouse gases [8]. Considering the importance of nuclear energy in the world, in the event of an accident, irreparable damages will be created, bringing many costs. One of the concerns about nuclear reactors is their protection and control

of the amount of pollutants that are spread in the environment since the reactors release radionuclides due to accidents, technical errors, terrorist attacks, war, or generally from the chimney. These polluting radionuclides, in addition to emitting ionizing radiation, also cause chemical poisoning [9]. If an accident occurs in a This Nuclear Power Plant (NPP), the gamma radiation resulting from the nuclear activities of this NPP causes environmental pollution [10]. Some of the factors that cause the spread of gamma rays are: nuclear accidents, technical errors, terrorist attacks, war, nuclear tests and radioactive waste [11]. Ionizing radiations, including gamma rays, cause various damages such as cancer, burns, genetic changes, anemia, reduction of blood cells, reduction of the immune system and death [12]. The effect of gamma rays on human health depends on various factors. Some of the factors are: the amount and type of radiation, the time and duration of exposure to radiation, the distance from the source of radiation and the location of radiation in the body [13]. However, in addition to economic and energy benefits, NPPs also have environmental risks and challenges [14]. One of the ways of pollution in the environment is the chimney of NPP. Chimneys of NPP are long and resistant structures that transfer the gases resulting from the nuclear fission process [15] to the top of the atmosphere [16]. The purpose of this article is to predict and advance the material from the BNPP due to a hypothetical accident and the release of dangerous gases in the atmosphere using Hysplit4 software in the first week of April 2023.

Material and Methods

Hysplit4 software has been used to simulate the airflow and spread of pollutants in the atmosphere. The National Oceanic and Atmospheric Administration (NOAA) developed this software and used NOAA meteorological data (GDAS) for atmospheric modeling. These data include information about pressure, temperature, humidity, wind speed and direction, height above the ground, and the concentration of pollutants in the atmosphere. These are available with a time interval of 3 hours and a spatial distance of 1 degree. To simulate the dispersion paths and the spread rate of radioactive substances in the atmosphere, the location and time of the leakage of radioactive substances must be determined first. This paper assumes a radioactive material leak occurred at the BNPP in the United Arab Emirates. The geographical coordinates of this NPP are 52°13'59.7"E, 23°58'01.1"N. The time of leakage of radioactive materials is assumed to be noon local time .Then, the amount of leakage of radioactive materials was determined, and 10, 100, 1000, and 10000 Ci were considered. The investigated radioactive materials include nuclear fission products such as ^{131}I, ^{137}Cs, ^{90}Sr, and ^{85}Kr. These radioactive materials have different half-lives and emit alpha, beta, and gamma particles.

Result and Discussion

The coordinates of the BNPP are located on the west coast of Abu Dhabi and are shown in Figure 1 by Google Earth Pro software.

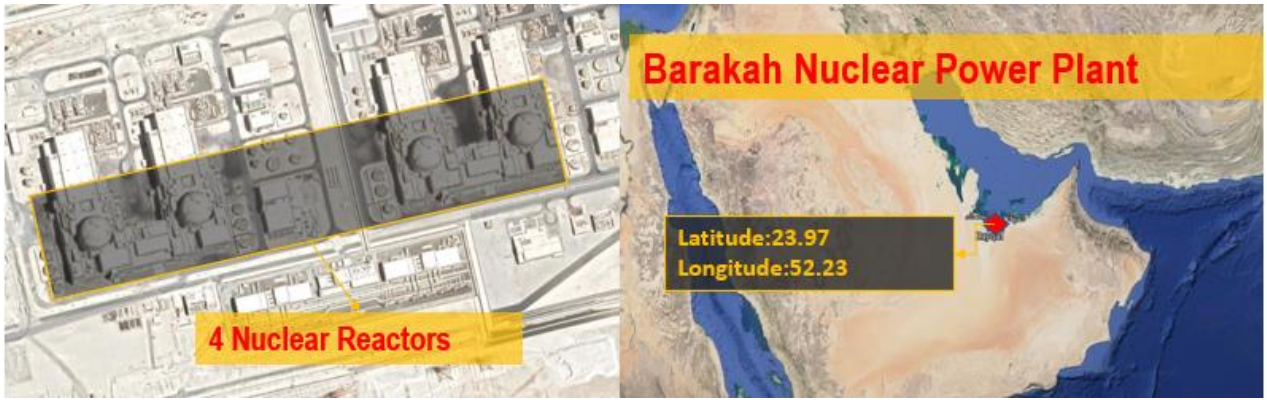

Figure1. Satellite map of Barakah nuclear power plant in the United Arab Emirates

This research assumes that the incident occurred in April 2023, according to the modeling of Hysplit4 software. Figure 2 shows the wind direction and forward paths in April 2023 using NOAA meteorological data at three different heights (50, 100, and 1000 m, sea level). Figure 1 shows the direction of the wind movement of the BNPP for the first week of April 2023.

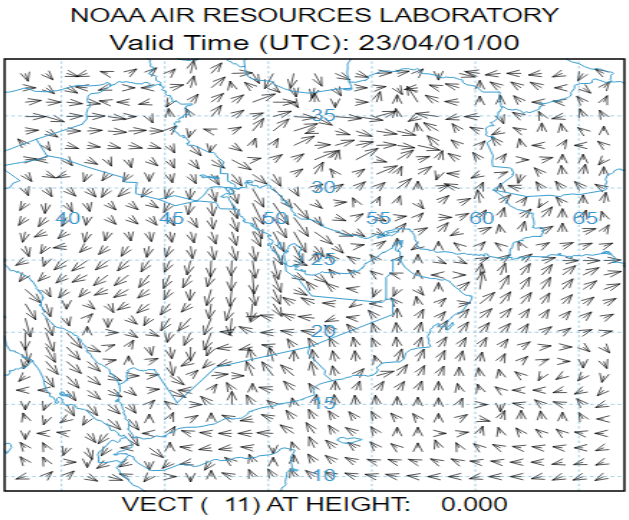

Figure2. Air movement path in the first week of April 2023

Figure 3 shows the forward path for three different distances (50, 100, and 1000 m), including 5 circles at a 50 km distance from each other.

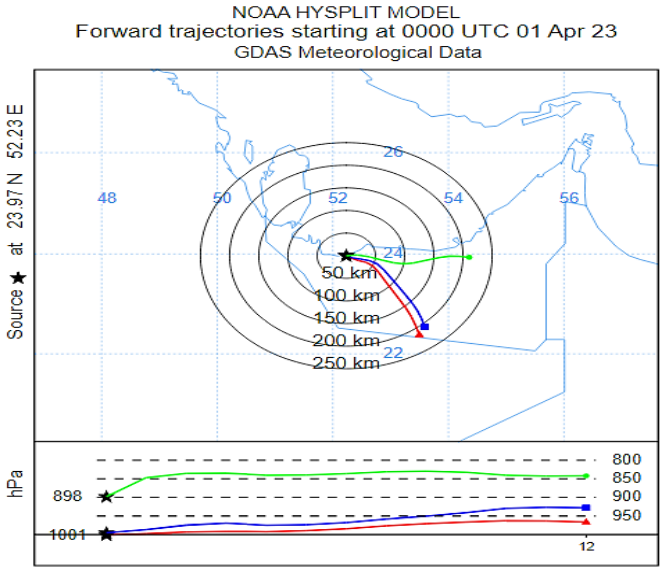

Figure3. Forward trajectories starting the first day of April 2023

To calculate the concentration in the Hysplit4 software, as shown in Figure 4, source parameters such as location, height, duration, and emission rate of the pollutant or substance were determined. Also, the meteorological data file was selected, and the geographical area was specified.

After calculating the radiological dose concentration, it was obtained using Hysplit4 software. (Figure 4) The maximum radiological dose is shown in red (with a 10mSv/h dose rat), and the maximum concentration is 6.7E+ 02 Bq/m3. The results of the maximum concentration and maximum dose show that this value is higher than the allowed value set by ICRP at the time of the accident.

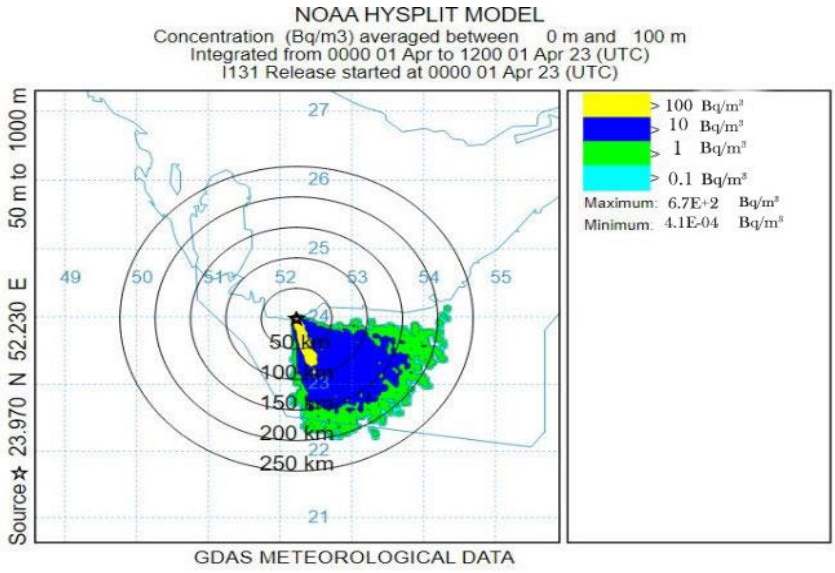

Figure 4. Concentration (Bq/m^3) for April 2023 for ^{131}I of radioactive materials for one day.

Due to the accident, materials that leak into the environment from the BNPP may include ^{131}I, ^{134}Cs,^{137}Cs, ^{90}Sr, and ^{239}Po that in this paper the ^{131}I was considered. Wind can be crucial in transporting and distributing these substances in the atmosphere. Radioactive materials may be transported to distant areas or neighboring countries (Figure 2) or fall on the ground depending on the wind's direction, speed, height, and season. These substances may pose environmental and health hazards to humans, animals, and plants. It is necessary to take preventive and control measures to prevent and reduce these risks. Some measures are setting standards for air quality and acceptable radiation limits, strict control of NPP activity and prevention of accidents or technical errors, planning for response in case of an accident or terrorist operation, and preparation for evacuation or shelter in the affected area. Since radioactive materials may enter groundwater, they can contaminate crops and animals and cause many environmental hazards.

Abu Dhabi is the largest City in the UAE and the capital of this country. BNPP plant is adjacent to the Persian Gulf. The possibility of leaking radioactive materials with higher energy from this part is very likely. The countries of Iran, Saudi Arabia, Qatar, Bahrain, Kuwait, and Iraq are the most damaged by the leakage of radioactive materials due to their proximity to the Persian Gulf. On the other hand, passing through the country of Oman, it enters the Indian Ocean and causes an environmental disaster for the neighboring ocean countries.

On the other hand, the desalination systems of these countries are also contaminated with radioactive substances. Therefore, NPP must implement adequate safety measures and emergency plans to prevent or reduce the consequences of a severe accident.

Validation

The results of this article are similar to the results of Athari et al.'s article (7), in which the Fars reactor was investigated in the normal operating mode and in this article the Barakeh reactor was investigated in the accident mode. Also, in another article, according to Table1, the radius examined in this article is up to 250 km, while the radius examined in the article by Khan Jani Bijjargah et al. (8) is up to 50 km due to the limitation in the Aermod software. Also, in this article, the data has been examined for a period of 7 days, while in the article by Khan Jani Bijargah et al., it has been examined for a period of 5 days after the incident.

Table1. Comparison of time and radius investigated in two similar works

Checked time after the incident		**The radius under investigation**	
In the article by Khanjani Bijargah et al	In this article	In the article by Khanjani Bijargah et al	**In this article**
5 day	7 day	50Km	**250 Km**

Comparing the results of this article with Chernobyl and Fukushima

On site measurements at the west gate of the Fukushima Daiichi nuclear power plant indicate the presence of 131I in the air in the close vicinity of the plant (within approximately 1 km). The concentrations in air reported for the period 31 March to 1 May ranged from 40 Bq/m3 to 1180 Bq/m3 for total 131I. the concentrations in air reported for 29 May were about 3 Bq/m3 for 131I.

Therefore, the comparison of BNPP activity with Chernobyl and Daichi Fukushima nuclear power plants is shown in the table below, the text and table were added to the article in the Validation Section. Also, in the stations near the Chernobyl nuclear power plant, the maximum activity of ^{131}I is according to the table2 and Figure 4 less than 100 and about 28.93 Bq /m^3 is reported[17]

Table2.Comparison of Fukushima and Chernobyl nuclear power plants with BNPP

Plant	BNPP	Daichi Fukushima	Chernobyl
^{131}I activity (Bq/m^3)	670 Bq/m^3	40-1180 Bq/m^3	180 Bq/m^3

Conclusion

It is assumed that the BNPP had an accident in the chimney system on April 1, 2023, and caused the release of radioactive materials from unstable nuclei into the atmosphere.

Using Hysplit4 software, the simulation of the future source and the places where the contamination is supposed to go was done and determined.

For this purpose, NOAA Meteorological Data (GDAS) was used to model the atmosphere. These data were received with a time interval of 3 hours and a spatial distance of 1 degree. Then, according to the location, time, and amount of leakage of radioactive materials, the boundary conditions were determined for Hysplit4 software. These conditions include height above the ground, wind speed and direction, pollutant concentration, injection rate, and simulation time. The simulation time is assumed to be one week from April 1 to April 7, 2023. Since radioactive contaminants are seen in the environment as smoke, dust, or fog, and after an accident and entering the body, each contaminant enters a specific body part and is located in that part. And causes serious problems. The elimination rate of these radioactive substances depends on its chemical nature and half-life. When an incident of ^{131}I, the alpha emitter is released in the environment, it is absorbed by the thyroid gland and causes thyroid cancer due to DNA damage. As a result, the NPP does not pose a risk to human health and the environment under normal conditions and a possible accident, and necessary measures must be taken before the accident to minimize the damage to the environment and humans. Of course, these results are based on the assumptions and models used in this research and may differ from reality. Therefore, it is necessary to use other methods besides the Hysplit4 software for a more accurate and comprehensive assessment of the risks caused by the BNPP.

References

[1] Singh, S. (2021). Energy Crisis and Climate Change: Global Concerns and Their Solutions. Energy: Crises, Challenges and Solutions, 1-17.

[2] Qazi, A., Hussain, F., Rahim, N. A., Hardaker, G., Alghazzawi, D., Shaban, K., & Haruna, K. (2019). Towards sustainable energy: a systematic review of renewable energy sources, technologies, and public opinions. IEEE access, 7, 63837-63851.

[3] Çakar, N. D., Erdoğan, S., Gedikli, A., & Öncü, M. A. (2022). Nuclear energy consumption, nuclear fusion reactors and environmental quality: The case of G7 countries. Nuclear Engineering and Technology, 54(4), 1301-1311.

[4] Bragg-Sitton, S. M., Boardman, R., Rabiti, C., & O'Brien, J. (2020). Reimagining future energy systems: Overview of the US program to maximize energy utilization via integrated nuclear-renewable energy systems. International Journal of Energy Research, 44(10), 8156-8169.

[5] Agyekum, E. B., Ansah, M. N. S., & Afornu, K. B. (2020). Nuclear energy for sustainable development: SWOT analysis on Ghana’s nuclear agenda. Energy Reports, 6, 107-115.

[6] Park, K., Son, S., Oh, J., & Kim, S. (2022). Sustainable Decommissioning Strategies for Nuclear Power Plants: A Systematic Literature Review. *Sustainability*, *14*(10), 5947.

[7] Analytica, O. (2020). Emerald Expert Briefings.

[8] Oxford Analytica. (2021). Countries' approaches to reviving nuclear power differ. *Emerald Expert Briefings*, (oxan-db).

[9] Eidemüller, D., & Eidemüller, D. (2021). Radioactive Incidents and Disasters. *Nuclear Power Explained*, 195-240.

[10] He, S., Tang, S., Xiao, Y., & Cheke, R. A. (2018). Stochastic modelling of air pollution impacts on respiratory infection risk. *Bulletin of Mathematical Biology*, *80*, 3127-3153.

[11] Ciottone, G. R., & Alexander, G. A. (2024). Nuclear and Radiation Disaster Management. In *Ciottone's Disaster Medicine* (pp. 492-497). Elsevier.

[12] Montesinos, C. A., Khalid, R., Cristea, O., Greenberger, J. S., Epperly, M. W., Lemon, J. A., ... & Jones, J. A. (2021). Space radiation protection countermeasures in microgravity and planetary exploration. *Life*, *11*(8), 829.

[13] Christodouleas, J. P., Forrest, R. D., Ainsley, C. G., Tochner, Z., Hahn, S. M., & Glatstein, E. (2011). Short-term and long-term health risks of nuclear-power-plant accidents. *New England journal of medicine*, *364*(24), 2334-2341.

[14] Draxler, R. R., & Hess, G. D. (1998). An overview of the HYSPLIT_4 modelling system for trajectories. *Australian meteorological magazine*, *47*(4), 295-308.

[15] Mathew, M. D. (2022). Nuclear energy: A pathway towards mitigation of global warming. *Progress in Nuclear Energy*, *143*, 104080.

[16] Chai, T., Ren, X., Ngan, F., Cohen, M., & Crawford, A. (2023). Estimation of power plant SO 2 emissions using HYSPLIT dispersion model and airborne observations with plume rise ensemble runs. *EGUsphere*, *2023*, 1-41.

[17] Fujak, M., Isajenko, K., Lipiński, P., Piotrowska, B. and Kwiatkowska, I., 2013. Radioactivity of the atmospheric aerosols measured in Poland following the accident in the Fukushima Dai-ichi nuclear power plant in 2011. *Nukleonika*, *58*(4), pp.497-503.

ICNST 2024 International Conference on Nuclear Science and Technology
6- 8 MAY 2024 | Isfahan, Iran

Studying the effects of B4C, H3BO3, W and Pb materials on shielding optimization for IECF device with D-T fuel (Paper ID: 1042)

Zanganeh H.[1*], Nasrabadi M N.[1,2]

[1]*Faculty of Physics, University of Isfahan, Isfahan, Iran*

[2]*Frank Laboratory of Neutron Physics, Joint Institute for Nuclear Research, Dubna, Russia*

Abstract

This research has been done to improve the flux and dose values of neutron and gamma in radiation shielding for 14.1MeV fusion neutrons. In this study, the effects of replacing B_4C instead of H_3BO_3 and W instead of Pb in the same thicknesses compared to the shield designed in our previous work. We used four different combinations of these materials in the shield layers. The best result for reducing the gamma dose was obtained using B_4C and W with a dose of 1.23μSv, but the best result for reducing the neutron dose and flux was obtained by using H_3BO_3 and W with a neutron dose of 15.40μSv compared to other compounds of layers for this shielding.

Keywords: Dose rate, Fluence, B_4C, H_3BO_3, W, Shielding

Introduction

Nuclear fusion is done in different ways such as magnetic confinement fusion, inertial confinement fusion, and inertial electrostatic confinement fusion (IECF) [1]. To perform nuclear fusion in an IECF device, fuel is injected through two nozzles towards the central grid of the device, which is placed on the grid holder. The products of the fusion reaction for D-T fuel are neutron and alpha, and if the fusion fuel changes, the reaction products also change [2, 3]. This device has a simple design, but it has many applications in nuclear research, industry, and medicine [4-6]. Based on the confinement time and other parameters, this device has different uses, but it is mostly used as a neutron source [7, 8]. In this study, our fuel is D-T, where neutron (14.1MeV) and alpha (3.5MeV) particles are reaction products. According to the reference book of this device, its neutron production rate is from 10^6 to $10^{12}s^{-1}$ [9]. Accordingly, for the safe use of this device as a neutron source, it is necessary to design a suitable shield with the energy of produced neutrons and other particles in this type of fusion reaction. Some papers and research have been done to design the shield and safety analysis for this fusion device [10, 11]. In one of these papers, paraffin, boric acid, wood, and stainless steel are among the materials used to make the shield for the IECF device [10]. Different thicknesses of material have been chosen for each layer. We also designed and simulated a shield for this device in our previous work [12] and we

achieved some good results. In this paper, we compared the results of the two new materials with the two materials used in our previous work. Our goal is to find the better results to optimize shielding for IECF devices with D-T fuel.

Research Theories

The energy of neutrons produced by the IECF device with D-T as fuel is 14.1 MeV. The shield must first reduce the energy of these neutrons by 000.. 3MeV. For such a reduction of energy, inelastic collisions are much more suitable than elastic collisions. A 14.1 MeV neutron will lose about 8 MeV of its energy in an inelastic collision, depending on the type of nucleus it collides with. Using the following equation, the residual energy for a neutron in an inelastic collision is obtained [13]:

$$T = 3.2 \times \sqrt{\frac{E}{A}} \quad (1)$$

Where E is the incident neutron energy and A is the mass number of the target nucleus. Accordingly, the higher the nuclear mass number, incident neutron loses the more energy in an inelastic collision. On the other hand, for the inelastic collision of the neutron produced from the D-T fusion reaction with a material, the target material must have low inelastic collision threshold energy to increase the probability of inelastic collision. The higher the mass number of the target nucleus causes the lower inelastic collision threshold energy. Using the following equation, we can calculate the inelastic threshold energy required for an incident neutron [13]:

$$E_t = \frac{A+1}{A} \times \varepsilon \quad (2)$$

According to the above equation, ε is the first state excitation energy which for instance for ^{12}C is 4.43MeV. Then for this nucleus, $E_t = 4.8MeV$. For heavier nuclei such as ^{56}Fe, the inelastic threshold energy is reduced. In the second step, after the inelastic collision with the target nucleus and reducing its energy to about 3MeV, it needs elastic collisions with appropriate materials to lose energy and thermalize. The energy of neutrons is reduced after elastic collisions based on the following equation [14]:

$$E_n \backsimeq E_0 e^{-n\xi} \quad (3)$$

Where ξ is given by:

$$\xi \backsimeq \frac{2}{A+{}^{2}/_{3}} \quad (4)$$

E_0 is the initial energy of the incident neutron and E_n is the neutron's energy after n collisions. Four points should be considered to select the suitable moderator material for elastic collisions: 1. It should have a high elastic scattering cross-section, 2. It should have high lethargy. Generally, lethargy is the

mean decrement of the logarithm of the energy of a neutron passing through matter in slowing down the process and is given by:

$$\xi = 1 + \frac{(A-1)^2}{2A} \ln\left(\frac{A-1}{A+1}\right)$$

3. It should have a high macroscopic slowing down power (MSDP) that is given by:

$$\text{MSDP} = \xi\Sigma_s \quad (6)$$

Where Σ_s is the elastic scattering cross section. 4. It should have a very low Thermalize Factor (TF):

$$\text{TF} = \frac{\text{Fast Neutron Yield } (s^{-1})}{\text{Thermal Neutron Flux } (cm^{-2}.s^{-1})} \quad (7)$$

Based on the above description, the materials in the Table 1 were selected as different shield layers for the IECF device.

Table 1. List of selected materials for the shield layers

Material	Composition,	Atom Fraction	Density (g/cm^3)	Chemical Formula
Reinforced Concrete (iron-Portland concrete)	H	0.135585	5.90	-
	O	0.150644		
	Mg	0.002215		
	Al	0.005065		
	Si	0.013418		
	S	0.000646		
	Ca	0.040919		
	Mn	0.002638		
	Fe	0.648869		
Paraffin	H	0.675311	0.93	$C_{25}H_{52}$
	C	0.324689		
Boric Acid	H	0.428571	1.50	H_3BO_3
	B	0.142857		
	C	0.428571		
Lead	Pb	1.000000	11.35	Pb
Cadmium	Cd	1.000000	8.65	Cd

Using these materials in the MCNPX code, the following thicknesses were selected as appropriate thicknesses based on ICRP60 standards according to the Table 2 [12].

Table 2. Appropriate thicknesses of materials used in the layers of shield [12].

Total Thickness (cm)	Iron-Portland Concrete (cm)	Paraffin (cm)	Boric Acid (cm)	Lead (cm)	Cadmium (mm)
58	36	10	10	1.3	7

B_4C is one of the suitable absorbers for thermal neutrons [15]. Tungsten is also one of the suitable materials for attenuation of gamma rays [16]. Tungsten is also used in the central grid holder in IECF devices due to its properties such as good radiation damage resistance. By replacing B_4C instead of H_3BO_3 and W instead of Pb in different modes, we investigated whether the neutron and gamma fluxes and doses will be better for the shielding of the IECF device. In this simulation, the neutron source strength for the IECF device is considered to be $10^9 s^{-1}$. Sufficient histories (2×10^6 nps) were performed so that the calculation error is less than 1%. The energy spectrum of all neutrons produced from this source is 14.1MeV. We considered the angular distribution of the neutron radiation from the source to be isotropic. Flux and dose on desired surfaces were calculated by using F2 surface Tally. For source energy, we used the fusion function (Gaussian function) defined for the fusion source in the MCNPX code. The energy spectrum of all neutrons produced from this source is 14.1MeV. We considered the angular distribution of the neutron radiation from the source to be isotropic in all directions based on reality and the neutron source strength is $10^9 s^{-1}$. In the X version of the MCNP code, some standard flux-to-dose conversion functions have been added as library functions. To use these standard flux-to-dose conversion functions, the DEn card must be removed and the DFn card must be used instead. We did the same in this work and used the DFn card. In the DFn card, we set the value of IU equal to 2 so that the dose unit is $\mathrm{Sv/h.source\ particle}$.

Results and discussion

The results of the fluxes and doses for neutrons and gammas after the boric acid layer and on the surface of the first layer of the user's presence environment, where users can be near the device after all the shield layers, were calculated and are given in Table 3.

Table 3. Dose and flux in the used layer of the shield with boric acid and lead

Dose and flux in the first layer of the user's presence environment out of the shield (for shielding with boric acid and lead)		Dose and flux on the surface of the first layer after boric acid in the shield	
Neutron Dose (μSv)	١٦,٤٤	Neutron Dose (μSv)	٤٤,٣٩
Neutron Fluence (cm^{-2})	1.08×10^{-8}	Neutron Fluence (cm^{-2})	5.67×10^{-8}
Gamma Dose (μSv)	٢,١٨	Gamma Dose (μSv)	١٠,٦١
Gamma Fluence (cm^{-2})	6.17×10^{-8}	Gamma Fluence (cm^{-2})	4.97×10^{-7}

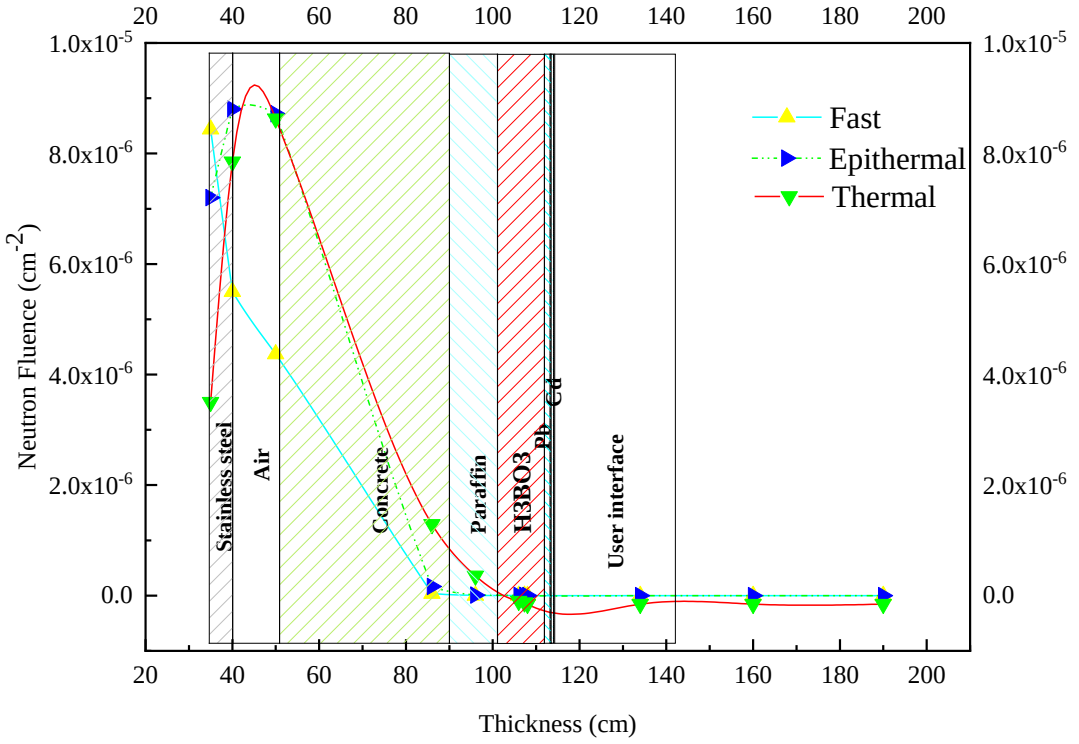

Fig. 1. Fast, Epithermal and Thermal neutron fluence for shield with boric acid and lead

Fig. 1 shows that in paraffin and boric acid layers, thermal neutron flux decreases much more than fast neutron flux. In the next step, compared to Table 2, only boron carbide (B_4C) was replaced instead of boric acid (H_3BO_3), and calculations of the fluxes and doses were done.

Table 4. Calculations for only replacing B_4C instead of H_3BO_3

Dose and flux in the first layer of the user's presence environment out of the shield (for shielding with boron carbide and lead)		Dose and flux on the surface of the first layer after boron carbide in the shield	
Neutron Dose (μSv)	۱۹,٤۷	Neutron Dose (μSv)	٥۸,۹۰
Neutron Fluence (cm^{-2})	1.92×10^{-8}	Neutron Fluence (cm^{-2})	8.79×10^{-8}
Gamma Dose (μSv)	۱,٦۹	Gamma Dose (μSv)	۸,۰٤
Gamma Fluence (cm^{-2})	4.72×10^{-8}	Gamma Fluence (cm^{-2})	4.03×10^{-7}

Based on the comparison between Tables 3 and 4, the neutron dose in the first layer out of the shield (that there is a possibility of the presence of the user), increased from 16.44 μSv to 19.47μSv. The gamma dose was 1.69μSv, which is lower than the shielding with boric acid and lead, which was 2.18μSv. In the next step, compared with Table 2, in addition to replacing boron carbide instead of boric acid, tungsten was also replaced instead of lead and the results were calculated.

Table 5. Calculations for replacing B_4C instead of H_3BO_3 and W instead of Pb

Dose and flux in the first layer of the user's presence environment out of the shield (for shielding with boron carbide and tungsten)		Dose and flux on the surface of the first layer after boron carbide in the shield	
Neutron Dose (μSv)	۱۷,۷٦	Neutron Dose (μSv)	٦۳,۹۲
Neutron Fluence (cm^{-2})	1.57×10^{-8}	Neutron Fluence (cm^{-2})	9.30×10^{-8}
Gamma Dose (μSv)	۱,۲۳	Gamma Dose (μSv)	۸,۷۷
Gamma fluence (cm^{-2})	3.63×10^{-8}	Gamma fluence (cm^{-2})	4.37×10^{-7}

According to Table 5 compared with Table 3, the calculation results showed that the dose of 14.1 MeV neutrons , has increased from 16.44μSv to 17.76μSv. Neutron fluence also increased. But the gamma dose has decreased from 2.18 μSv to 1.23 μSv, which is a positive result even compared to Table 4. In another step, compared with Table 2, tungsten was used instead of lead, but boric acid was used instead of boron carbide, that is, boric acid was used along with tungsten, and the results were calculated.

Table 6. Calculations for H_3BO_3 with W instead of Pb

Dose and flux in the first layer of the user environment out of the shield (for shielding with boric acid and tungsten)		Dose and flux on the surface of the first layer after boric acid in the shield	
Neutron Dose (μSv)	١٥,٤٠	Neutron Dose (μSv)	٤٧,٧٠
Neutron Fluence (cm^{-2})	9.94×10^{-9}	Neutron Fluence (cm^{-2})	5.31×10^{-8}
Gamma Dose (μSv)	١,٥٩	Gamma Dose (μSv)	١١,٢٤
Gamma Fluence (cm^{-2})	4.60×10^{-8}	Gamma Fluence (cm^{-2})	5.29×10^{-7}

Based on the comparison between Tables 6 and 3, the gamma dose was obtained 1.59μSv, which is better than the results of Table 4 with 1.69μSv, but from the results of Table 5, which replaces boron carbide (B4C) instead of boric acid (H3BO3) and tungsten (W) instead of Lead (Pb), and its value is 1.23μSv is not better. The results of Table 6 show that the neutron dose (which is the most effective parameter in determining the total dose) in the first layer of the user's presence environment after the shield (out of the shield), was obtained 15.40μSv. This amount was lower than the amount of neutron dose in the first layer after the shield (which is the user's presence environment) for shielding with boric acid and lead, which was 16.44μSv, and from various other compounds. Also, the neutron fluence was lower than all the previous values, which is the best one in different combinations, because this is the most important layer after the shield and in the user's presence environment. The first layer outside of the shield, should have the lowest amount of neutron dose and the total dose, in order to reduce the radiation damage to minimum possible amount.

Conclusions

The results of this study show that using boron carbide and tungsten in the shield is a better choice for reducing the gamma dose. But the use of boric acid along with tungsten in the shield layers has better results in terms of flux and dose of neutrons (compared to boron carbide and tungsten) for a D-T fusion as a neutron source (IECF device) with 14.1 MeV neutrons. Since, the most important and effective parameter (more effective than the gamma dose) in determining the total dose reached to the user's presence environment to maintain safety by the standards is the neutron dose, therefore, choosing using boric acid along with tungsten in this shield is more suitable.

References

[1] Black, J., Wood-Thanan, M., Maroni, A., & Sánchez, E. (2021). Study of inertial electrostatic confinement fusion using a finite-volume scheme for the one-dimensional Vlasov equation. Physical Review E, 103(2), 023212.
[2] Chan, Y. A., & Herdrich, G. (2019). Jet extraction and characterization in an inertial electrostatic confinement device. Vacuum, 167, 482-489.
[3] Farnsworth, P. T. (1966). Electric discharge device for producing interactions between nuclei (No. US 3258402).
[4]. Gueibe, C., Rutten, J., Camps, J., Moyaux, D., Schroeyers, W., Auer, M., & Schreurs, S. (2022). Application of silver-exchanged zeolite for radioxenon mitigation at fission-based medical isotope production facilities. Process Safety and Environmental Protection, 158, 576-588.
[5]. Damideh, V., Sadighzadeh, A., Koohi, A., Aslezaeem, A., Heidarnia, A., Abdollahi, N., & Damideh, R. (2012). Experimental study of the Iranian inertial electrostatic confinement fusion device as a continuous neutron generator. Journal of fusion energy, 31, 109-111.
[6]. Bhattacharjee, D., Buzarbaruah, N., Mohanty, S. R., & Adhikari, S. (2020). Kinetic characteristics of ions in an inertial electrostatic confinement device. Physical Review E, 102(6), 063205.
[7]. Buzarbaruah, N., Mohanty, S. R., & Hotta, E. (2018). A study on neutron emission from a cylindrical inertial electrostatic confinement device. Nuclear Instruments and Methods in Physics Research Section A: Accelerators, Spectrometers, Detectors and Associated Equipment, 911, 66-73.
[8]. Ghammas, H., & Nasrabadi, M. N. (2023). Investigating the effect of changing parameters in the IEC device in comparative study. Nuclear Engineering and Technology, 56, 292-300.
[9]. Miley, G. H., & Murali, S. K. (2014). Inertial electrostatic confinement (IEC) fusion. Fundamentals and Applications.
[10]. Lee, S. M., Yoriyaz, H., & Cabral, E. L. (2020). Development of neutron shielding for an inertial electrostatic confinement nuclear fusion device. International Nuclear Atlantic Conference, Santos, Brazil, 5088–5095.
[11]. Bakr, M., Ahmed, R., Smith, T. W., Firston, T., & Scott, T. B. (2024). Radiation shielding for inertial electrostatic confinement fusion system utilizing concrete and water. Radiation Research and Applied Sciences, 17(2), 100908.
[12]. Zanganeh, H., & Nasri Nasrabadi, M. (2023). Simulation of neutron and gamma shielding for an inertial electrostatic confinement fusion device. Radiation Physics and Engineering, 4(3), 29-41.
[13]. Lamarsh, J. R. (1966). Introduction to nuclear reactor theory. Addison.
[14]. Cember, H. (2009). Introduction to health physics, McGraw Hill Professional.
[15]. Mansouri, E., Mesbahi, A., Malekzadeh, R., Janghjoo, A. G., & Okutan, M. (2020). A review on neutron shielding performance of nanocomposite materials. International Journal of Radiation Research, 18(4), 611-622.
[16]. Asgari, M., Afarideh, H., Ghafoorifard, H., & Amirabadi, E. A. (2021). Comparison of nano/micro lead, bismuth and tungsten on the gamma shielding properties of the flexible composites against photon in wide energy range (40 keV–662 keV). Nuclear Engineering and Technology, 53(12), 4142-4149.

ICNST 2024 International Conference on Nuclear Science and Technology
6- 8 MAY 2024 | Isfahan, Iran

Comparison of barite concrete, paraffin and borated paraffin for Tehran Research Reactor D channel main shield using computational method (Paper ID: 1050)

Gholamzadeh Z.

Safety and Nuclear Research Reactor School, Nuclear Science and Technology Research Institute, Tehran, Iran,

E-mail for correspondence author: Cadmium_109@yahoo.com

Abstract

Radial channels of the research reactors are used for material analysis by using neutrons emerged from the nuclear reactor core. Inside these channels mainly is equipped with different neutron collimators and neutron filter crystals so that not only shape the neutron beam in parallel, convergent or divergent propagation but also filter some parts of the neutron spectra. However, at the radial channel exit after all equipment just at the beam port or the final exit of the radial channel a strong shield is needed to protect the reactor staff of high exposures related to the exited neutrons and gammas from the radial channel. The present work investigates barite concrete, paraffin or paraffin-borated shielding supremacy for the first layer of Tehran Research Reactor D channel main shield using computational method. MCNPX code was used to model the radial channel in details. In addition, radioactivity of the mentioned materials during short and long exposures would be investigated using ORIGEN code. The obtained results showed borated paraffin could has positive effect on thermal neutron background reduction at the sample position.

Keywords: Shielding power, Barite concrete, Paraffin, Borated-paraffin, MCNPX code, ORIGEN code

1. Introduction

Usually heavy concrete is used as shielding material in neutron research facilities. It attenuates both neutron and gamma radiations [1].

Heavy concrete is the most common material used in radiation shielding. Heavy concrete is obtained by adding high-density aggregates into normal concrete. Normal-weight concrete density varies between 2200 and 2450 kg/m^3 while heavy concrete's density is ranging from about 2900 and 6000 kg/m^3. Boron-containing multi-layered new heavy concretes were produced and radiation-shielding properties were determined. It is known that the concrete has large neutron absorption cross section at

14 MeV. In addition, heavy concrete was made using lead-zinc slag waste instead of sand, which can be used as gamma radiation shielding [2].

One of the main advantages of concrete in comparison to the others is that it is a composite type material and there is a possibility to optimize its constituents for better mechanical properties. However, in radiation protection, the geometry of radiation shielding is designed according to the efficiency of shielding properties of an element and not to the static conditions [3].

However, for shielding performance in a beam port of a research reactor radial channel, it should be noted that the neutron shielding is of most importance. Paraffin is a form of an alkene compound that is composed of a hydrocarbon bond. Paraffin has a high cross section and capability for capturing and moderating the fast neutrons [4].

Paraffin wax is a material that is widely used for radiation shielding construction. The advantage of paraffin wax is that it can absorb slow neutrons and has a large macroscopic cross-section that can efficiently moderate fast neutrons. This advantage is important for shielding materials. The main component of paraffin wax is normal paraffin hydrocarbons. Paraffin is a hydrocarbon alkane with the formula C_nH_{n+2}. It is a white or even colorless solid and it consists of hydrocarbon molecules containing twenty to forty carbon atoms while its density varies between of 0.77 to 0.93 g/cm^3 [5].

Toyen and Saenboonruang (2017) investigated paraffin and paraffin/bitumen composites with additions of boron oxide (B_2O_3) to evaluate the viscosity, flexural, and thermal neutron shielding properties for use as thermal neutron shielding materials. Their results indicated that an increase in B2O3 contents improved the shielding properties but slightly reduced the flexural properties [6].

Calzada et al. (2011) were investigated the application of a shielding material composed of steel resin, paraffin/polyethylene, and a boron compound for the redesign of the ANTARES facility at FRM-II (located at a cold neutron beam line; beam line number 4). The composition was optimized by help of Monte Carlo simulations using the code MCNP5 considering the local neutron and gamma spectra. They indicated that the optimal composition depends on the spectra and the neutron/gamma ratio in the beam line [1].

For SAMOP facility with a 100 kW TRIGA reactor, paraffin wax and concrete were used, in which the first material composed of carbon and hydrogen ($C_n H_{2n+2}$), with the typical formula of ($C_{31} H_{64}$) is a good neutron moderator that can be effectively used to slowdown the fast neutrons. It is easy to manufacture and inexpensive and therefore it was used as the main component of beam catcher. The outer shield made of ordinary concrete, which is commonly used for gamma ray shielding [7].

Beer et al. (2015) addressed Monte Carlo neutron-particle transport simulations to theoretically optimize the shielding capabilities of the biological shield for the SANRAD facility at the SAFARI-1 nuclear research reactor in South Africa. The entire facility is designed for the steel boxes to interlace with each other in order to prevent radiation leakage through a straight path at any part of the shielding. Casted concrete with a 4.22 g/cm^3 density was used to shield the facility [8].

Hence, the present work aimed to investigate paraffin, borated-paraffin and barite concrete materials as neutron/gamma shield of Tehran Research Reactor (TRR) D channel.

2. Material and methods

Construction of the light water Tehran Research Reactor (TRR) began in 1960, while the first achieved criticality and operation began in 1967. This reactor was designed to produce a thermal power of 5 MW. The normal operation mode of the reactor core involves 22 to 33 fuel assemblies. This reactor is equipped with 8 radial beam channels called A, B, C, D, E, F, H (tangential one which is considered as two beam channels). Beam channels A, D, E, and G have a diameter of 6 inches and are arranged radially at an angle of about 30°. Beam channels B and F have diameters of 12 inches and 8 inches, which are respectively arranged radially and as directly-faced toward the reactor core [9].

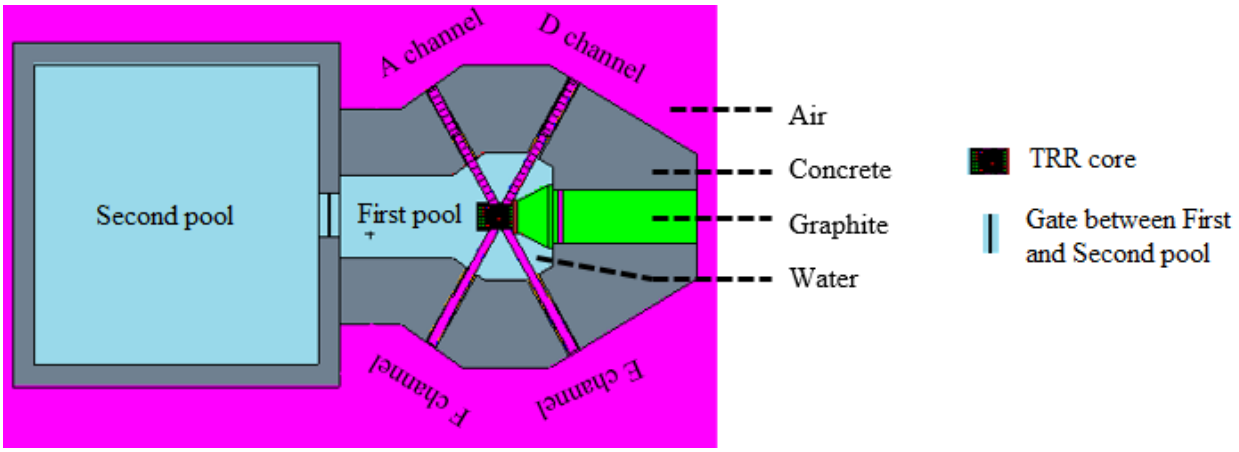

Fig.1. Schematic view of TRR pool and position of its four radial channels (A, D, E, F)

The simulations were performed by using the MCNPX and ORIGEN2 codes. MCNPX is a general-purpose Monte Carlo radiation transport code with a multi-tasking capability that can be used to reduce the time needed to obtain the computational result [10]. Its powerful, fully 3D, combinatorial geometry

of bodies and surfaces enables the users to model most real problems. The use of point-wise cross-sections allows the reproduction of neutronic and photonic materials transport properties with a high degree of accuracy. Statistical measures (tallies) of particle flux are allowed on user-defined surfaces and volumes. Several statistical tests check the convergence criteria of each tally and prevent under sampling [11].

ORIGEN2 is a versatile point-depletion and radioactive-decay computer code for use in simulating nuclear fuel cycles and calculating the nuclide compositions as well as characteristics of materials contained therein. It represents a revision and update of the original ORIGEN computer code, which was developed at the Oak Ridge National Laboratory (ORNL) and distributed worldwide beginning in the early 1970s. Included in ORIGEN2 are provisions for incorporating data generated by more sophisticated reactor physics codes, a free-format input, and a highly flexible and controllable output; with these features, ORIGEN2 has the capability for simulating a variety of fuel cycle flow sheets [12, 13].

The MCNPX simulated main shield details are shown in Fig.2. As in the figure is seen, the shield is consisted of three layers; 55 cm paraffin, 5 cm boric acid, 15 cm lead respectively, in which the final layer is lead. A monochromator room is seen in the figure with dimension of 30×40 cm^2 which a 60 cm-long Soller collimator installed on its corner so that it would guide the reflected monochromatic neutrons at 20° angel toward outside the shield. After paraffin layer, 1.5 cm thick borated-polyethylene (7%-borated) and 2 mm cadmium sheets of 20×25 cm^2 were used as thermal neutron beam stop inside the second layer (boric acid) [14].

D channel of TRR is a 6-in radial beam tube, which guides the emerged neutrons from the TRR core toward the reactor hall. A high-density concrete collimator holder was used inside the channel according to Fig.1, the concrete part length is 120 cm. A Soller collimator with 120 cm length consist of a stainless steel frame and three narrow sheets which have divided the empty cubic space of the collimator used inside the concrete holder. After the concrete holder, an iron disc-shaped part with 10 cm thickness is used. Then 15 cm thick polyethylene disc has been used. As final part, a 5 cm thick borated-polyethylene (7%) has been used. Because the main shield would not stand completely fit with the concrete wall of the TRR research reactor, 2 cm Nitrile Butadin Rubber (NBR) was used between the wall and main shield as flexible neutron shield material [14].

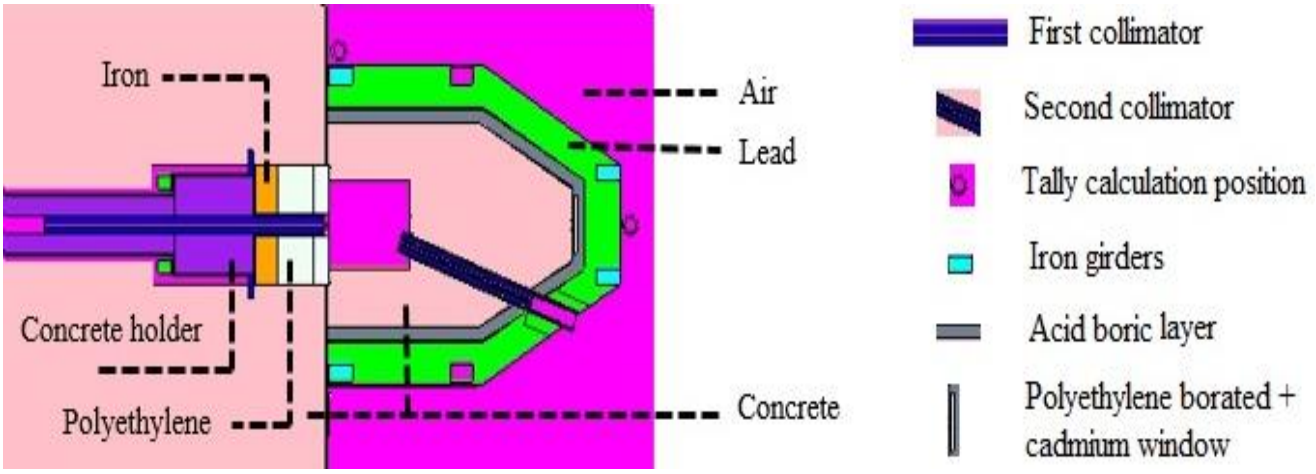

Fig. 2. Details of the used parts inside D channel and the main shield simulated using MCNPX

Neutron and gamma sources of TRR developed in MCNPX input and the gamma and neutron dose rates in front of the modeled shield and beside the wall near to NBR layer were calculated. DE/DF card and ANSI/ANS-6.1.1-1977 flux to dose conversion factors were used to calculate the gamma dose rates. Flux to dose conversion factor of NCRP-38, ANSI/ANS-6.1.1-1977 was used to calculate the neutron dose rates [14].

Neutron source emerged from TRR core was defined at a position exactly before the collimator holder beginning (Fig.3). The source neutrons propagate through the D channel shield after entering monochromator room, which is seen in Fig.3. Neutron and gamma dose rates were calculated using F4 tally of the MCNPX code inside the first layer of the main shield. This study aims to compare the neutron/gamma shielding power of the D channel shield first layer when paraffin, paraffin-borated or barite concrete materials are used for this layer. Also average thermal, epithermal and fast neutron flux inside the first layer of the shield was calculated using F4 tally card of the MCNPX code.

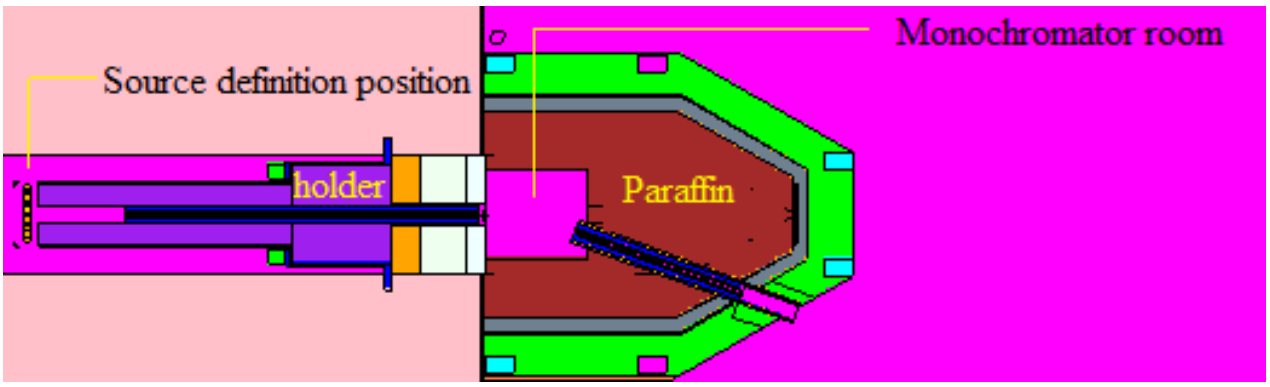

Fig.3. Schematic view of D channel shield and position of the first neutron source emerged from TRR core

The calculated average neutron flux inside the first layer was used in the ORIGEN code input to calculate the shield secondary gamma emission rate because of the induced activation by the neutron flux exposure during the TRR core operation. The gamma emission rate was used to define a gamma source inside the first layer volume using MCNPX code. Then using mesh tally capability of the MCNPX code, the gamma dose rate produced by these secondary gammas was calculated around the D channel shield.

3. Results and discussion

MCNPX calculations using F4 tally inside the first shield layer volume showed that the layer experiences an average neutron flux of 1.8E+05 n/s.cm^2. The value was used as input for ORIGEN code to calculate the activation rate of first layer material. The produced radioactive isotopes inside the first layer of the shield causes gamma dose rate around the shield not only during the system operation but also after its shutdown. The ORIGEN code calculations showed paraffin and paraffin-borated materials will not noticeably be radioactive because their total gamma intensities are 2.57E-07 #/s and 6.62E+02 #/s respectively. While in the case of barite concrete, the value is 1.53E+07 #/s for one-year exposure in the emerged neutron field from TRR core. Hence, total gamma intensity induced inside the barite concrete, as the material is to be used as the first layer of the shield was investigated for two continues exposures of 1-year and 10-year as the worse condition. In reality, the TRR reactor has not continues operation during one year so the gamma intensity of the produced radioisotopes inside the first layer is less than the overestimated values. The gamma intensity of the barite concrete for the exposure times were calculated using ORIGEN code by the assumption of an average neutron flux of 1.8E+05 n/s.cm^2. ORIGEN code results showed there is not noticeably difference for gamma intensity of 1-year and 10-year exposures (Fig.4). This means that most of the produced radioisotopes inside the barite concrete are short and medium half-life ones so that reach to an equilibrium after a short time of neutron exposure. In addition, the ORIGEN code output shows after the system shutdown, the total intensity of the delayed gammas (those emitted from the produced radioactive nuclides inside the barite concrete) drops approximately 10 times after 28 days of the system shutdown (Fig.5).

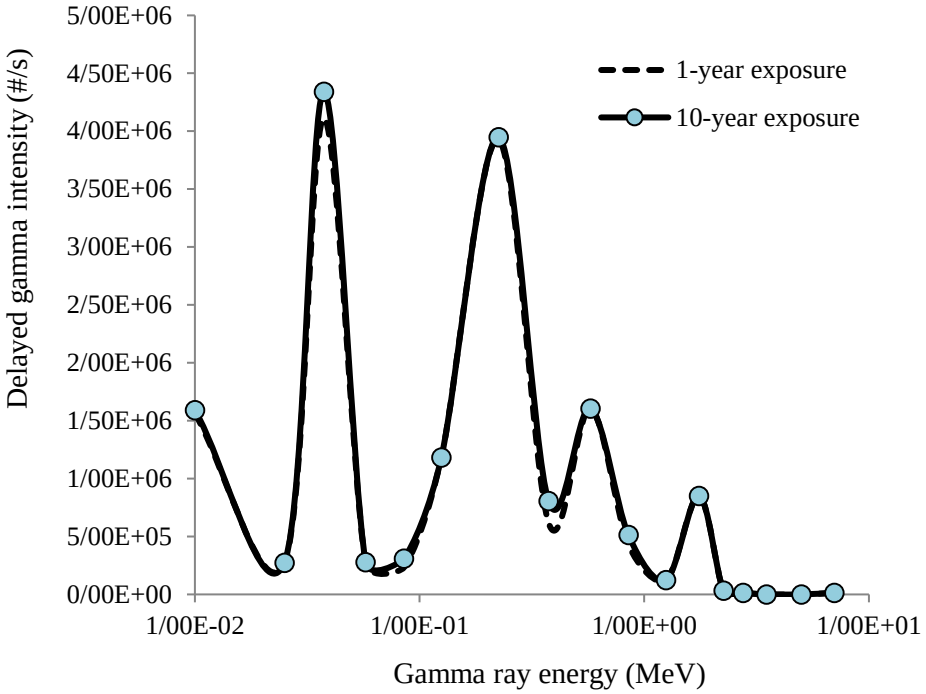

Fig.4. Comparison of delayed gamma spectra inside the barite concrete material as the first layer of the investigated shield during different neutron exposure times

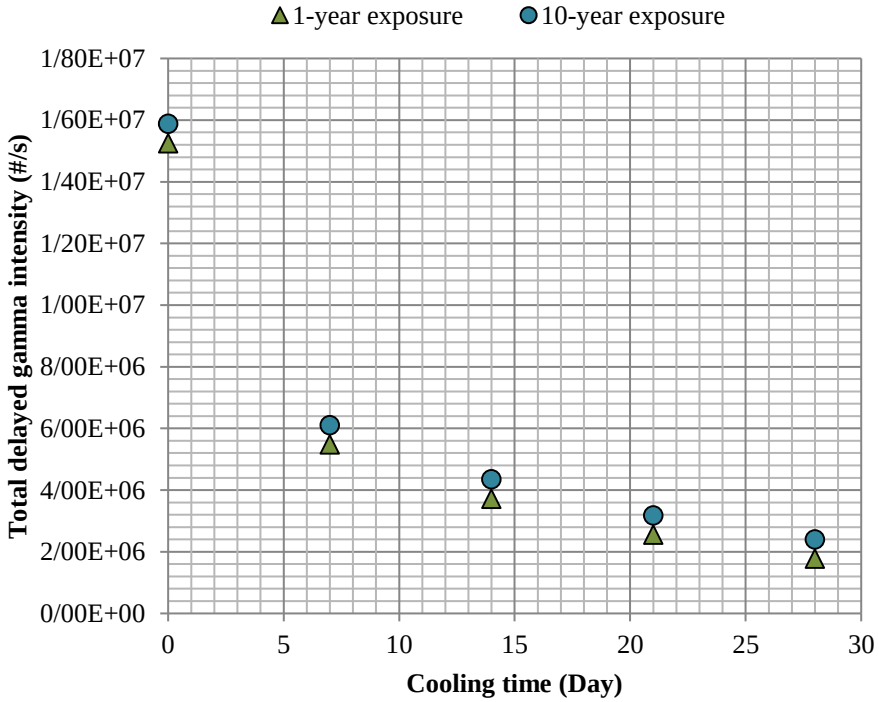

Fig.5. Examination of total delayed gamma intensity variation inside the barite concrete material as the first layer of the investigated shield during 28-days cooling times

After extraction of the delayed gamma from ORIGEN code, a gamma source was defined in MCNPX code input in the case of barite concrete material, which shows that the first layer material is emitting the delayed gammas (Fig.6). The source distribution is seen in the Figure 6 as dots inside the first layer volume.

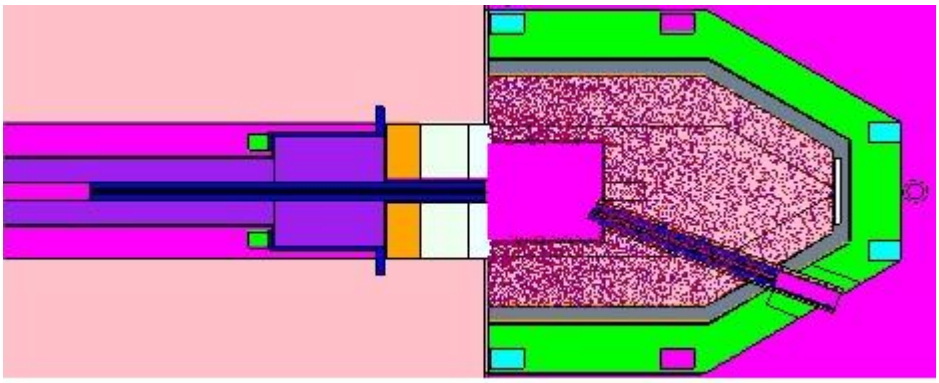

Fig.6. Simulation of delayed gamma source distribution inside the barite concrete material as the first layer of the investigated shield during TRR operation

Then mesh tally capability of MCNPX code was used to model the gamma dose rate around the shield produced by these delayed gammas. The MCNPX code results show a dose rate of about 1.7 nSv/h is available around the shield during TRR operation (Fig.7) when barite concrete is used as the first layer. The value drops about 6 times after one-week of TRR shutdown. Hence, the barite concrete activity level dose not noticeably effect on gamma dose rate values around the D channel shield when barite concrete material is used as the first layer of the D channel shield.

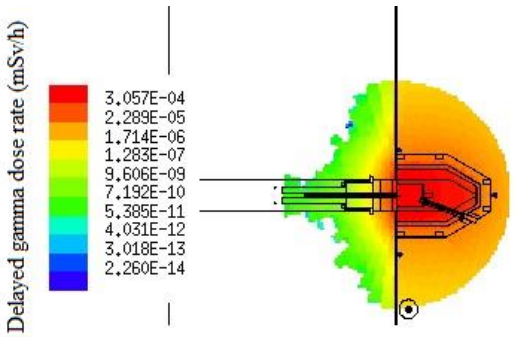

Fig.7. Distribution of delayed gamma dose rate inside the barite concrete material as the first layer of the investigated shield during TRR operation

In next step, primary gamma dose rate was calculated around the D channel and its shield using MCNPX code. The primary gammas are those emerging directly from TRR core. Fig.8 clearly shows the barite concrete could shield the primary gammas much better than the paraffin and paraffin-borated layers.

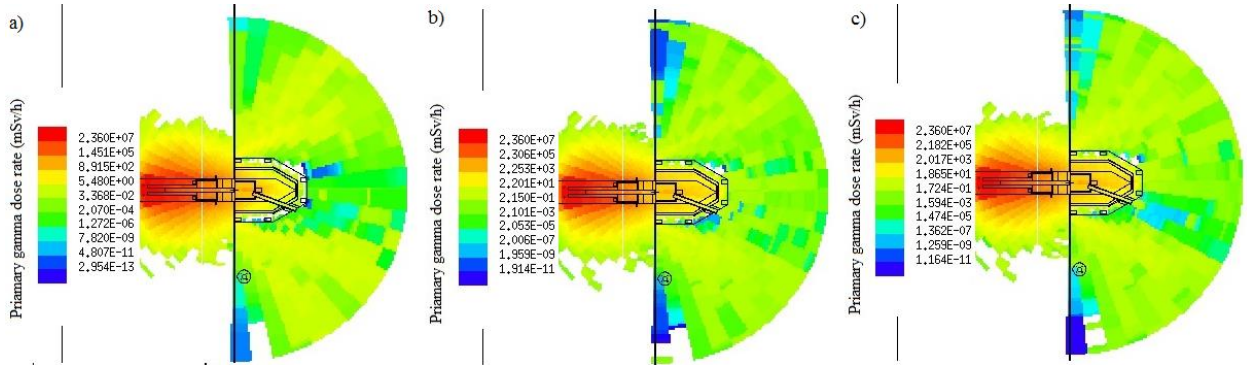

Fig.8. Primary gamma dose rate distribution inside and around the D channel shield a) barite concrete as the first layer b) paraffin-borated as the first layer c) paraffin as the first layer

The calculations using MCNPX code showed the neutron dose rate is not much different between paraffin and borated-paraffin involved 7% of acid boric (about 3% when 30 cm of the mentioned materials are compared with each other). However, secondary gamma dose rate decreases about 16% when borated-paraffin is used as the first layer of the D channel shield clearly because of carbon content reduction inside the first layer. In addition, the results showed barite concrete is not an appropriate neutron shield when it is used with the same thickness of paraffin or borated-paraffin (Fig.9). In the last case, the neutron dose rate after 30 cm of the used shield is about 98 times higher than borated-paraffin.

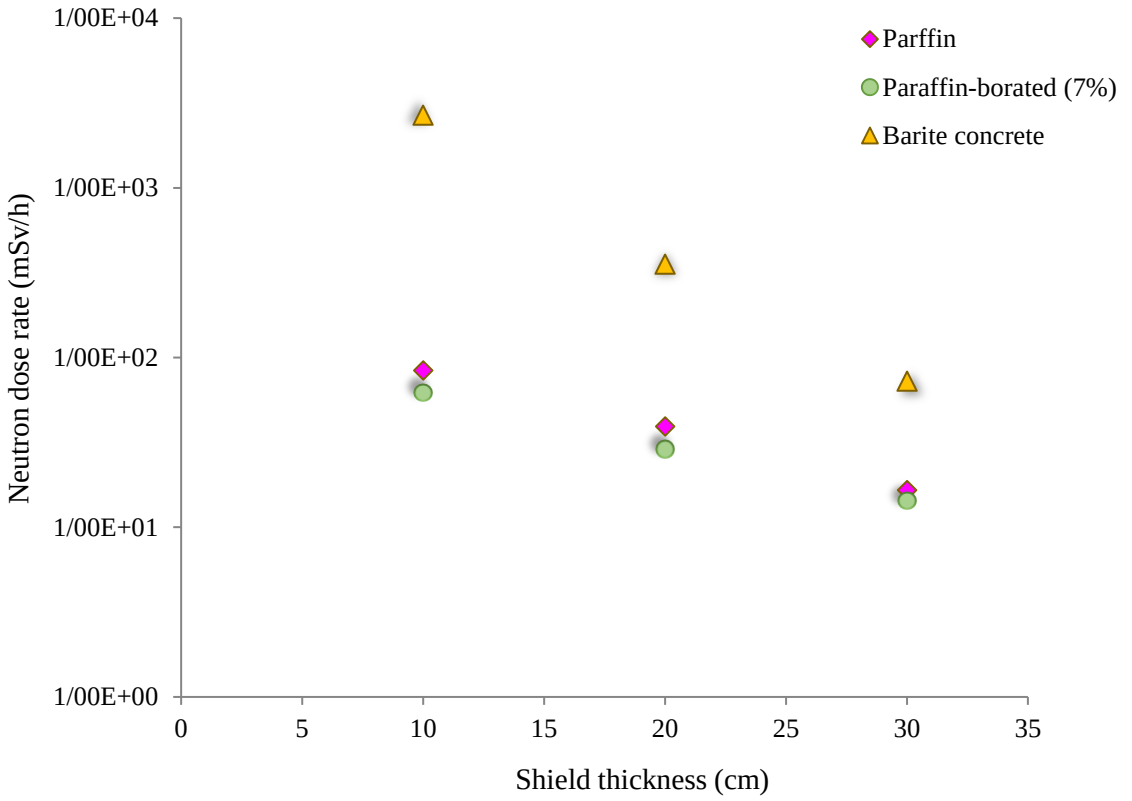

Fig.9. Neutron dose rate on the barite concrete, paraffin, paraffin-borated material thickness when are used as the first layer of TRR D channel shield

Table 1 shows however 30 cm of paraffin would result in less fast neutron flux in comparison with borated-paraffin but the material is more attractive regarding the higher low energy neutron absorption rate.

Table 1. Some neutron and gamma ray parameters after 30 cm paraffin, borated-paraffin or barite concrete shield material

Material	Gamma dose rate (mSv/h)	Neutron flux E_n<0.02 eV	Neutron flux E_n>1 keV
Paraffin	16.6	Non detectable	1.75E05
Borated-paraffin	14.3	Non detectable	2.64E05
Barite concrete	2.92	1.83E05	1.36E06

It should be noted that the calculated value conformity with the experimental values depends on different parameters such as precise modeling of all geometries, material composites, material densities, gaps maybe are available at any section of the components as well as the neutron and gamma source intensity and spectra. Hence, some uncertainty should be evaluated to select the best material

thickness before the shield construction. For example, the result obtained by Sardjono et al. (2019) shows that at 60 cm of the paraffin thickness, the dose rate has significantly reduced to 12.4 μSv/h. They reported that the correction factor of 10% was then added to the calculated values to include the reactor power calibration factor [6].

Conclusions

The present study investigated paraffin, borated-paraffin and barite concrete materials for first layer of the TRR D channel shield. MCNPX and ORIGNE code calculations showed regarding the radioactivity of the shield exposed to neutrons emerging from TRR core and neutron shielding power the borated-paraffin is the best choice while it decreases thermal neutron background that is very important turbulence parameter for diffraction spectra acquisition because it causes noise. However, the fast neutrons lose their energy with collisions and may increase the background but fast filter crystals decrease their leakage from the shield. So, thermal neutron background should be as low as possible at diffraction table sample to minimize the nose or background at diffraction pattern.

References

Calzada, E., Gr¨unauer, F., Schillinger, B., Turck, H., (2011). Reusable shielding material for neutron- and gamma-radiation, Journal of Nuclear Instruments and Methods in Physics Research Section A 651(1): 77-80.

Aygün, B., (2019). Neutron and gamma radiation shielding properties of high-temperature resistant heavy concretes including chromite and wolframite, Journal of radiation research and applied science, 12(1): 352–359.

Piotrowski, T., Tefelski, D. B., Polanski, A. and Skubalski, J., (2012). Monte Carlo simulations for optimization of neutron shielding concrete, Cent. Eur. J. Eng. 2(2): 296-303.

Khanifah, L., Widodo, S., Widarto, Made Dharma Putra, N,, and Satrio, A., (2018). Characteristics of Paraffin Shielding of Kartini Reactor, Yogyakarta, ASEAN Journal on Science & Technology for Development, 135(3): 195-198.

Sardjono, Y., Walhikmah, R., Widiatmono, R., Mahmudah, R. S. N., Wijaya, G. S., Triatmoko, I. M. and Widarto, (2022). Safety analysis of paraffin wax based biological shielding for cancer therapy with BNCT method on piercing beamport of Kartini nuclear reactor Yogyakarta, Journal of Physics: Conference Series 2190: 012014

Toyen, D. and Saenboonruang, K., (2017). Development of paraffin and paraffin/bitumen composites with additions of B2O3 for thermal neutron shielding applications, Journal of Nuclear Science and Technology, 56(8):871-877.

Sutondo Tegas, S., (2019). Radiation shielding design of neutron source from Kartini reactor's beam-port for SAMOP test facility, 7th Asian Physics Symposium, IOP Conf. Series: Journal of Physics: Conf. Series 1204, 012061.

de Beer, F.C., Radebe, M.J., Schillinger, B., Nshimirimana, R., Ramushu, M. A. and Modise, T., (2015). Upgrading the Neutron Radiography Facility in South Africa (SANRAD): Concrete Shielding Design Characteristics, Physics Procedia, 69:115 – 123.

Aslani Menarebazari, Z., Jafari, H. and Gholamzadeh Z., (2023). The design and construction of a collimator holder to equip beam tube D of the Tehran Research Reactor, Nuclear Engineering and Design, 405(15):112226

Pelowitz D. B., (2008). MCNPX User's manual version 2.6.0, LA-CP-07- 1473

Jafari, H., Choopan Dastjerdi, M.H. and Rajabi Moghadam, S., (2020). A Monte Carlo evaluation of neutron images quality in a research reactor based neutron radiography facility, Nucl. Instrum. Methods in Phys Reas Sec A, 976(1):164258.

Croff, A.G. (1983). ORIGEN2: A versatile computer code for calculating the nuclide compositions and characteristics of nuclear materials, nuclear technology, 62(3): 335-352.

Croff, A.G., (1980). A user's manual for the ORIGEN2 computer code, Oak Ridge National Laboratory.

Gholamzadeh, Z., (2023). The effect of sapphire neutron filter on neutron and secondary-gamma dose rate reduction around the D channel main shield of TRR, Radiation Physics and Engineering, 4(2):25–33.

ICNST 2024
International Conference on Nuclear Science and Technology
6- 8 MAY 2024 | Isfahan, Iran

Calculating the annual effective dose of radioactive elements in Graduate University of Advanced Technology source hole (Paper ID: 1075)

Esmaeili Ranjbar L [1*], Rezaie M [1]

[1] *Department of Nuclear Engineering, Faculty of Sciences and Modern Technologies, Graduate University of Advanced Technology, Kerman, Iran*

Abstract

For nuclear, atomic and scientific research in most universities, a special place (source hole) is assigned for keeping of radioactive sources. These places should be safe for radiation hazards caused by those sources. In this research, an attempt has been made to investigate the annual effective dose caused by the placement of an adult MIRD phantom at 4 points around of the source hole of the Graduate University of Advanced Technology (KGUT), which has been approved by the Atomic Energy Organization of Iran, using the MCNPX code simulation. The location of the adult MIRD phantom is considered inside and outside of the source hole, near and far away (50 meters) of the source hole room where the research greenhouse of the university is located. The results of Monte Carlo simulation show that the annual effective dose in those 4 locations is equal to 12 .29, 4.47, 0 and 0 mSv/year respectively. Except for inside the source hole, the annual effective dose of KGUT radioactive sources is lower than the maximum level reported by ICRP reports (5 mSv/year). Therefore, the environments out of KGUT source hole room are safe for employments and student.

Keywords: Radioactive Source, MCNPX, Annual Effective Dose, Research Greenhouse, KGUT

Introduction

The Atomic Energy Organization of Iran is responsible for providing radioactive sources according to the rules of the International Commission on Radiological Protection (ICRP) with full supervision of universities and research centers in the nuclear field [1,2]. Calculating the annual effective dose from radioactive sources in the research centers and universities of the country is one of the most important tasks that must be done by the health physics unit and researchers to check the permissible level of radiation and the safety of people working in laboratories and the public. Usually, most of work in complete safety because they generally have low activity. But a limited number of radioactive sources have high activity at millicurie level. Graduate University of Advanced Technology is one of Iran's academic centers, whose nuclear laboratory has recently been equipped with two sources of ^{60}Co and ^{137}Cs with an activity of 100 mCi. In this research, it has been tried to calculate the annual effective

dose and the allowed time of research with ^{60}Co and ^{137}Cs sources for the experts and researchers of the laboratory according to the space considered for it and also based on the location of these sources. The annual effectiveness should be checked and calculated by individuals and students. According to the reports of the International Commission on Radiological Protection (ICRP), the maximum annual effective dose of workers must be less than 5 mSv/y and each normal person is less than 1 mSv/y [3-5]. In order to conduct this research, the Monte Carlo N Particle 2.7 X version (MCNPX) simulation code was used, which has the ability to track 32 atomic and nuclear particles based on Monte Carlo principles [6]. Using the adult MIRD phantom [7], the annual effective dose of radiation from ^{60}Co and ^{137}Cs sources has been extracted using gamma spectrum of they [8,9]. How to calculate the annual effective dose for adult MIRD phantom in 4 specific locations is mentioned in the next steps.

Experimental

According to Figure 1, first an adult MIRD phantom code is used in the MCNPX code, and then the space and chamber of the source hole include ^{60}Co and ^{137}Cs sources are defined in input file. In order to design the input file to calculate the annual effective dose in different organs, the adult MIRD phantom is placed in 4 locations of the source hole room, including inside source hole, inside and outside of the source hole room, and at a distance of 50 m from it that make the research greenhouse of the KGUT university.

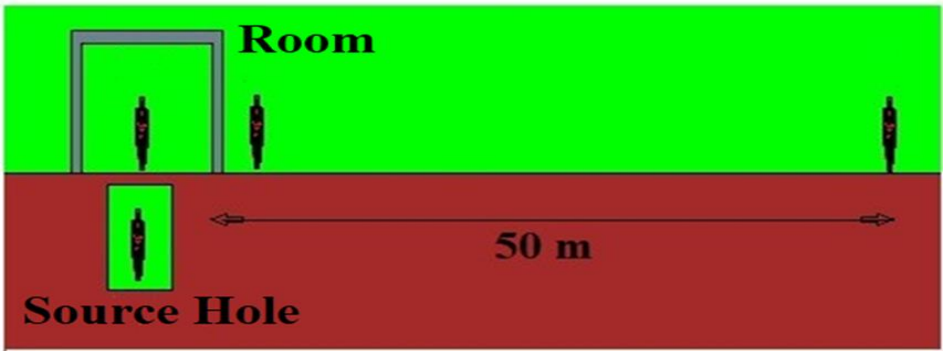

Fig. 1. A view of the adult MIRD phantom in the considered locations

The wall material of the source hole chamber is made of concrete, the material around the source hole is soil, and the space inside and outside the source hole chamber is also made of air g/cm^3 in the MCNPX code. Table 1 shows materials density that used in this simulation.

Table 1. Density of materials that used in MCNPX code

Material	Density (g/cm^3) [11-13]
Concrete	2.3
Soil	1.4
Air	0.001293

Also, using the ^{60}Co and ^{137}Cs sources information (Table 2), the source card is simulated in the MCNPX code. After the running of the simulation, the results can be obtained by F6 tally card, which are in MeV/g unit per single particle, that converted to mSv/y by applying the relevant coefficients. To reach an error below 1%, the number of particles is considered to be 10^8.

Table 2. ^{60}Co and ^{137}Cs sources information

Source	Decay energy (MeV)	Radioactive Decay mode [14,15]	Half-life [14,16]	Activity
^{60}Co	1.173 & 1.332	γ	5.3 y	100 mCi
^{137}Cs	0.5120	β^-	30.17 y	100 mCi
^{137}Cs	0.6617	γ	30.17 y	100 mCi

In order to calculate the annual effective dose, the adult MIRD phantom was placed in 4 points around source hole room as: inside the hole(P1), inside (P2) and outside (P2) the room, as well as at a distance of 50 m from room (P2), which is the location of the university's research greenhouse. Then the dose per single particle in different organs was calculated using F6 tally command that results are listed in Table 3.

Table 3. Gamma dose per single particle in different organs in 4 points (in MeV/g)

Organ	Tissue Weighting Factor [16]	^{60}Co				^{137}Cs			
		P1 Place	P2 Place	P3 Place	P4 Place	P1 Place	P2 Place	P3 Place	P4 Place
Skull & Brain	0.01	1.38e-05	4.47e-05	0	0	7.56e-12	4.43e-12	0	0
Adrenals	0.015	0.00015	0.00013	0	0	5.64e-11	7.23e-11	0	0
Gall Bladder	0.015	0.00018	0.00017	0	0	6.7e-14	1.14e-11	0	0
Stomach	0.12	0.00046	0.00233	0	0	3.02e-11	8.33e-12	0	0
Small Intestine	0.015	0.00019	0.00034	0	0	4.75e-11	1.49e-11	0	0
Heart	0.015	0.00012	0.00015	0	0	2.06e-11	2.47e-13	0	0
Kidney	0.015	0.00011	0.00014	0	0	1.27e-10	2.51e-12	0	0
Liver	0.04	0.00031	0.00032	0	0	1.95e-11	1.3e-11	0	0
Lungs	0.12	0.00073	0.00081	0	0	3.55e-11	6.05e-12	0	0
Pancreas	0.015	0.00017	0.00012	0	0	7.85e-13	8.49e-12	0	0
Spleen	0.015	6.34e-05	0.00017	0	0	3.32e-13	7.88e-13	0	0
Thymus	0.015	0	0	0	0	1e-10	0	0	0
Thyroid	0.04	0.00051	0.00098	0	0	3.04e-14	0	0	0
Urinary Bladder	0.04	0.00081	0.00212	0	0	2.71e-10	0.00158	0	0
Head & Neck Skin	0.01	2.35e-05	7.31e-05	0	0	2.52e-11	1.63e-11	0	0
Trunk Skin	0.01	0.000155	0.000305	0	0	2.62e-10	4.6e-11	0	0
Leg Skin	0.01	0.000459	0.0023	0	0	8.55e-09	6.82e-10	0	0
Esophagus	0.04	1.84e-05	0.00019	0	0	7.78e-12	1.14e-12	0	0

The results of Table 3 are determined based on the simulation of different organs in 4 places, which are in terms of MeV/g, which is converted to Gy/y by using the coefficient of 1.6×10^{-10}(MeV/g to Gy) ,A(Activity(Bq)) and 365×86400 (s to y). The output of f6 tally for each organ in the MCNPX code is for one decay in source. Therefore, to calculate the dose due to the activity of the source in the amount of 100 milliCuries (100mCi), the activity of the source must be multiplied to 3.7×10^{10}($A=100\times10^{-3}\times3.7\times10^{10}=3.7\times10^{9}$). Because the weight coefficient of gamma is 1 [17], the results in terms of Gy can be declared based on Sievert (Sv). Finally, the results of Table 3 are multiplied by the weighting factor of each organs and summation of them the annual effective dose can be calculated. The annual effective dose in 4 point are given in Table 4.

Table 4. The results of annual effective dose (mSv/y) in 4 points around the KGUT source hole

Annual Effective Dose(mSv/y)	^{60}Co				^{137}Cs			
	P1 Place	P2 Place	P3 Place	P4 Place	P1 Place	P2 Place	P3 Place	P4 Place
	10.712	4.467	0	0	1.59	9.56E-06	0	0

Also, Table 5 and figure 2 was shown the total annual effective dose of ^{60}Co and ^{137}Cs source in 4 locations around the KGUT source hole.

Table 5. The total annual effective dose (mSv/y) of ^{60}Co and ^{137}Cs sources in 4 locations around the KGUT source hole.

P1 Place	P2 Place	P3 Place	P4 Place
12.29	4.47	0	0

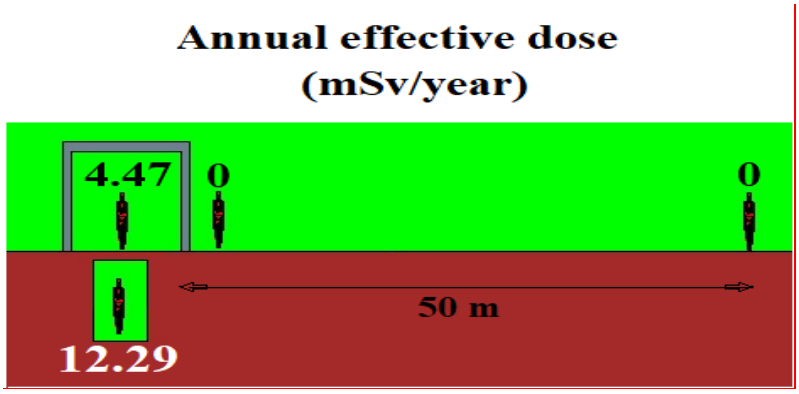

Fig. 2. A view of annual effective dose of ^{60}Co and ^{137}Cs sources in 4 locations

Conclusions

In this research, first, the source hole room of the Graduate University of Advanced Technology is simulated. Then the adult MIRD phantom in 4 locations around source hole room as: inside the hole (P1), inside (P2) and outside (P2) the hole room, as well as at a distance of 50 m from hole room (P2) which is made the research greenhouse was defined for annual effective dose calculation by definition of ^{60}Co and ^{137}Cs sources inside the source hole without shield. The results show that the annual effective dose caused by the 100 mCi of ^{60}Co source in 4 points is equal to 10.712, 4.467, 0 and 0, respectively, and100 mCi of ^{137}Cs source is equal to 1.59, 9.56 E-6, 0 and 0, respectively. Also, the

total annual effective dose of two sources in 4 locations is 12.29, 4.47, 0 and 0, respectively. The total results obtained from of ^{60}Co and ^{137}Cs sources show that inside the source hole, the annual effective dose exceeds the maximum amount due two sources without its shields. Therefore, it is required to comply with the principles of radiation protection, to use appropriate equipment in source hole. But outside the hole and room and at distance of 50 m from it, where the research greenhouse of the university is located, no annual effective dose is recorded due to the presence of a concrete wall and layers. Therefore, in terms of radiation, the presence of people outside the source hole room, as well as the presence of workers inside the source room is safe.

References

[1] ICRP. 2007. Publication No. 103, The 2007 Recommendations of the International Commission on Radiological Protection. ICRP 37(2-4):1-332.

[2] Webb, Geoffrey AM, and Ian F. Robinson. "International radiation safety standards." Journal of Radiological Protection 23.3 (2003): 337.

[3] Abel, J. (1994). Radiation safety: New international standarcis.

[4] US Nuclear Regulatory Commission. (1991). Subpart D—Radiation dose limits for individual members of the public. nrc. gov.

[5] National Council on Radiation Protection and Measurements. (2004). Recent applications of the NCRP public dose limit recommendation for ionizing radiation. Statement No. 10.

[6] Kahn, H., & Mann, I. (1957). Monte Carlo (p. 1165). Rand Corporation.

[7] Pakravan, D. (2023). Presentation of Organ Dose and Effective Dose Conversion Factors in Dual-Energy Computed To mography: A Monte Carlo Simulation Study. *Journal of Biomedical* Physics & Engineering, 13(4), 333.

[8] Rühm, W., Azizova, T., Bouffler, S., Cullings, H. M., Grosche, B., Little, M. P., ... & Woloschak, G. E. (2018). Typical doses and dose rates in studies pertinent to radiation risk inference at low doses and low dose rates. Journal of radiation research, 59(suppl_2), ii1-ii10.

[9] Stewart, F. A., Akleyev, A. V., Hauer-Jensen, M., Hendry, J. H., Kleiman, N. J., Macvittie, T. J., ... & Wallace, W. H. (2012). ICRP publication 118: ICRP statement on tissue reactions and early and late effects of radiation in normal tissues and organs–threshold doses for tissue reactions in a radiation protection context. Annals of the ICRP, 41(1-2), 1-322.

[10] Tekin, H. O. (2016). MCNP-X Monte Carlo code application for mass attenuation coefficients of concrete at different energies by modeling 3× 3inch NaI (Tl) detector and comparison with XCOM and Monte Carlo data. Science and technology of nuclear installations, 2016.

[11] Wielopolski, L., & Doron, O. (2012). Nuclear spectroscopy for in situ soil elemental analysis: Monte Carlo simulations. Applied Radiation and Isotopes, 70(7), 1085-1088.

[12] Kima, J. W., & Leea, Y. O. (2016). Generating Importance Map for Geometry Splitting using Discrete Ordinates Code in Deep Shielding Problem.

[13] Deutsch, M., Elliott, L. G., & Roberts, A. (1945). Disintegration Schemes of Radioactive Substances VIII. Co 60. Physical Review, *68*(9-10), 193.

[14] Magill, J., & Galy, J. (2005). Types of Radioactive Decay. Radioactivity Radionuclides Radiation*:* Including the Universal Nuclide Chart on CD-ROM, 59-87.

[15] Martin, R. H., & Taylor, J. G. (1990). A measurement of the half-life of ^{137}Cs. Nuclear Instruments and Methods in Physics Research Section A: Accelerators, Spectrometers, Detectors and Associated Equipment, 286(3), 507-513.

[16] Abdoulahpour, M. A., Rezaie, M. R., & Mohammadi, S. (2023). Measurement and simulation of the effective annual dose and radiation hazards of Jooshan hot spring in Kerman province. Radiation Physics and Engineering.

[17] ICRP. Publication No. 103, The 2007 Recommendations of the International Commission on Radiological Protection. ICRP. 2007;37(2–4):1–332.

ICNST 2024
International Conference on Nuclear Science and Technology
6- 8 MAY 2024 | Isfahan, Iran

Operational safety assessment program for near-surface disposal; A Case Study of Anarak Repository (Paper ID: 1138)

Zare Ganjaroodi S.[1], Fani M.[1*], Maleki Farsani A.[2]

[1]Energy and Physics Department, Amirkabir University of Technology, 424 Hafez Ave., Tehran, Iran

[2]Iran Radioactive Waste Company (IRWA), Atomic Energy Organization of Iran (AEOI), Postcode: 1439955931, Tehran - Iran

Abstract

Anarak radioactive waste repository, a near-surface trench-type, is the most suitable site for the LLW and ILW disposal which is selected according to the national and international requirements during eight years site selection phase. In this study, the safety assessment of Anarak repository has been performed for the operational phase in conservative terms to considerate the possible events in treatment building for both normal operation and accident scenarios using Monte Carlo code. Results show, the dose reached to the personnel during waste acceptance phase is almost to 8 mSv/year for thirty minutes for six times a year. Moreover, in the case of collecting the leaked waste in the accident scenario, 1.55 mSv/year will be reached to the workers within thirty minutes at distance of 20 cm from the radioactive waste.

Keywords: Near-surface, Disposal, Safety assessment, Anarak, Operational.

Introduction

The radioactive waste consists of any material that is either intrinsically radioactive or has been contaminated by radioactivity. According to the IAEA reports, nuclear waste is typically classified as Low-Level Waste (LLW), Intermediate-Level Waste (ILW), and High-Level Waste (HLW). Most of the LLW is sent to land-based disposal immediately after packaging for long-term management. Near-surface repositories have been used for the LLW and ILW disposal in many countries. Near-surface disposal facilities for LLW are designed to provide long term isolation of the wastes from the human environment by means of a system of barriers both natural and man-made. The basic principle of near-surface disposal is to keep the radiation dose and risk from the disposal practice to levels as low as reasonably achievable. In such manner, the safety of these facilities needs to be ensured during all stages of their lifetimes in two modes; the operational and post closure phases [1-2].

The radioactive waste disposal safety assessment is typically based on the consideration of various scenarios that are selected with the aim to envelope the possible performance of the disposal system

and the associated radiological impact [1-3]. A complete safety assessment program for radioactive disposal facility must include all possible scenarios of release and exposure including human intrusion. In terms of severity of risk, the human intrusion scenario may become important in the safety analysis of radioactive waste facilities [4].

Anarak site, a near-surface trench-type repository, is the most suitable site which is selected according to the international atomic energy agency (IAEA) and Iran Nuclear Regulatory Authority (INRA) standards and fundumentals during eight years site selection phase; for both LLW and ILW, which are produced in Bushehr Nuclear Power Plant (BNPP) and other medical and research industrial applications in a period of seventy years. These wastes contain a wide range of radionuclides including Uranium, Plutonium, Iodine, Technetium, Americium, Strontium, Cobalt, and Cesium. The Anarak site has located in a syncline structure that consists of lower red formation sediments. The Anarak site is located in the center of Iran and has an area of about 1 Km^2. The nearest town to Anarak disposal site is Anarak with less than 1300 population. According to geophysical studies, Anarak disposal site does not contain any confined aquifer and the water level reaches a depth of about 300 m. Furthermore, there is not an effective groundwater flow at this depth [5-6].

In order to provide assurance that radioactive waste disposal system is functioning properly, it is necessary to predict the individual dose as a part of safety assessment. Safety assessment is an iterative procedure to evaluate the performance of the disposal system and its potential impact on human health and the environment. Several reports and essays on various technical aspects of safety asessment programs of radioactive waste repositories have been investigated in recent years. In this paper, the operatinal safety assessment programs for Iran's radioactive waste repository in Anarak site is studied for the treatment building in two modes of normal operation and accident scenarios. The IAEA published some reports as guide and standatrd framework for near-surface disposal safety assessment. The objective of these Safety Guides are to provide recommendations on how to meet the requirements for assessing the safety of near-surface repositories [7-9]. Mitrakos et al, investigated the preliminary safety assessment for planning near-surface disposal of LLW in Greece which is published in the Journal of Environmental Radioactivity in 2023 [10]. In another paper, in 1999, Nair and Krishnamoorthy studied the probabilistic safety assessment model for near-surface radioactive waste disposal facilities [11]. In 2015, Sujitha et al, worked on the risk assessment of LLW in near-surface disposal facilities. In this project, they developed a radiological model for the risk assessment for the

near-surface disposal facilities of Cesium, Strontium and Cobalt. Also, the risk to the critical individual is estimated [12].

Material and method

Anarak site is a near-surface repository which consists of storage building, treatment building, health physics building, laboratories, and disposal site. Treatment building, which is built for the solid and liquid wastes management, includes storage zone, radioactive sources, overpacking, and temporary storage of cemented radioactive waste. The building area is approximately 2300 m^2. In order to reduce the dose to the employees, forklifts and overhead cranes are used in this building to move barrels and overpacks, which are controlled by remote operators. According to the reactor final safety reports [13], the wastes produced in BNPP are divided into two types of wastes, in which surface dose rates vary from 0.01 to 0.3 and from 0.3 to 10. On the other hand, the wastes are categorized into two categories, solid and solidified radioactive wastes according to their physical nature. The number and characteristics of solid and solidified waste with low and medium radiation are listed in the Table 1.

Table 1. Solid and solidified waste characteristics [14].

Radioactive waste	Total exposure (Bq/y)	No. of barrels per year
Solidified waste includes: VLLW, Radioactive waste including concentrated salt, Radioactive waste including high temperature titanium filters, Sludge residues from ion exchange filters, and Radioactive waste including sludge	1.7 E9 ≤ TE ≤ 2.5 E13	815
Solid waste includes: VLLW & LLW	-	765

Solid and solidified wastes are placed inside special disposal for transportation and burial. Next, the barrels are placed individually or in concrete overpack (In order to increase the reliability factor and reduce the penetration of substances such as water into the barrel) for final disposal. The geometric parameters and materials of the barrel and overpack are presented in Table 2.

Table 2. Barrel and overpack design parameters [14].

Parameter	Value	
	Barrel	Overpack
Shape	Cylindrical	Cube
Diameter (cm)	57.50	-
Height (cm)	81.00	130.00
Length (cm)	-	155.00
Width (cm)	0.30	155.00
Thickness (cm)	-	10.00
Material	Iron	Concrete

MCNPX is a based Monte Carlo code designed to track many particles over broad ranges of energies. This code can be used in several transport modes of neutron, photon, electron, and combined neutron/photon transport to solve the equation. The MCNPX does not solve an explicit transport equation. MCNPX code uses the Monte Carlo method to simulate the geometry and solve transport equations by tracing individual particles and recording some tallies of their normal operation [15].

The purpose of the various scenario used in the safety assessment of radioactive facilities is to model and present the uncertainty related to human behavior in the two modes of normal operation considerations and accident conditions. In general, a scenario can be considered a hypothetical outcome of processes and events that lead to human radiation. The considered scenarios are intended to visualize possible future states of the disposal site.

In this paper, operational phase and accident scenarios in treatment building were investigated. Next, all the activities that lead to employees being absorbed the dose were modeled in order to calculate the dose that reached to personals in a specific time steps.

Results and discussion

In this paper, the safety assessment of the treatment building is divided into two parts, normal operation and accident scenarios. Hence, different conditions are studied and analyzed in each part.

Normal operation

First, the employee's radiation dose in the storage zone of the treatment building at different distances from the barrel and the concrete overpack has been calculated using MCNPX code simulation for both solid and solidified waste. Results show, the dose values are less than the acceptable limit according to the IAEA reports [16-17]. The dose calculation from waste barrels and overpack are shown in Tables 3 and 4.

Table 3. The dose rate calculation from barrel.

Radioactive waste	Dose rate (mSv/h)		
	Surface dose	From 100 (cm)	From 300 (cm)
Solid waste	3.45	0.145	0.020
Radioactive waste including concentrated salt,	15.00	0.528	0.075
Radioactive waste including high temperature titanium filters	6.80	0.240	0.034
Sludge residues from ion exchange filters	15.11	0.522	0.075
Radioactive waste including sludge	0.305	0.010	0.001

Table 4. The dose rate calculation from overpack.

Radioactive waste	Dose rate (mSv/h)		
	Surface dose	From 100 (cm)	From 300 (cm)
Solid waste	0.0030	0.0010	0.0002
Radioactive waste including concentrated salt,	1.56	0.121	0.024
Radioactive waste including high temperature titanium filters	0.64	0.052	0.010
Sludge residues from ion exchange filters	1.47	0.116	0.023
Radioactive waste including sludge	0.030	0.0023	0.0004

In normal operation, three working shifts have been considered for treatment building, where three people are working in each shift. In this study, as a conservative assessment, the operational process with the highest probability of radiation exposure have been considered for employees. The different types of operation process, people involved and the radiation time in the treatment building are illustrated in Table 5.

Table 5. Operational process, people involved, occurrence frequency per year and the radiation time in the treatment building.

Stage	Frequency (per year)	Time (min)	No of people	Distance (cm)
Waste acceptance	6	30	2	150
Waste transportation	20	20	2	150
Source transportation	12	60	1	150

No accidents are considered during the waste acceptance phase. On the other hand, in the transportation of waste barrels, the accident of falling and breaking, as well as in the stage of moving radioactive sources, incidents such as falling and missing the source are considered. Normal operations results are presented in Table 6.

Table 6. Dose calculations for normal operation process.

Stage	Frequency (per year)	Time (min)	No of people	Dose (mSv/y)
Opening containers	132	1	2	1.12
Emptying the barrel	1580	5	2	0.57
Inspection and scanning of the barrel	158	30	2	0.35
Moving the barrels to the basket	1580	5	2	0.57
Moving the basket to the cells	264	15	2	0.29
Moving the basket to the trenches	0.2	20	8	1.91

Accident scenario

There is a possibility of accidents such as falling, breaking, and missing the radioactive source in waste and radioactive source transportation stages.

Considering that the length of the human arm is about 40 to 50 cm, the National Council of Radiation Protection (NCRP) [18] has also recommended the value of the arm length in calculations of 40 cm. For conservative considerations, it has been assumed that after the accident for the waste barrel, about 10% of the waste inventory will leak, and after the contamination is removed, 1% will still remain. The different types process, people involved and the radiation time in the treatment building for barrel and basket accident scenario are given in Tables 7 and 8.

Table 7. Barrel accident scenario, people involved, occurrence frequency per year and the radiation time in the treatment building.

Stage	Frequency (per year)	Time (min)	No of people	Distance (cm)	Dose (mSv/y)
Collection of waste and damaged barrels	6	30	2	20	1.15
Filling new barrels	6	30	2	100	3.21
Barrels transportation	6	30	2	200	0.92

Table 7. Basket accident scenario, people involved, occurrence frequency per year and the radiation time in the treatment building.

Stage	Frequency (per year)	Time (min)	No of people	Distance (cm)	Dose (mSv/y)
Collection of waste and damaged barrels	1	40	10	20	8.64
Filling new barrels	1	30	10	100	1.58
Barrels transportation	1	10	10	200	0.18

A possibility of another Accident scenario in the treatment building is the fall of radioactive source. Results showed that, for the Cobalt-60 radioactive source, less than one mSv/y dose will reach the person in the time of sixty minutes from a distance of 150 cm.

Conclusions

For the majority of all of the waste types produced by nuclear technologies, a satisfactory disposal has been developed and is being implemented around the world. Near-surface facilities are on or below the surface where the protective covering is of the order of a few meters thick. Waste barrels are placed in constructed vaults and when full the vaults are backfilled. Anarak site, a trench type near-surface repository includes storage and treatment buildings and also burial site. In this paper, the possible events in treatment building were divided into two categories of normal operation and accident scenarios to show that, the building is designed safely in accordance with national and international laws and limitations. Next, the safety parameters such as accident probability and dose were calculated in different scenarios using MCNPX code. Normal operation results show, the dose parameter during the Barrel transportation is reached to below than 2 mSv/year for twenty minutes for twenty times a year. The annual absorbed dose rate of personnel in normal operation is less than 2.5 mSv/year. On the other hand, in the case of collecting the leaked waste in the accident scenario, 1.55 mSv/year will be reached to the workers within thirty minutes at a distance of 20 cm from the radioactive waste. Moreover, the annual absorbed dose rate of personnel in accident scenario is less than 4 mSv/year. According to IAEA and INRA guidelines and standards, the average absorption dose of personnel in 5 years should not exceed 100 mSv/year (also more than 1.5 mSv per season), which conservative calculations presented that the personnel absorbed dose does not exceed in normal operation and accident scenarios. Finally, the treatment salon floor cover is designed to prevent radioactive radionuclides leakage into the underground water. Due to the 25 km distance of repository site from the city center, there is no possibility of danger for people during the accident scenario. Also, the present structure is resistant to an earthquake with a magnitude of nine Richter.

References

[1]- IAEA, (2004), Safety Assessment Methodologies for Near-surface Disposal Facilities, IAEA-ISAM-1, Vienna.

[2]- IAEA, (2009), Classification of Radioactive Waste, IAEA Safety Standards Series No. SSG-1, IAEA, Vienna.

[3]- IAEA, (1999), Near-surface Disposal of Radioactive Waste, IAEA Safety Standards Series No. WS-R-1, IAEA, Vienna.

[4]- T.M. Krishnamoorthy et al, (1997), Evaluation of disposal limits for shallow land burial facilities: Application to the back end of nuclear fuel cycle Applied Radiation and Isotopes, Applied Radiation and Isotopes, Volume 48, Issue 9.

[5]- Iran Radioactive Waste Management Company (IRWA), (2022), Site selection report, Atomic Energy Organization of Iran (AEOI).

[6]- Iran Radioactive Waste Management Company (IRWA), (2022), Site description report, Atomic Energy Organization of Iran (AEOI).

[7]- IAEA, (1999), Safety Assessment for Near-surface Disposal of Radioactive Waste, Safety guide, WS-G-1.1, Vienna.

[8]- IAEA, (2012), The Safety Case and Safety Assessment for the Disposal of Radioactive Waste, Safety guide No. SSG-23, Vienna.

[9]- IAEA, (1995), Safety Assessment of near-surface Radioactive Waste Disposal Facilities: Model Intercomparison Using Simple, TECDOC 846, Venna.

[10]- D. Mitrakos et al, (2013), Preliminary safety assessment for planning near-surface disposal of low level radioactive waste in Greece, Journal of Environmental Radioactivity, Volume 263, July 2023, 107163.

[11]- R.N. Nair, T.M. Krishnamoorthy, (1999), Probabilistic safety assessment model for near-surface radioactive waste disposal facilities, Environmental Modelling & Software Volume 14, Issue 5, March 1999, Pages 447-460.

[12]- S. Sujitha et al, (2015), Risk Assessment of Low Level Radioactive Waste in Near-surface Disposal Facilities, Geotechnical Safety and Risk, doi:10.3233/978-1-61499-580-7-425.

[13]- FSAR of BNPP-1. (2003). Final Safety Analysis Report of Bushehr Nuclear Power Plant (chapter 11), Ministry of Russian Federation of Atomic Energy (Atomenergoproekt), Moscow.

[14]- Iran Radioactive Waste Management Company (IRWA), (2022), Radiation shielding and criticality evaluation of waste disposal concrete containerreport, Atomic Energy Organization of Iran (AEOI).

[15]- Pelowitz, D.B., (2008), MCNPXTM User's Manual Version 2.6.0. Los Alamos National Laboratory.

[16]- IAEA, (2011), Disposal of radioactive waste, specific safety requirements No. SSR-5, IAEA, Venna.

[17]- IAEA, (2018), Regulations for the Safe Transport of Radioactive Material, specific safety requirements No. SSR-6, IAEA, Venna.

[18]- National Council of Radiation Protection (NCRP), (2005), Performance Assessment of near-surface Facilities for Disposal of Low Level Radioactive Waste, NCRP Releases Report No. 152.

ICNST 2024 International Conference on Nuclear Science and Technology
6- 8 MAY 2024 | Isfahan, Iran

Evaluation of Radiation Shielding Effectiveness of Iron Oxide-Enhanced Polyvinylidene Dichloride Composites via Attenuation Coefficient (Paper ID: 1147)

Yazdankish, Enayatolah

Applied Chemistry Department, Faculty of Gas and Petroleum, Yasouj University, Gachsaran, Iran

Abstract

This study explores the use of polyvinylidene dichloride composite reinforced with iron oxide (Fe_3O_4) nanoparticles as a radiation shielding material for applications such as clothing, gloves, and aprons. Three different composites containing 20%, 40%, and 60% weight fractions of iron oxide were analyzed for their shielding properties. The mass attenuation coefficient, linear attenuation coefficient, half-value layer (the thickness at which radiation intensity is reduced by half), and one-tenth value layer were calculated using PY-MBLUF software. Additionally, the effective atomic number (Z_{eff}) and effective electron density (N_{eff}) of the composite materials were determined. Furthermore, it was observed that the mass and linear attenuation coefficients decrease with higher incident radiation energy, and the composite with 60% iron oxide by weight exhibited superior performance compared to the other two composites. These findings highlight the potential of these composites as effective radiation shields and provide valuable insights for their practical application.

***Keywords**: Radiation Shielding, Mass Attenuation Coefficient, Polyvinylidene dichloride.*

1. Introduction

Radiation technology is utilized across various industries, including nuclear power plants, particle accelerators, food irradiation, nuclear waste storage sites, biological studies, defect detection in metal castings, nuclear medical imaging and therapy, and space exploration. This underscores the importance of protection against radiation. As nuclear technology and safety standards continue to develop, the storage and handling of useful radioactive materials in radiological institutions has emerged as a crucial issue. Given the detrimental effects of radiation on human health, safeguarding against unwanted radiation is imperative. Since humans work with radiation under different conditions, various materials such as clothing, gloves, aprons, glasses, and fixed materials in doors and walls are used as radiation shields. Radiation is typically divided into two types: ionizing and non-ionizing rays. Non-ionizing radiations like radio waves, microwaves, IR, UV, and visible light generally do not pose a significant risk to human health. On the other hand, ionizing radiation encompasses particles (such as alpha, beta, and neutrons) and photons (X and gamma rays). Protection against alpha and beta particles can be

achieved with thin sheets of paper and aluminum, while shielding materials such as construction and buildings, as well as wearable protective garments, are necessary for protection against neutrons, X-rays, and gamma-rays[1-4].

Lead is the most commonly used material for radiation protection, but due to its toxicity, heaviness, and inflexibility, alternative materials are employed in certain applications. Many radiation protection garments tend to be uncomfortably heavy if worn for long periods. A moderate reduction in weight can result from using appropriate non-Pb materials. In the literature, there are a variety of materials have been provided by researchers for radiation protection including modified concrete, polymers, composite materials, glasses, metallic alloys, stainless steel, and ceramics. These materials have been evaluated for their suitability as shielding materials in various applications. Advanced materials, such as nanocomposites and metamaterials, are being explored for their potential to provide superior radiation shielding properties. Using these innovative materials could lead to improved radiation protection and dosimetry in various applications[5-7].

Polyvinylidene dichloride (PVDC) is prepared from the polymerization of dichloroethylene. This crystalline polymer has high strength, good abrasion resistance, high melting temperature (about 180 degrees), good thermal resistance, good chemical resistance against acids, alcohols, solvents, and fats, and excellent impermeability against oil. It shows grease, water vapor, oxygen, and carbon dioxide. Films prepared from this polymer with extrusion have high transparency and flexibility. PVDC is used in food packaging, wrapping paper, parts, fittings in the chemical industry, and acid waste disposal pipes. This material can also be used as a radiation shield in the form of clothes, gloves, aprons, etc. [8-10]. Polyvinylidene dichloride is a polymer that has been chosen as a radiation shield in this research, and to increase its effectiveness as a radiation shield, various reinforced composites of it with a weight percentage of 20%, 40%, and 60% of iron oxide Fe_3O_4 has been used. Therefore, in the following section, the necessary theory is presented, the results and discussion are obtained in section 3, and finally, the conclusion is obtained in section 4.

2. Theory

In the range of radiation with X and gamma energies, photon interaction with matter occurs mainly through the photoelectric effect, Compton scattering, and pair production phenomenon. In the energy above *10 keV* (which is considered in this paper), the Rayleigh interaction has a small cross-section and little effect, so its effect has been ignored. Based on the photoelectric effect, all the energy of the

photon is absorbed by the electrons of the valence layer and separated from the nucleus, thus leaving the atom. In this process, the incoming photon is destroyed. In addition to being dependent on the atomic number of the target nucleus, the cross-sectional area of the photoelectric effect decreases with the increase of the incoming photon energy and at low energies is given by the following approximate relationship[11].

$$\sigma_{ph} \approx 3 \times 10^{12} \frac{Z^4}{E^{3.5}} \quad (1)$$

where, σ_{ph} is the photoelectric cross-section, Z is the atomic number of the nucleus, and E is the incident photon energy. In Compton scattering, the incoming photon spends part of its energy to knock out the atomic electron, and another part leaves the atom in the form of a photon with a larger wavelength and lower energy. The relative reduction of the output photon energy to the input is the cause of the attenuation of the intensity of the input radiation. In the phenomenon of pair production, a photon in the vicinity of matter turns into a particle and anti-particle. The electron, which is the lightest particle, has a rest mass of *512 KeV*. Therefore, the minimum radiation photon energy for the pair production phenomenon is *1.024 MeV*. At energies above the pair production threshold energy, this phenomenon becomes the dominant interaction of photons.

Beer-Lambert law (Equation (2)) [12] is used to obtain the linear attenuation coefficient (μ). In this method, by passing incoming mono-energetic radiation through an object of thickness x and measuring the intensity of the out-coming radiation the linear attenuation coefficient will be obtained. The mass attenuation coefficient (μ/ρ) which is equal to dividing the linear attenuation coefficient by the density is also obtained. This quantity is necessary to obtain other characteristics of the radiation shielding material. The half-value layer or the half-intensity layer expresses the thickness of the material through which the intensity of radiation decreases to half of its initial value through passing the matter.

$$I = I_0 e^{(\mu/\rho)\rho x} \quad (2)$$

where, I and I_0 are incoming and outgoing radiation intensity respectively, x is the thickness of matter, ρ is the material density and μ is the linear attenuation coefficient. The mass attenuation coefficient is denoted by (μ/ρ). As mentioned before, the half-value layer (HVL) and tenth-value layer (TVL) are the required thickness of material (in cm) which attenuates the radiation intensity by half and one-tenth respectively. The mean free path or relaxation length (λ) is also calculated, which represents the average distance between two successive interactions of photons with the material. Therefore, by considering Eq. (2) the HVL, TVL, and λ are as follows:

$$HVL = \frac{0.693}{\mu}, \quad TVL = \frac{2.303}{\mu}, \ and \ \ \lambda = \frac{1}{\mu} \tag{3}$$

The effective atomic numbers (Z_{eff}) and effective electron densities (N_{eff}) are essential factors for determining the ability of X and gamma photons to penetrate materials containing multiple elements. Many research studies have investigated these parameters for a variety of materials, including biological substances, alloys, compounds, glass, and minerals. When dealing with the energy range at which photon interactions occur, it is difficult to represent the number of atoms in a compound, alloy, glass, mineral structure, or biological material as a single quantity. A method is introduced to address this challenge by calculating the effective atomic numbers, taking into account the atomic number of all constituent elements in the material. The effective atomic numbers and the effective electron densities yield insights into the scattering and absorption of total cross-sections of gamma rays within a specific energy range. The effective atomic number is determined using the mass attenuation coefficient values for absorbed photons and varies with energy. For composite materials, the effective atomic number (Z_{eff}) is the equivalent atomic number of a composite material that produces the same effect as a single element when interacting with photons and obtained as [13, 14]:

$$Z_{eff} = \frac{\sigma_a}{\sigma_e} = \frac{\sum_i f_i A_i (\mu/\rho)_i}{\sum_i f_i (A_i/Z_i)(\mu/\rho)_i} \tag{4}$$

where, σ_a and σ_e are atomic and electronic cross-sections respectively, and f_i is the relative abundance of element *i*th for the total number of atoms, such that $\sum_i f_i = 1$. A_i and Z_i are the mass and atomic number of *i*th element, respectively. The effective electron density is a parameter that is related to the effective atomic number of a substance. It is defined as the number of electrons per unit mass and can be expressed mathematically using the following equation [15, 16].

$$N_{eff} = \frac{N_{eff}}{\langle A \rangle} Z_{eff} \tag{5}$$

where, $\langle A \rangle$ is the average atomic mass of the composite or sample.

3. Methods and Py-MLBUF software

A comprehensive understanding of a range of gamma-ray shielding parameters is crucial for evaluating the effectiveness of gamma-ray shielding in a building. In such investigations, computers play a pivotal role in determining gamma-ray shielding parameters. Multi-layered shields offer enhanced shielding efficiency when compared to single-layered protectors. In this research, the Py-MLBUF code was utilized to assess the protective characteristics of PVDC composites reinforced with iron oxide. Parameters such as density, atomic number of constituent elements, and weight percentage of each

element were gathered for these composites. Additionally, an empirical formula was selected as the basis for the calculations conducted. The computer code for this platform, developed in Python and named Py-MLBUF, calculates gamma-ray shielding parameters across the energy spectrum of 0.015–15 MeV, assuming perpendicular radiation incidence on the shield surface. The calculations were carried out with a primary focus on comparing calculation errors with empirical data. In comparison to the Phy-x/PSD [17] and BXCOM [18] software, Py-MLBUF has exhibited superior performance in this context [19].

4. Results and Discussion

Polyvinylidene chloride was selected as the base material and three composites reinforced with iron oxide (Fe_3O_4) were selected. The weight percentage of iron oxide used in these composites is 20%, 40% and 60%. As the proportion of iron oxide in the composite material rises, its plasticity diminishes while its brittleness and hardness increase. Beyond a concentration of 60%, the plasticity of the composite becomes nearly negligible. The density of iron oxide is 5.18 g/cm^3 and the density of PVDC polymer is 1.63 g/cm^3. The density of the composite is obtained from the following equation, which can be obtained with some algebraic calculations for the mixture.

$$\frac{1}{\rho} = \frac{w_p}{\rho_p} + \frac{w_F}{\rho_F} \tag{6}$$

In this regard, ρ, ρ_p, ρ_F, w_p and w_F are respectively the density of the composite, the density of polyvinylidene dichloride, the density of iron oxide, the weight percentage of polymer and the weight percentage of iron oxide. (It should be mentioned that the density of a compound cannot be obtained from this relationship and it is only suitable for composites and mixtures.) Based on this, the density of the composites was 1.889, 2.246, and 2.768 grams per cubic centimeter for composites with 20%, 40%, and 60% of iron oxide. Py-MLBUF software is used to calculate radiation shielding parameters [19]. Table 1 shows the mass attenuation coefficient and linear attenuation coefficient for all three composites and lead for comparison. As the energy increases, the mass and linear attenuation coefficient decrease. In addition, when the weight percentage of iron oxide in the composite is higher, the mass and linear attenuation coefficient also increase. As a comparison, the lead element has a higher mass attenuation coefficient than composites.

Table 1: Mass and linear attenuation coefficient of lead and three polyvinylidene dichloride (PVDC) composites reinforced with 20%, 40%, and 60% by weight of iron oxide

Energy (MeV)	PVDC -Fe_3O_4 %20		PVDC -Fe_3O_4 %40		PVDC -Fe_3O_4 %60		Pb	
	MAC (cm^2/g)	LAC (1/cm)	MAC (cm^2/g)	LAC (1/cm)	MAC (cm^2/g)	LAC (1/cm)	MAC (cm^2/g)	LAC (1/cm)
1.50E-02	19.0	35.9	247	55.5	30.4	84.2	111	1265
2.00E-02	8.39	15.9	110	24.7	13.6	37.7	86.3	979
4.00E-02	1.24	2.34	1.61	3.61	1.97	5.45	14.4	343
6.00E-02	0.482	0.911	0.593	1.33	0.704	1.95	5.02	162
8.00E-02	0.290	0.548	0.337	0.757	0.384	1.06	2.42	91.2
1.00E-01	0.217	0.410	0.241	0.541	0.265	0.732	5.55	56.9
2.00E-01	0.130	0.246	0.133	0.298	0.135	0.374	0.999	27.4
4.00E-01	0.096	0.180	0.095	0.214	0.095	0.263	0.232	62.9
6.00E-01	0.080	0.151	0.079	0.178	0.079	0.219	0.125	22.8
8.00E-01	0.070	0.132	0.069	0.156	0.069	0.191	0.089	11.3
1.00E+00	0.063	0.119	0.062	0.140	0.062	0.171	0.071	4.57
2.00E+00	0.044	0.084	0.044	0.099	0.044	0.121	0.046	2.63
4.00E+00	0.032	0.061	0.032	0.072	0.032	0.090	0.042	1.83
6.00E+00	0.028	0.053	0.028	0.063	0.028	0.079	0.044	1.41
8.00E+00	0.026	0.049	0.026	0.059	0.027	0.074	0.047	1.01
1.00E+01	0.025	0.047	0.026	0.057	0.026	0.072	0.050	0.805
1.50E+01	0.024	0.045	0.025	0.056	0.026	0.071	0.057	0.592

In Figure 1, the mass attenuation coefficient for all three composites and lead is plotted in terms of energy. As can be seen, the mass attenuation coefficient is higher at low energies. It is clear from the comparison of the three composites that the higher the percentage of iron oxide, the higher the mass attenuation coefficient. The mass attenuation coefficient, as expected, is greater than those for composites.

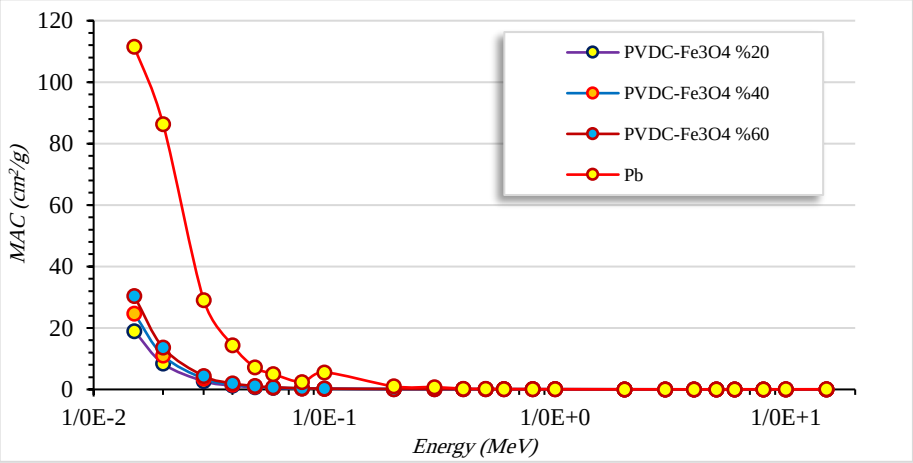

Figure 1: Mass attenuation coefficient for three polyvinylidene dichloride composites reinforced with iron oxide with weight percentages of 20%, 40%, and 60%, and compare them with mass attenuation coefficient Pb.

Table 2 shows the half-value layer (HVL) and the tenth-value layer (TVL) in centimeters. The half-value layer and the tenth-value layer are the thickness of material that when the radiation passes through it, the intensity of the radiation is reduced to half and one-tenth of its initial value, respectively. These thicknesses depend on the radiation intensity. As the radiation intensity increases, the thickness of the half-intensity layer and the tenth-intensity layer also increases. Figure 2 shows the HVL, measured in centimeters, plotted against radiation energy (in MeV) for three composites and the lead element. At lower energy levels, all materials have a low HVL, which then increases as the energy rises. It can be observed that the higher the percentage of iron oxide, the lower the HVL. As expected, the HVL for lead is lower than considered composites.

Table 2: Half-value layer and tenth-value layer of lead and three polyvinylidene dichloride (PVDC) composites reinforced with 20%, 40%, and 60% by weight of iron oxide

Energy	**PVDC-Fe_3O_4 %20**		**PVDC-Fe_3O_4 %40**		**PVDC-Fe_3O_4 %60**		**Pb**	
(MeV)	HVL(cm)	TVL(cm)	HVL(cm)	TVL (cm)	HVL(cm)	TVL(cm)	HVL(cm)	TVL(cm)
1.50E-02	0.0193	0.0642	0.0125	0.0415	0.0082	0.0274	0.001	0.002
2.00E-02	0.0437	0.1452	0.0281	0.0932	0.0184	0.0611	0.001	0.002
3.00E-02	0.1368	0.4545	0.0877	0.2915	0.0575	0.1911	0.002	0.007
4.00E-02	0.2958	0.9825	0.1923	0.6387	0.1271	0.4223	0.004	0.014
5.00E-02	0.5115	1.6991	0.3403	1.1303	0.2284	0.7586	0.008	0.025
6.00E-02	0.7606	2.5266	0.5203	1.7286	0.3558	1.182	0.012	0.040
8.00E-02	1.2638	4.1984	0.9156	3.0415	0.6525	2.1674	0.025	0.084
1.00E-01	1.6887	5.6096	1.2808	4.2548	0.9464	3.1438	0.011	0.037
2.00E-01	2.8124	9.3426	2.3236	7.719	1.8527	6.1547	0.061	0.203
3.00E-01	3.3927	11.2704	2.8472	9.4583	2.3053	7.6579	0.152	0.504
4.00E-01	3.8438	12.7689	3.2414	10.7676	2.6371	8.7601	0.263	0.874
5.00E-01	4.2357	14.0707	3.5791	11.8894	2.9177	9.6925	0.379	1.258
6.00E-01	4.5944	15.2623	3.8862	12.9097	3.1715	10.5354	0.490	1.628
8.00E-01	5.2474	17.4315	4.443	14.7593	3.6295	12.0569	0.689	2.289
1.00E+00	5.8451	19.4171	4.9513	16.4478	4.0465	13.4423	0.861	2.859
2.00E+00	8.2952	27.5561	7.0182	23.314	5.7288	19.0306	1.327	4.408
3.00E+00	10.0736	33.4638	8.4888	28.1993	6.9014	22.9259	1.444	4.796
4.00E+00	11.4054	37.8879	9.5656	31.7762	7.7399	25.7115	1.456	4.837
5.00E+00	12.4122	41.2324	10.3623	34.4227	8.3465	27.7266	1.431	4.753
6.00E+00	13.1733	43.7607	10.9495	36.3736	8.7817	29.1722	1.392	4.624
8.00E+00	14.192	47.1448	11.7047	38.8822	9.3167	30.9494	1.308	4.344
1.00E+01	14.7762	49.0856	12.1095	40.2268	9.5806	31.8261	1.229	4.084
1.50E+01	15.3495	50.9898	12.4375	41.3163	9.7358	32.3417	1.080	3.589

The average atomic number of atoms present in a material can be measured using the effective atomic number, as illustrated in Figure 3. In composites with a higher weight fraction of iron oxide, their Z_{eff} value increases, indicating a higher average atomic number of the constituent atoms. Consequently, these composites are more effective at reducing radiation due to the presence of atoms with higher atomic numbers. The increased likelihood of interactions between radiation and the atoms in the material contributes to the superior radiation attenuation properties of the composite. Generally, as the

radiation energy increases, the Z_{eff} value decreases. In Figure 4, the effective electron density, measured as the number of electrons per unit mass, is plotted for three composites of PVDC reinforced with 20%, 40%, and 60% weight fractions of iron oxide. Similar to the effective atomic number, the N_{eff} value varies with the energy of radiation, reaching its minimum value at around 1 to 2 MeV.

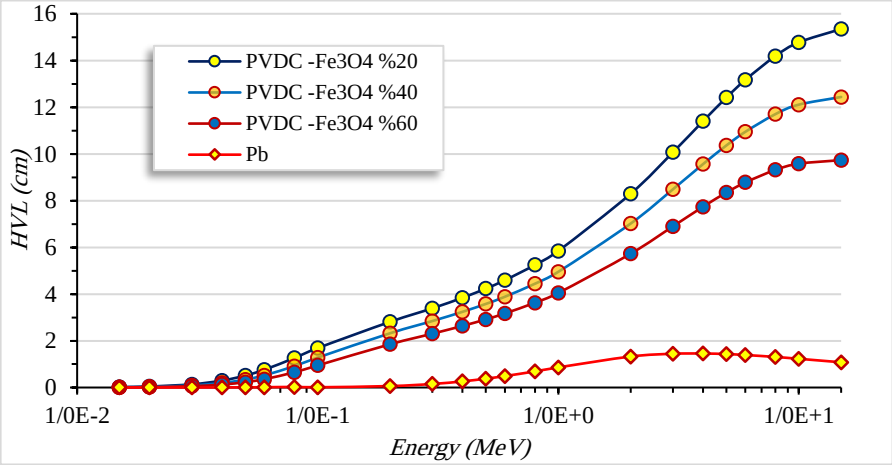

Figure 2: Half-value layer or HVL, a thickness of the material through which the intensity of the radiation decreases to half the initial value during the passage of the radiation. The thickness of the half-value layer increases with increasing energy.

The atomic number of a material plays a crucial role in determining how radiation interacts within that substance. The effective atomic number is key for predicting how photons interact with a substance, as certain types of photon interactions rely on the atomic number. The effective atomic number can vary depending on the energy range being utilized. In Figure 3, the effective atomic number is presented against the photon energy for three PVDC composites. For the lead element, this is constant and equal to 82. The effective electron density, N_{eff}, is closely linked to the effective atomic number density, Z_{eff}, which is measured in the number of electrons per unit mass and plotted against photon energy in Figure 4. For the lead element, this is constant and equal to 2.383×10^{23}.

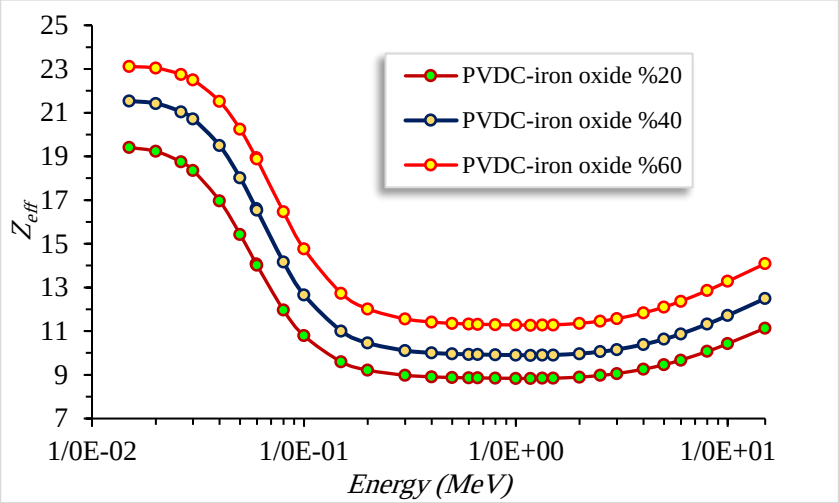

Figure 3: The effective atomic number of three PVDC reinforced with iron dioxide. The effective atomic number of lead is constant and equal to 82.

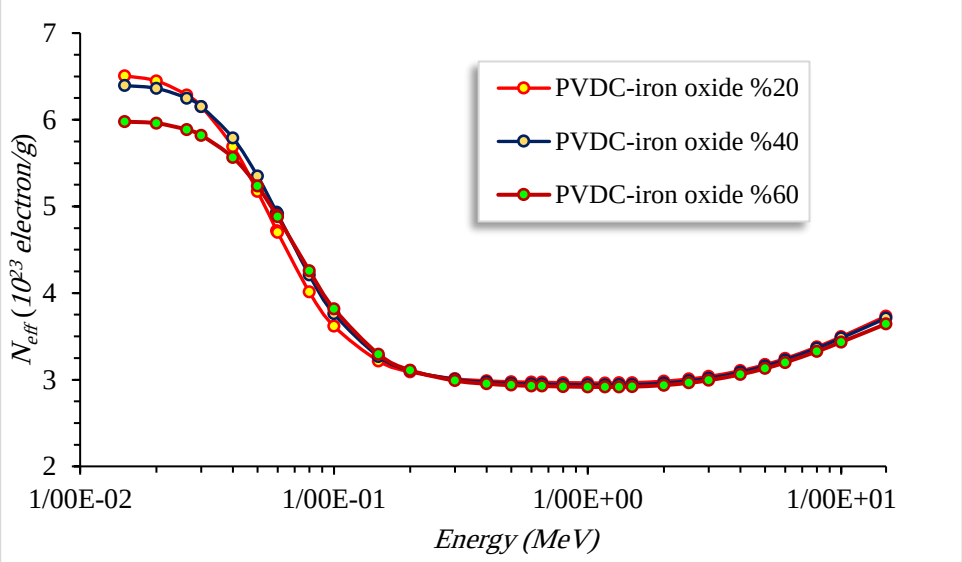

Figure 4: Effective electron number, which shows the number of electrons per gram of matter versus photon energy. For lead, this number is 2.383×10^{23}.

5. Conclusion

Polyvinylidene dichloride is utilized as a material for radiation shielding. To improve its performance, a composite was created by reinforcing the polymer with iron oxide nanoparticles. Three composites were produced with weight fractions of 20%, 40%, and 60%. Using the PY-MBLUF software, various properties including mass and linear attenuation coefficients, half and tenth value layers, and effective

atomic and electronic numbers were calculated. The results demonstrate that at lower photon energies, the mass attenuation coefficient increases, indicating better performance of the composite as a radiation shield. Additionally, it was observed that composites with higher weight fractions of iron oxide exhibited greater mass and linear attenuation coefficients, illustrating their superior performance as radiation shields. Furthermore, the protective efficacy of lead was taken into account for comparison. While lead offers superior protective properties compared to these composites, there are instances where the use of these composites proves advantageous due to factors such as flexibility, weight, ease of use, and other relevant features.

References

1. Yazdankish, E., M. Foroughi, and M.H.A. Azqhandi, Capture of I131 from medical-based wastewater using the highly effective and recyclable adsorbent of g-C3N4 assembled with Mg-Co-Al-layered double hydroxide. Journal of Hazardous Materials, 2020. **389**: p. 122151.
2. Barabash, A., D. Barabash, V. Pertsev, and D. Panfilov, Polymer-composite materials for radiation protection, in Energy Management of Municipal Transportation Facilities and Transport. 2018, Springer. p. 352-360.
3. Bhosale, R.R., et al., Radiation shielding and gamma ray attenuation properties of some polymers. Nuclear Technology and Radiation Protection, 2017. **32**(3): p. 288-293.
4. Yazdankish, E. and M. Nejatolahi, Improved calculation of alpha decay half-life by incorporating nuclei deformation shape and proximity potential. Physica Scripta, 2023. **98**(11): p. 115309.
5. Özdemir, T., et al., Nano lead oxide and epdm composite for development of polymer based radiation shielding material: Gamma irradiation and attenuation tests. Radiation Physics and Chemistry, 2018. **144**: p. 248-255.
6. Howard, B., et al., Protection of the environment from ionizing radiation in a regulatory context—an overview of the PROTECT coordinated action project. Journal of Radiological Protection, 2010. **30**(2): p. 195.
7. Azqhandi, M.H.A., M. Foroughi, and E. Yazdankish, A highly effective, recyclable, and novel host-guest nanocomposite for Triclosan removal: a comprehensive modeling and optimization-based adsorption study. Journal of colloid and interface science, 2019. **551**: p. 195-207.

8. Wang, Y., et al., Design strategy of barium titanate/polyvinylidene fluoride-based nanocomposite films for high energy storage. Journal of Materials Chemistry A, 2020. **8**(3): p. 884-917.

9. Behera, R. and K. Elanseralathan, A review on polyvinylidene fluoride polymer based nanocomposites for energy storage applications. Journal of Energy Storage, 2022. **48**: p. 103788.

10. Keshavarz, M., M. Tabatabaee, M. Shahabi, and E. Yazdankish, A Sulfonated Phenanthrolinum Salt of Phosphotungstate as Novel Catalyst for the Efficient Synthesis of 3, 3′-Diaryloxindoles. Polycyclic Aromatic Compounds, 2021. **41**(2): p. 427-439.

11. Al-Buriahi, M.S., et al., Radiation attenuation properties of some commercial polymers for advanced shielding applications at low energies. Polymers for Advanced Technologies, 2021. **32**(6): p. 2386-2396.

12. Mayerhöfer, T.G., H. Mutschke, and J. Popp, Employing theories far beyond their limits—the case of the (Boguer-) beer–lambert law. ChemPhysChem, 2016. **17**(13): p. 1948-1955.

13. Özkalaycı, F., et al., Lead (II) chloride effects on nuclear shielding capabilities of polymer composites. Journal of Physics and Chemistry of Solids, 2020. **145**: p. 109543.

14. Hosamani, M., et al., Determination of effective atomic number of multifunctional materials using backscattered beta particles–a novel method. Spectroscopy Letters, 2020. **53**(2): p. 132-139.

15. Tekin, H., et al., Photon and neutron shielding performance of boron phosphate glasses for diagnostic radiology facilities. Results in Physics, 2019. **12**: p. 1457-1464.

16. Kaewkhao, J., J. Laopaiboon, and W. Chewpraditkul, Determination of effective atomic numbers and effective electron densities for Cu/Zn alloy. Journal of Quantitative Spectroscopy and Radiative Transfer, 2008. **109**(7): p. 1260-1265.

17. Şakar, E., et al., Phy-X/PSD: development of a user friendly online software for calculation of parameters relevant to radiation shielding and dosimetry. Radiation Physics and Chemistry, 2020. **166**: p. 108496.

18. Eyecioğlu, Ö., et al., BXCOM: a software for computation of radiation sensing. Radiation Effects and Defects in Solids, 2019.

19. Mann, K.S. and S.S. Mann, Py-MLBUF: Development of an online-platform for gamma-ray shielding calculations and investigations. Annals of Nuclear Energy, 2021. **150**: p. 107845.

ICNST 2024 International Conference on Nuclear Science and Technology
6- 8 MAY 2024 | Isfahan, Iran

Decision support system for managing nuclear and radiation emergencies. (Paper ID: 1160)

Heidary P[1], Abbasi F. Correspondent[1*]

[1]IRAN Nuclear Authority Regulatory, Tehran, Iran

Abstract

The JRODOS-DSS is developed by Karlsruhe Institute of Technology for the management of nuclear and radiological emergencies. It was evaluated and improved in various projects, such as PREPARE, CONFIDENCE, and EURANOS. The system is installed and maintained on INRA (Iran Nuclear Regulatory Authority) servers since 2021 to ensure proper preparedness and response to potential nuclear and radiological incidents. The system has significant capabilities in atmospheric dispersion modeling at mid-range and long-range scales followed by estimating doses through dominant pathways. The system has a special ability to suggest countermeasures (distribution of iodine tablets, relocation, evacuating, and sheltering) or other protective actions (like food banning) and evaluate their impact which should be reported to decision makers to make decision about if and how these actions shall be implemented. The system will be described in this study and an exercise conducted by Rodos User Group in 2023 (RUG2023) is illustrated as an example.

Keywords:

JRODOS-DSS, Dose assessment, Dispersion modeling

Introduction

Proper preparedness and to response to nuclear and radiological emergencies is one of the fundamental safety requirements in any usage of nuclear facilities, that shall be met before licensing, while operating and even after decommissioning which requires a robust decision-making approach for handling multiple phases and aspects of emergency to ensure making effective and consistent decisions by response organizations (i.e., national authorities, stakeholders, regulatory bodies).

Assessing consequences of a nuclear or radiological accident is a significant part of the emergency preparedness and is vital for decision making process, which requires a multidisciplinary and comprehensive system of tools to support decision makers.

The most well-known and widely used decision support system (DSS) for handling nuclear and radiological emergencies is called JRODOS which stands for Java-based Real-time On-line Decision

Support System. It is developed and maintains by Karlsruhe Institute of Technology under the support of the European Commission's RTD Framework programs since 1992.

The system is designed and developed to manage off-site emergency situations by exploring the consequences of radioactive release, effectiveness of protective measures. The main task of JRODOS is to support decision makers providing them a large scale of information in different aspects and phases of an accident, especially in the response phase that faster decisions and more reliable information are needed.

The system can be installed and run alongside other disaster management structure in national or regional emergency center for preparing and response to nuclear emergencies initiated from facilities inside and near the country. Data transfers channels can be used to fetch the status of the facilities periodically and prepare for probable accident in near future. Also, estimation and measurement from contaminated urban and agricultural area can be imported to the system to manage the situation and transition to normal condition (if any).

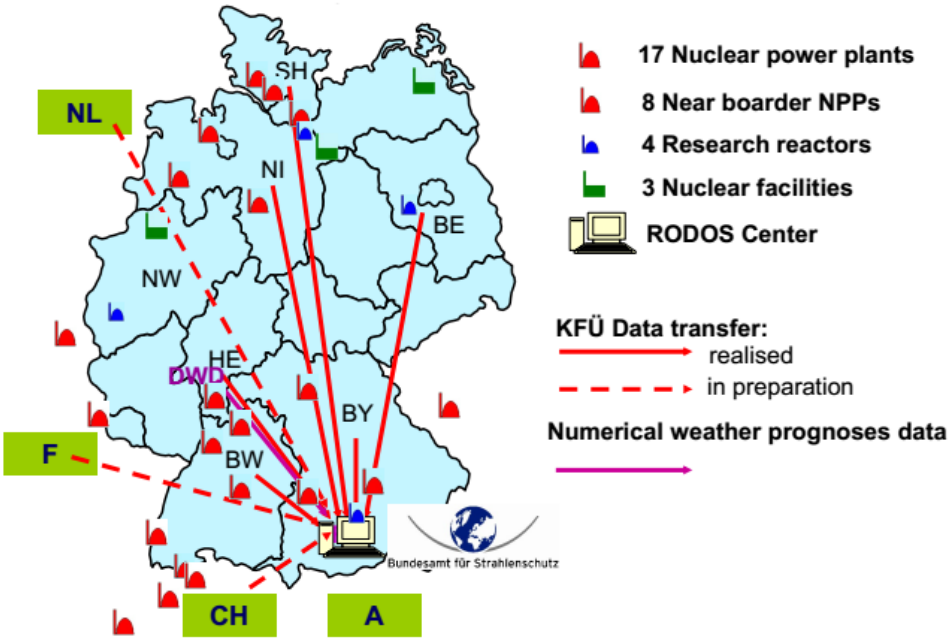

Fig. 1. National emergency center in BFS, Germany with JODOS installed.

There are data transfer channels with facilities inside and nearby countries [7].

There are wide range of countermeasures that can mitigate an emergency and alleviate or avoid radiological consequences. Some of them were stated in [1], however, according to IAEA GSR7 major useful countermeasures during emergency are: sheltering, evacuation and relocation of people,

distribution of iodine tablets which are implemented by special module in JRODOS. Also, it is possible to analyze the effectiveness of each countermeasure. This phase is called urgency emergency phase and starting directly after the nuclear accident, may last up to several weeks following the accident. Food restrictions and agricultural countermeasures also may be proposed as countermeasure for later times. Regions need these actions and timetable of them can be found by geo-analyzing JRODOS output. The system may also be used for simulating long time after accident for restoration of contaminated land in which JRODOS can make us sure that health risk and doses would not exceed some predefined criteria. This phase is called transition or post-accident phase and begins when the external inhalation exposure from the radioactive cloud is terminated and deposition of radioactive contaminant is trivial or they do not occur in the region of interest, which may last from weeks to months to years. Whereas the primary objective of the emergency phase is to protect human health, the transition phase focuses on the detailed evaluation of the radiological situation in the contaminated areas and on the preparation of plans for the recovery to resume social and economic activities.

It is worth mentioning the German Commission on Radiological Protection (SSK) suggests to break down an accident into phases that reflect the varying status of release, type and urgency of measures, type and availability of resources, and relevance of exposure pathways [2,5]. (Figure 2)

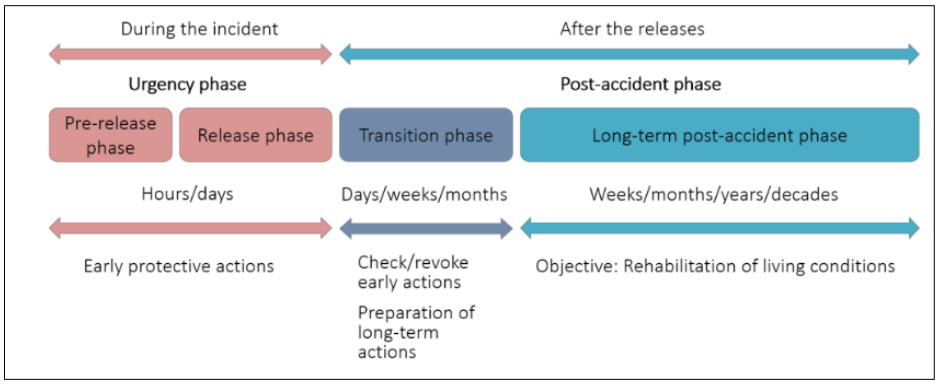

Fig. 2. Phases of a nuclear accident by SSK

Other important features of the system are: [3,4,6]

Considering Using the reference levels for action proposition dose (ICRP-103) and ICRP screening model.

Considering the main routes of radiation exposure (External effective dose induced by radionuclide deposited on the ground (Ground Shine), external effective dose induced by the radioactive cloud

(Cloud Shine); internal dose induced by food intake (Ingestion), and the dose induced by inhalation. These pathways are shown in Figure 3

Importing measurement (i.e., from nearby mast) for modifying calculation and construct initial cloud shape. Input data shall be in RTTF format which is the native format for RODOS.

Minimal source term reconstruction module which (theoretically) can estimate place and time of the release probabilistically by using of simultaneous activity and meteorological measurement. However, almost no station has such measurement ability so this module has a few applications.

Compatibility with gamma dose rate stations (GDRS). Measurement from GDRS can be used for triggering an action or source reconstruction. Also, it is possible to guess gamma dose rate in place of GDRS.

Calculation in residential area is implemented in ERMIN module which can be applied to very low range problems (couple of meters). Special issues like retention from surfaces (i.e., roof, walls, plant, etc.) and indoor/outdoor re-suspension are considered. Also, there are couple of calculation endpoints (as output) like, public and worker dose rate and surface contamination. Using the module requires very fine topology and measured meteorological data inside the domain.

There are a couple of modules ("Statistic Output", "Ensemble Generator") for generating and running many simulations to comparing some feature or statistical calculation. Also, there are other tools ("Recurrent Job Launcher" and "continuous chain") that can run the simulation periodically with updated meteorological data.

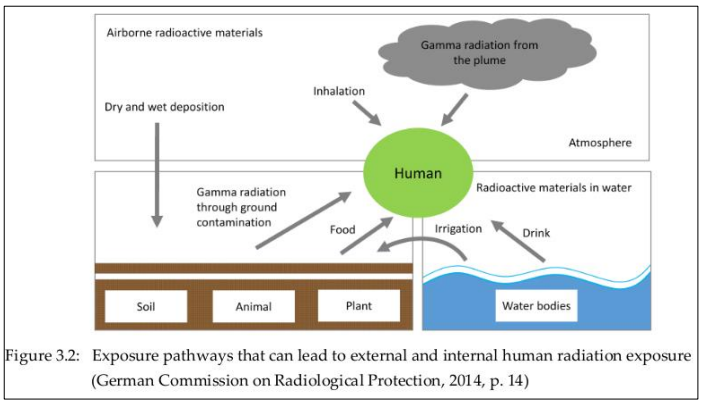

Figure 3.2: Exposure pathways that can lead to external and internal human radiation exposure (German Commission on Radiological Protection, 2014, p. 14)

Fig. 3. Exposure pathways that can lead to external and internal exposure of human [2,5]

JRODOS is widely used in emergency centers especially in European and Asian countries. There is a workgroup called Rodos User Group (RUG) which is the community for discussing about the system and maintaining the code. RUG also conducts annual exercise (with hypothetical scenario and given

inputs) for keeping the community active and assessing preparedness. At the time of writing this paper Iran is the only country in the middle east that actively contributed to all RUG exercises.

The purpose of this study is to assess the capabilities of JRODOS as a decision support system and various usage of the system in preparedness and response to an emergency. First, we depict the architecture of the system and explain most important parts. Then necessary inputs for running a simulation will be described and the desired results will be mentioned. After that we describe about customizing the system with domestic data and layers. Finally, we illustrate last RUG exercise as an example of facing with a hypothetical emergency.

Methods Describing Simulations:

Software architecture for a typical JRODOS installations shown in Figure 4. Numerical calculation is done in central server equipped with a geo-referenced database, meteorological Providers and connection to other essential infrastructure. This configuration ensures that every connected client will perform the simulation with the same assumption and data. So, their results would not vary significantly. Moreover, the customization procedure (which is time-consuming and crucial) can be done once. JRODOS tracks transfer of activity to food, feed and environment and it can calculate dose quantities by using related coefficient.

Also, there are separate tools for downloading/generating meteorological data needed for the simulation. Meteorological data in many formats can be imported to JRODOS but NOMADS is the most popular one and it is usually used in exercises. However, it is possible to import other good quality data or down scale them by atmospheric models (like WRF).

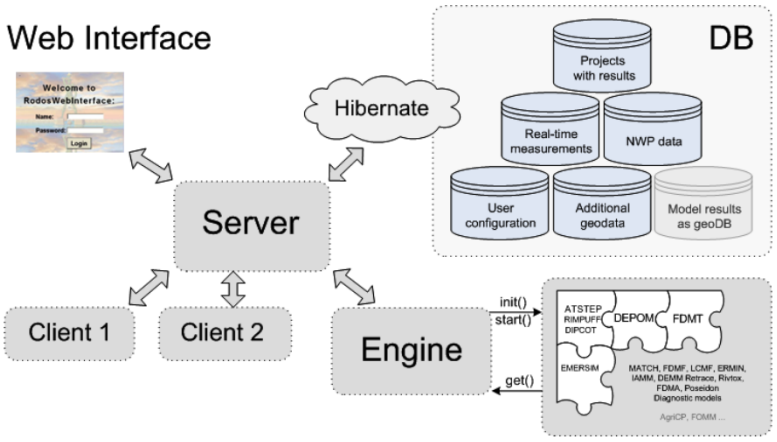

Fig. 4. Architecture of a typical JRODOS installation.

Technically, JRODOS is a container for variety of models and modules each perform distinct calculations. They can be aligned in a model chain to reach to definite end point. A typical model chain usually starts with a dispersion (atmospheric or hydrodynamic) model followed by dose assessment or countermeasure module. Then we can explore the results for proposing protective action. The most important pathway in emergency situation is through atmosphere so we will describe different parts of this chain (Figure 5). The whole process is divided into three parts: input, dispersion models and modules.

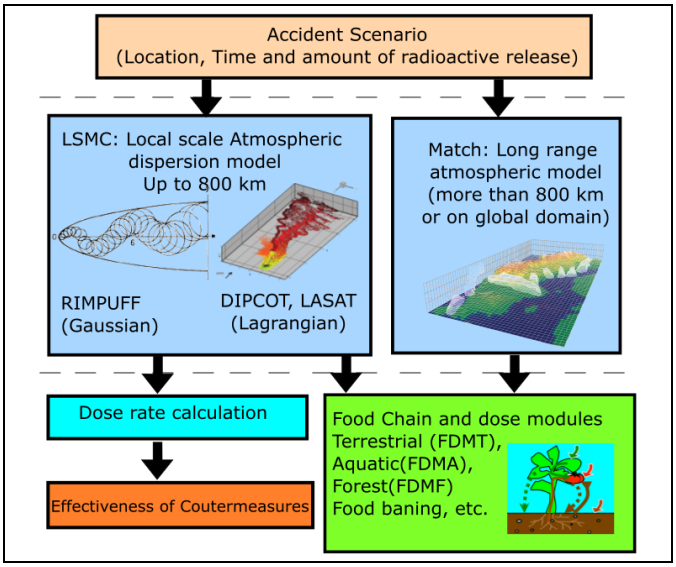

Fig. 5. workflow of a typical atmospheric dispersion simulation.

Scenario: Each simulation in JRODOS starts with input data consist of source term (radioactive contaminant released) Usually, emergency is detected from early warning stations or abnormal operation of facilities. So, at the very first times usually the source term is not fully characterized. In case of radiological emergency, we can estimate the source term by the available information about the radioactive source and type of the accident (i.e., explosion, espionage, etc.). However, predefined source terms for probable accidents are available for NPPs. These source term along with timing forms the whole scenario for the accident that is the starting point of the simulation. A simulation scenario shall at least contain following items:

Precise radioactive material released shall be stated. The individual elements with mixing ratios are required for atmospheric transport calculations. Furthermore, any related information about the released activity like released height and duration, chemical form, particle size and half-life of radionuclide must be determined in the scenario. Amount and ratio of radionuclide is released from

facility is significantly depend on type of reactor, performance of containment, fuel cycle and accident type.

Geo-location of the nuclear power plant or a release location for a radiological emergency where the assumed event takes place

Date and time of the accident: whether the accident date lies within the growing season or outside plays a crucial role for food-chain model assessments. Also, dispersion models are chaotic systems so a tiny change in release timing may result in a huge difference.

Detailed information about the meteorological conditions during the assumed dispersion and deposition phase for airborne releases, and about hydrological and possibly also meteorological conditions in the considered dispersion time interval for aquatic releases

Dispersion models: Local atmospheric simulations (less than 800 km) are implemented in LSMC (Local Scale Model Chain) which is equipped with three engines: RIMPUFF is the light wave puff model, DIPCOT and LASAT are Lagrangian particle models. If the NPP located farther than 800 km it can be simulated with MATCH model which is a far-range and global dispersion model. Dispersion modes track the fate of contaminant step by step inside the computational grid with finite difference or other numerical methods. The activity concentrations obtained by these models can then be used by other modules (next in chain) for deposition or dose calculations. Although LSMC itself has minimal capability for generating dose quantities and activity concentrations required for countermeasures and food screening but detailed information about activity and dose quantities shall be fetched by other modules. The most useful output produced by dispersion models is “Cloud Arrival Time” and “Cloud Leaving Time”. They can be used for determining evacuation priority between different sectors and finding proper routes and places for relocation. Running the dispersion models is the most time-consuming part of the simulation and usually is parallelized.

Modules: Human will receive doses from very different and independent pathways each are considered with a separate module in JRODOS. Inhalation and external exposure are trivial and can be produces by LSMC itself but for finding hot-spots we need to know places where wet deposition occurs. Dry deposition occurs more smoothly and is the starting point for transferring activity to food and feed. Ther is a module called DEPOM that can calculate dry and wet deposition. Terrestrial pathways (though plant and animal) are also considered by FDMT and FDMA does the same for aquatic products.

EMERSIM module is able to suggest needed countermeasures based on national or international criteria. The module is able to analyze effectiveness and cost of each countermeasure which can be used for deciding on prioritizing or postponing a definite countermeasure. However, there are no module to depict food banning area and we shall find out interested region by spatial analysis or simply by drawing contour around them.

These tools are managed by comprehensive user interfaces and operated with real-time database and GIS functionalities to show geographical characteristics (elevation, land use, soil type, population density and agricultural production) for the surroundings of the release location with Google Maps (hybrid view) or OpenStreetMap as background layer. This sublime GIS tools can be used for probing spatial outputs. There are more than 140 outputs for a single simulation in JRODOS and important outputs are:

Cloud arrival time: It records at a given location on the map the time elapsed between the start of release and when the plume reaches to the point.

Area affected by: The time and location when some condition satisfies (like following conditions) for the first time.

The time integrated air concentration (nuclide sum) near ground exceeds 1000 $Bq.s/m^3$

The total cloud GDR is larger than 1 nSv/h

Total Ground contamination is larger than 100 Bq/m^2

These are useful indicators for the time window suitable for initiating emergency actions, in particular with respect to sheltering, evacuation and thyroid blocking by the intake of stable iodine

Air concentration: calculated activity concentration of the radioactive cloud for a height of 1m above ground

Total cumulative dose: Summation of the received dose from all pathways.

Countermeasure: An action aimed at alleviating the radiological consequences of an accident (Evacuation, Iodine tablet distribution, relocation).

Food Banning: Any limitation for production or consumption of food and feed due to probable radioactive contamination.

More complex analysis can be done with GIS software (i.e., QuantumGIS or ArcGIS) that is directly connected to JRODOS database. There are other none spatial outputs like time-table of countermeasures that will be shown in tables.

Results and Discussion

As an example, the first RODOS User Group exercise in 2023 (RUG2023) is illustrated. The scenario was sent to RUG users via email and there was a two-week time window for working and publishing results. Results shall be self-assessed by comparing with KIT results and other participants. The scenario (consequence of events resulted to accident) will be stated first. Then assumptions for running the project is mentioned and finally the desired results are shown.

Scenario: In this session, we will explain the first exercise scenario for the RODOS User Group (RUG) in 2023, along with the corresponding result generation. The exercise included one EMERGENCY model chain run with either the KIT-CN site. Gamma dose rate measurement stations close to Karlsruhe, Germany measured elevated levels of radioactivity in the afternoon of 21 June 2022. After deploying measurement teams, a release of Cs-137 from a local steel mill at the KIT-CN site, coordinates 8.426° E and 49.092° N, is identified. At 06:00 (UTC) on 21 June 2022, a delivery of scrap metal from a demolished hospital was added to the steel production line. It is assumed that the sealed radioactive source capsule of a medical teletherapy unit was part of the scrap metal delivery by accident. The activity in the radioactive source capsule is estimated as 50 TBq Cs-137 from old hospital licensing records. The start of the release from the stack at 50m height was estimated to be 07:00 (UTC) on 21 June 2022. The steel mill is shut down at 04:00 (UTC) on 22 June 2022. It is assumed that the release stops at this time and that all the Cs-137 from the source capsule was released into the environment.

Preparation: It is recommended to use these setting for simplicity of comparison.

The default computational grid of 800(2) is used. This grid spans 800 km on each side with the smallest cell of 2 km size.

NOMADS 0.5° x 0.5° prognostic data were used that was downloaded on 20.06.2021 07:07 UTC and on 21.06.2021 07:15 UTC. Attendees may use their own meteorological data source for 96h duration.

A file called “export-stations.csv” is sent with the scenario which is the location of gamma dose rate stations in Germany. This file shall be copied to client folder of JRodos installation, so that user can use use the interpolate to points tool which will interpolate values of total gamma dose rate to the place of stations.

Result: Desired results consist of geographical results that were generated as map with OSM as background and text results that were organized in tables. Users usually choose one of the dispersion models comes with JRODOS, however, all three models of LSMC were used here for comparison and probing trivial differences. Results that were supposed to report are:

1. **Cloud arrival time**

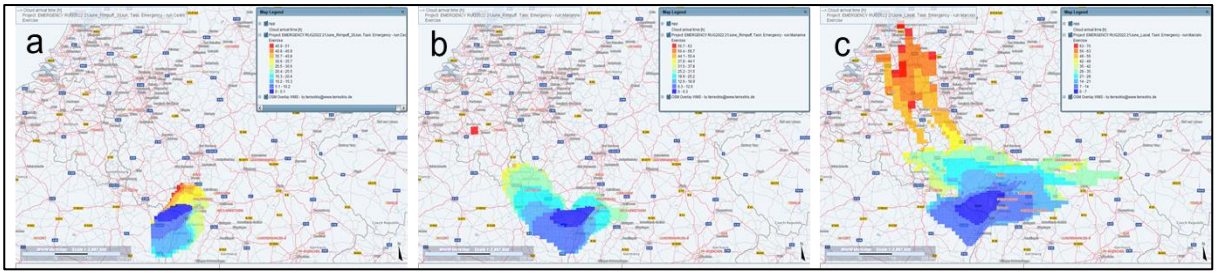

Fig. 6. Cloud arrival time a) RIMPUFF with weather data downloaded 20.06.2021, b) RIMPUFF with weather data downloaded 21.06.2021, c) LASAT with weather data downloaded 21.06.2021

The cloud arrival time is the most important outputs, in early time and can be used for prioritizing protective actions. As shown in figure 6 radioactive cloud moves slightly to the south (blue color) and then headed to north (yellow and red colors) in case of LASAT it was expected to reach to the shore in about 60 hours. So, evacuation of the people in the north is more essential and evacuated or relocated people shall be moved to south or west where the initial plume may not reach them soon.

2. **Air concentration of Cs-137. (map; table with maximum concentration in 1, 10 and 100 km distance)**

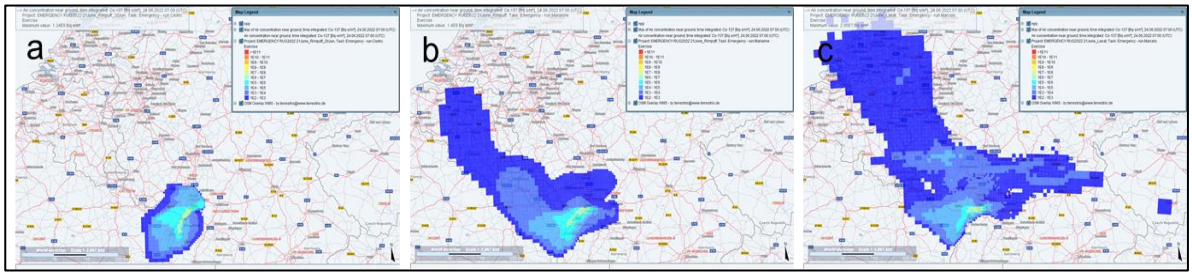

Fig. 7. Air concentration near ground time integrated Cs-137 a) RIMPUFF with weather data downloaded 20.06.2021, b) RIMPUFF with weather data downloaded 21.06.2021, c) LASAT with weather data downloaded 21.06.2021

Table 1. the maximum concentration was determined at distances of 10 and 100 km.

Distance [km]	1	10	100
Air concentration near ground time integrated Cs-137 [Bq s/m^3]	A: 1.24E8 B: 1.4E8 C: 2.03E7	A: 1.3E7 B: 7.04E6 C: 5.43E6	A: 1.3E4 B: 4.78E4 C: 1.66E4

Air concentration of radioactive pollutant (Cs-137 in this case) can be used for performing other protective actions. For instance, people living at 100 km from the accident (depending on the country regulation) may be sheltered and stay there until plume passes that area but for inhabitant areas located 1km or 10km from accident place sheltering is not effective and they shall be evacuated or relocated because the radioactive pollutant is bigger.

Total dose (w/o ingestion; integrated over 7 days; map with contour lines of 1 and 100 mSv; table with maximum distance in which 1 and 100 mSv is exceeded)

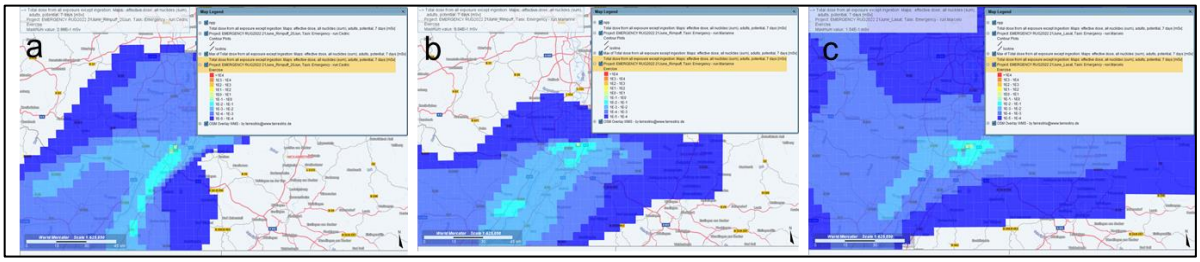

Fig. 8. Total dose (w/o ingestion; integrated over 7 days) a) RIMPUFF with weather data downloaded 20.06.2021, b) RIMPUFF with weather data downloaded 21.06.2021, c) LASAT with weather data downloaded 21.06.2021

Exploring legend of figure 8, it is clear that 1 mSv criteria is not exceed with this calculation grid due to low source term. So, relocated people can comeback to their home after accident unless other accident happens because the annual dose limit will not exceed due to this accident.

Activity concentration of Cs-137 in leafy vegetables and cow milk (table with maximum distance in which WHO/FAO maximum levels in leafy vegetables – 1250 Bq/kg - and cow milk – 1000 Bq/kg - are exceeded)

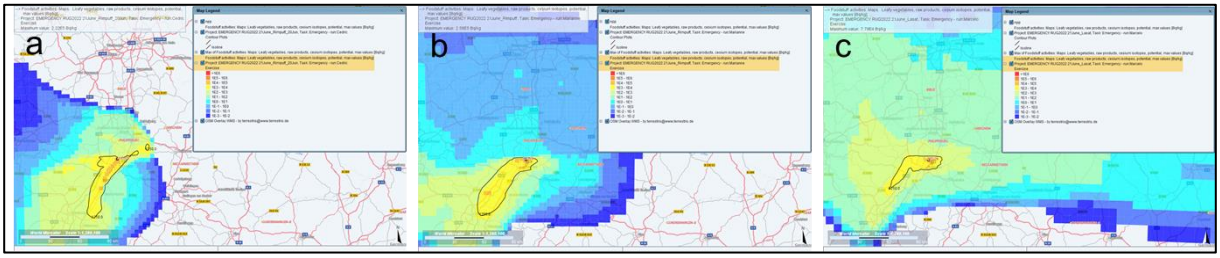

Fig. 9. Leafy vegetables, max Cs-137 activity a) RIMPUFF with weather data downloaded 20.06.2021, b) RIMPUFF with weather data downloaded 21.06.2021, c) LASAT with weather data downloaded 21.06.2021

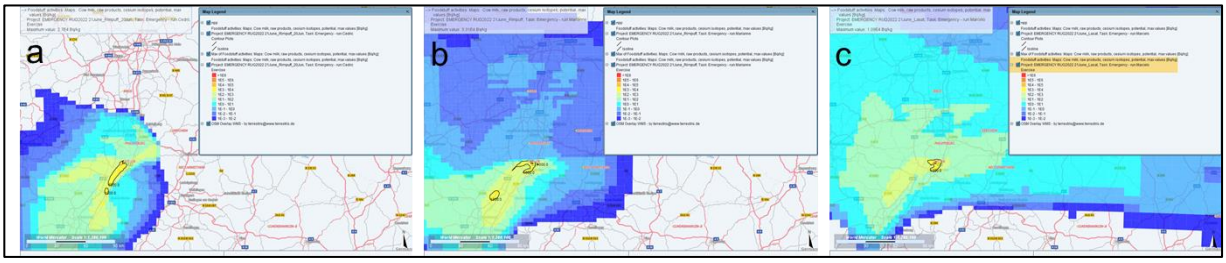

Fig. 10. Cow milk, max Cs-137 activity a) RIMPUFF with weather data downloaded 20.06.2021, b) RIMPUFF with weather data downloaded 21.06.2021, c) LASAT with weather data downloaded 21.06.2021

Table 2. Maximum distance where WHO/FAO level for activity concentration in leafy vegetable and cow's milk is exceeded.

Maximum Distance where levels are exceeded	RIMPUFF with weather data downloaded 20.06.2021	RIMPUFF with weather data downloaded 21.06.2021	LASAT with weather data downloaded 21.06.2021
Leafy vegetables, max Cs-137 activity above 1250 Bq/kg	67 km	71 km	50 km
Cow milk, max Cs-137 activity above 1000 Bq/kg	37 km	53 km	10 km

As shown in figure 9 and 10 the contour is drawn around areas in which WHO/FAO criteria is exceeded, however, for administrative purposes usually maximum distance is reported. So, in this case authorities shall ban or limit production and consumption of leavy and cow's milk distances stated in table 2.

Which GDR measurement stations in the region should report elevated radioactivity according to the model runs? Make a list of up to ten of these stations. A shapefile with the German GDR Stations was provided with the exercise material and can be used for visualization.

Table 3. GDR stations that may detect high dose rate

No	RIMPUFF with weather data downloaded 20.06.2021	RIMPUFF with weather data downloaded 21.06.2021	LASAT with weather data downloaded 21.06.2021
1	Z1049	Z3279	Z3279
2	Z2200	Z1049	Z2201
3	Z1059	Z1059	Z1059
4	Z3279	Z2200	Z2196
5	Z2201	Z1046	Z2230
6	Z1046	Z1170	Z1045
7	Z2233	Z2233	hP020
8	Z2235	Z3182	hP022
9	Z2234	Z1249	hP023
10	Z1170	Z1245	hP021

With the aforementioned assumptions we suppose that stations mentioned in table 3 raise alarm messages, however, if that would not the case, the assumptions are not correct or the conditions prevailing (e.g., wind speed) has been changes. So, for better managing the situation we shall update the simulation with the new details.

Propose a list of protective actions for the affected areas and/or for your countries for the early phase (first week) of the accident. An extensive example list of potential actions can be found in chapter 2.8 of CONVEX-3 (2013) [1].

Considering above information one can propose following protective actions:

Informing the public and relevant authorities.

Monitoring and if necessary, banning of foodstuff in the contaminated area.

Contamination and dose measurements for steel mill staff.

Contamination measurement of steel mill products, waste and equipment.

There are tiny differences between result of each model due to different computational method. So, for robust preparedness and response it is recommended to run multiple models evaluate them with measurement (is possible) and compare the results.

Conclusions

It is crucial to implement suitable measures to reduce human exposure and protect the environment in order to preserve human health following a nuclear incident. Hence, the decision support system was created with the primary objective of aiding decision-makers by offering a wide range of information throughout all phases of a nuclear or radiation emergency. This system needs weather data and multiple layers of information (land use, population, soil type and etc.) and radiological data (transfer of radioactive pollutant between food, agricultural product and animals). Once the scenario is developed, movement of radioactive materials in the air, their deposition on land and water surfaces, within the ecosystem, and ultimately the calculation of potential radiation exposure to individuals can be simulated. After the simulation has done, the system has the capability to assist in selecting appropriate countermeasures and developing suitable decision-making strategies. Usually, JRODOS centers manage periodic runs for NPPs in near range and they are ready to perform modeling for other radiological accident as soon as they declared.

References

[1] AL MAGHRIB, B. A. B. (2014). Exercise Report (ConvEx-3). IAEA, Vienna.
[2] German Commission on Radiological Protection. (2014). Basic Radiological Principles for Decisions on Measures for the Protection of the Population against Incidents involving Releases of Radionuclides. Retrieved May 5,2018, from https://www.ssk.de/SharedDocs/Beratungsergebnisse_PDF/2014/RadiologischeGrundlagen_e.html
[3] ICRP Publication 103. (2007). The 2007 recommendations of the International Commission on Radiological Protection, Ann. ICRP 37, Elsevier.
[4] Landman, C. Raskob, W. Trybushnyi, D. and Ievdin, I. (2016). An application example for the new ICRP screening tool of JRodos. Radioprotection, 51(HS1): S17-S22.
[5] Möhrle, S. (2020). Case-Based Decision Support for Disaster Management. KIT Scientific Publishing (p. 322).
[6] Pirouzmand, A. Kowsar, Z. and Dehghani, P. (2018). Atmospheric dispersion assessment of radioactive materials during severe accident conditions for Bushehr nuclear power plant using HYSPLIT code. Progress in Nuclear Energy, 108:169-178.
[7] Trybushnyi, D. (2024). Practical demonstration on JRODOS use in Germany, workshop Workshop on the role of JRODOS for supporting decision making process in a nuclear emergency. Yerevan, Armenia.

Cyber security in peaceful nuclear facilities (Paper ID: 1174)

Samaneh.T. Correspondent[1*], Recabian ,R. Co-Author[2]Saeedi, S. Co-Author[3]
[1]Doctoral student of Allameh Tabatabai, Tehran-Iran
[2]Associate Professor of Ayat Azami University of Borujerdi, Borujerd-Iran
[3]Master's degree at Ayat Azami University of Borujerdi, Borujerd, Iran

Abstract

Cybersecurity is very important in peaceful nuclear installations. Maintaining cybersecurity at these facilities is necessary due to their sensitive and high-risk nature and involves taking action to protect information, network and data against internal or external threats. Cybersecurity communication, due to the nature of cyberspace is very difficult to operate, cyber technology can undoubtedly be used, as with conventional warfare tools, to attack government organizations, financial institutions, national energy and transportation infrastructure, cybersecurity, not only involves insecurity in information systems, but also includes all infrastructure that is somehow related to information technology. Therefore, the present research with the aim of reviewing cybersecurity in peaceful nuclear installations is accepted and attempts to answer this fundamental question of how to investigate and analyze the place of cybersecurity in peaceful nuclear installations? This paper uses a descriptive and analytical approach to the hypothesis that"supply chain vulnerability means that equipment deployed in nuclear facilities is at risk at any stage, and that the nuclear industry, regulatory groups, security agencies, governments, and international organizations must work with cybersecurity experts to develop resolute policy responses through coordinated action to address the technical, managerial, and cultural weaknesses identified in this report on a cooperative basis."

Keywords: Cybersecurity, Peace Facilities, Nuclear Facilities, Cyber Space

Introduction

One of the most volatile environments dominating today's activities is cyberspace and cyberspace; cyber space security, followed by cyberspace, is subject to constant change, and due to the fact that maintaining security in this space is an important issue in the national security of the country, as well as the lack of synergies of cybersecurity research institutions in Iran, the use of a model for the governance of this space in order to make appropriate use of all capacities is an appropriate solution for governance. Cybersecurity is not the same as data protection but more about privacy and how we use data. Placing iron bars in a window provides greater security, but does nothing to protect privacy, while placing a curtain has the opposite effect. Cybersecurity is not the same as data backup, which falls under the scope of business continuity. Having a good backup and recovery plan in place is vital

after any scenario as it can result in data loss or compromise. Nuclear power is a reliable, low-carbon energy source and canbe dramatically harnessed. The industry can optimize complex procedures by combining digital simulations of real nuclear installations with AI systems, and improve the design, performance and safety of the reactor. This optimization increases operational efficiency and reducesmaintenance costs. Nuclear energy is also an emerging science in human life, but thanks to the enormous capabilities of this technology in the short term, it has been able to penetrate into various spheres of human life and play a huge role in the industrial, medical and agricultural dimensions. If we categorize activities related to the field of nuclear energy, one part of it relates to the applications that lead to the generation of electricity. For example, the area of the nuclear fuel cycle, from the exploration to the fuel production stage, and finally, the nuclear reactors that generate electricity, if we leave this area, the second part is the non-electric part, activities that are related to the areas of agriculture, environment, health and food and other related topics, called peaceful nuclear facilities, are also the petrochemical and polymer industry, and such are the equipment broadcasting systems that are used for these applications, for example, in the field of agriculture and food, filling this food that reduces waste.

All these nuclear activities are peaceful and for civilian purposes. Therefore, it must be said that cybersecurity can contribute in various ways to nuclear security and safety. The detection and detection of nuclear and other radioactive materials can be improved by using it in the data processing process of radiation detection systems. It can also be used to analyze data from physical protection systems to improve intrusion detection. While cybersecurity can help identify anomalies that indicate a cyber attack onnuclear facilities. It should be noted that given the sensitivity inherent in the nature of peaceful activities, the adoption of new strategies in the structural, software and hardware dimensions to fully ensure security in nuclear installations should be on the agenda of the IAEA officials. One of these strategies concerns cybersecurity in peaceful nuclear installations, which is the subject of current research, and seeks answers to the question of how to investigate and analyze the place of cybersecurity in peaceful nuclear installations?

Theoretical Foundations

Concepts

A.Cyber Security: The simplest definition of "cyber security" is through comparing and contrasting information security. While information security protects your information from any unauthorized

access, cybersecurity protects it from unauthorized online access. This definition was simple, but for a more formal and comprehensive alternative: cybersecurity is a set of tools, policies, security concepts, guidelines, risk management approaches of actions, training, best practices, assurance, and technologies that can be used to protect the cyber environment and user organizations and assets (Nuclear Regulatory Commission, 2010).

B. Nuclear safety: Nuclear security means preventing, detecting, and responding to theft, vandalism, unauthorized access, illegal transfer, or other hostile actions involving nuclear material, other radioactive material, or their affiliated entities. Safety and security are both imperative, which means that there is a two-way relationship between them and they are interdependent. Essentially, nuclearsafety and security are both at the service of goals that overlap, differentiate, and conflict dramatically between the two. Defence, for example, is an important structural principle for safety and security that depends on the use of several independent dams and barriers; although security considerations challenge the efficiency and independence of safety barriers. Overall, nuclearsafety and security both serve goals that overlap, including protecting workers, the public, and the environment from unintentional releases of radioactive material. In addition, security equipment includes controlling access to nuclear facilities and other facilities to prevent damage to or the removal, seizure, transfer and unauthorized use of radioactive materials; safeguarding sensitive information and cybersecurity; accountability and control of materials (Paraghdam,2009:49).

C. Peaceful Nuclear Facilities: Peaceful nuclear installations shall mean the use of nuclear technology to meet industrial, scientific, medical and energy needs in compliance with international obligations and shall have the appropriate care and supervision to prevent the misuse or violation of international law in the area of non-proliferation of nuclear weapons. The Peace Facility is a priority on the implementation of the Far Eastern Partnership (Bertrand,G.1981:66).

Theoretical Framework

From a realistic point of view, every international unit wants its own security and survival and is always fearless of destruction. In such a space, war is not only possible but also quite likely and even common. In their view, states are made up of a community of power-loving, plentiful, and anxious human beings from the threat of death, and the international scene is a roundabout of opposing governments that seek to gain, maintain, and increase credibility in order to secure and sustain themselves permanently, and that, like humans whose social impulses are facilitated, governments will seek violence on their own

and otherwise, by coalitioning with each other against any government or other factor that prevents them from achieving their goals. The link between the two factors of power and fear is one of the most important issues that these thinkers raise, and it is from the link between the two that the balancing behaviour takes on meaning and significance as the most natural reaction of the actors in international politics (Little,13:1389). Introducing his theory of nuclear deterrence in 1981, Kenneth Waltz stated that the fear of nuclear weapon failure was the most enduring feature of the international system and therefore there was no reason to worry about the proliferation of these weapons in the international system. One of the reasons for the increasing importance of deterrence in Waltz theory is its strong reliance on the “balance of power” as the conventional method and the governing rule in shaping the international order; because for him deterrence is a form of distribution of power among states resulting from their efforts to survive, survive and achieve security (Zagre,2004,29).

In his theory, Waltz states that, in principle, a state that acquires nuclear weapons acts more cautiously than a state that does not (Wheeler, 2009:432). the result of this theory is that the possibility of war among nuclear-weapon states reaches zero, and this is because heads of states with nuclear capabilities, regardless of their personal and military character, have fully acted as rational actors and, to the extent possible, refrained from creating nuclear war. The option of nuclearization of states due to the reduction of the occurrence of war in the international system is regarded as one of the surest ways of maintaining the status quo in this system (Waltz,2000,5). because the logic of deterrence works in any case and prevents countries that have these years from using it from endangering "nuclear peace"(Walts and Sagan,1995,34).

Thus, in accordance with the Waltz deterrence theory, deterrence by inducing a threat to the other party to inflict the initial blow and cause the second blow brings peace and stability in the international anarchic system and prevents war and conflict between governments. Therefore, this topic of cybersecurity in peaceful nuclear installations can also act as a deterrent.

Findings

Cybersecurity as a Process

It is better not to think that “cyber security” is not a solution, a technology and nothing more. Yes, it includes tools and technologies used in the daily struggle to maintain compliance and information integrity; however, cybersecurity is the business process. This means that managers' attention is directed to the required level and understanding that, like any other business process, it can adapt to

the needs of the business and react to changes in the threat. Enterprise cybersecurity capabilities must align not only with your risk appetite, but also with wider business strategic goals. Cybersecurity is not only a business process, but a strategic business priority. If it is not, then it is likely not to be taken seriously at C-level and instead as something that can and should be fully transferred to IT. One of the things that cybersecurity refers to is an SSL certificate. An SSL certificate actually encrypts information that is not heard or hacked between the server and the user (cybersecurity.html,2019).

Cybersecurity must be understood within the context of the organization in which you are based. Everyone must do something to ensure that businesses are protected from threats that can be dangerous. But the threat landscape is constantly changing and so it can be hard to know what to do and how to protect an organization. Cybersecurity is a very broad topic that can be greatly simplified, only when your organization understands the meaning of cybersecurity can you begin to plan a strategy. Cybersecurity involves a series of protocols that a company or an individual follows to ensure information from their ICA. ICA stands for Integrity, Confidentiality, and Availability, and if you have proper security, you can recover hard power, errors, or malfunctions very quickly in certain situations, as these types of incidents make your efficiency more vulnerable to external intrusion and hackers. Cybersecurity is an important component of the company's infrastructure. Success in a company's ability to protect proprietary information and customer data from people who abuse it. Business continuity and disaster recovery concepts are fundamental cybersecurity strategies. Business continuity is essential to the survival of a business. Quick Recovery of Threats means you can keep your audience in problematic situations. Disaster recovery means preserving the integrity of your data and infrastructure after a catastrophic event. These threats are ultimately categorized by the level of cybersecurity currently implemented in your digital infrastructure (www.reblaze/product).

The Importance of Cybersecurity

Why should security be at the top of every company's agenda? Why should senior management concern itself with cybersecurity? There is an undeniable reason: the digital world in which we do business is vulnerable and vulnerable to cyberattacks. Secure, which to set up and control the global network still has to go through a transition before it becomes a fully self-programmed ecosystem. Decision makers must ensure that all of their company's systems adhere to the latest standards with proper security. Employees should also be trained in basic cybersecurity protocols. This is especially the case for non-tech workers. For example, everyone should know how to accept a phishing email and how to avoid it. Without a proper security strategy, irreparable events may occur. Attackers know how to find and

exploit weaknesses, opening gaps that cause powerful systems to fall apart (Deibert and Rohozinski,2010).

Cybersecurity Challenges

The best cybersecurity strategies go beyond the principles outlined in Baal. Any advanced hacker can get through this simple defense. As a company expands, cybersecurity also becomes more difficult. For example, a Fortune 1000 company's “attack surface” is much larger than a small and medium-sized business.

A. Stuxnet and its nature as a cyber weapon: Staxnet is a very large and complex threat whose primary purpose is an industrial control system (ICS)or a set of similar systems. Its ultimate goal is also to reprogram the ICS through code modifications on the PLC to work in a way that the attacker has in mind while hiding any changes from the equipment operator. To increase their success in achieving this goal, the creators compiled a vast collection of components, including zero-day extensions, Windows rootkit, the first PLC rootkit, antivirus escape techniques, injecting code into running programs, buckling codes, network infection routines, peer-to-peer (P2P) updates, and a command-and-control interface (Bahramzadeh and Adeli,2023:7).

B. The possibility of carrying malware like StaxNet: After the StaxNet attack, which has been unparalleled in its time in terms of complexity, other armed rogue software has been created, such as Dooku, Flame, Gauss, and Simon. These attacks can be different types of StaxNet or inspired by them, and their design aims to steal information and destroy industrial control systems. I would like to point out that the StaxNet source code was posted on the web shortly after it was first identified, and as a result the likelihood of malware attacks inspired by StaxNet has increased considerably. In other words, hackers can simply use proprietary components and technologies that are available online in their attacks; while reverse engineering of the binary execution file can also restore the structures and core components of the standalone code. Numerous analytical reports have been submitted about StaxNet, which can be used as a reference for the publication and modification of StaxNet. With these points in mind, it can be concluded that StaxNet is indeed representative of the next generation of cyberattacks (Dunn, Cavelt. 2008). Mutual action against cyber threats The progress of industrial unit data networks (PDNs) used in nuclear power plants demonstrates the potential for cyber threats, which are exacerbated in IT environments, however, PDNs improve the efficiency and reliability of protection, control and monitoring systems and enhance overall plant efficiency. A reciprocal action that can be taken to protect the security system against malicious cyber threats is to create a security policy within

which factory staff can define plans for network access security and its operations by identifying six critical network segments. It is necessary to note that network monitoring requires aspects of anomalous and innovative analysis with network traffic and deployment of IPS / IDS firewalls and security tools in the network environment. The PLC is the most common hardware tool for implementing a rigorous control system and instrumentation in the NPP. Among the security methods available to prevent malicious programs from replicating within the PLC, the following can be noted: Ensure that the Flash update plan requires an authentication system. Provide appropriate access control to protect hardware images during storage by preventing remote updates and disabling removable media such as tamp drives. Eslmer and StaxNet are types of worm viruses that attack the nuclear C&I system, but the target of the Doku, Flame, Gauss, and Cimon viruses is to attack the ICS industrial control system. Digital Code Signing Certificate, which is the main tool to protect a computer system from malware, is actually the process of creating an encrypted digital signature. Creating restrictions for software is another way of protecting the system against malware (Cyberspace Policy Review:2012).

C.Create attacking opportunities for hackers: Another cybersecurity challenge is tackling the increasing overlap between the physical and virtual worlds of information exchange. The more common driverless cars and other self-regulated devices are, the Internet of Things (IoT)and BYOD's business policies give criminals greater access to cyber-physical systems. This includes cars, factories, smart refrigerators and toasters in your kitchen, even for a medical pacemaker. In the future, penetration into one of these systems may mean penetration into all of them (https://www.reblaze.com).

D.Complex Locations: An important challenge in cybersecurity is the lack of qualified professionals to do the job. Many people are at the bottom of the spectrum of cybersecurity with general skills. Security experts who know how to protect companies from advanced hackers are rare. Those who know how to do things know how important it is. Only the largest and richest companies in the world can afford this special level of service, which is another barrier SMBs must overcome to compete online(Bahramzadeh & Adeli,9:2023).

DataProtection and Critical Infrastructure Assurance Function

All technologies have disadvantages and advantages. Digital technologies are transforming how people communicate with each other, how machines are used, and how machinesconnect with each other. Huge amounts of data are being circulated and [then] stored; our world is increasingly reliant on the Internet and digitalizationto sustain life. The vulnerability caused by stealing this information has

become one of the biggest weaknesses of financial and business transactions. Data protection and critical infrastructure assurance functions – such as energy sources, food and water, transport and communications – depend on the safe operation and assurance of digital technologies. Individuals' personal affairs, for example, background information and health insurance, continue to be severely undermined. The report also focuses on such situations in the context of a much more dangerous category of cyberattack – when industrial monitoring systems of an establishment are disrupted or even come under the control or aggression of intruders inside or outside the same establishments where such systems are located (The UK Cyber Security Strategy:2012).

Nuclear Safety and Security

Reducing the risks and incidents arising from nuclear proliferation has been achieved by adhering to the safety tips established by the International Energy Agency. Reducing the likelihood of exposure to hazardous pollutants is a product of compliance with international conventions on the prohibition of the transport and illegal distribution of hazardous cross-border pollutants. In this regard, reference can be made to the Basel Convention on the Control of Transboundary Movements of Hazardous Pollutants and their Distribution, the Convention with Macao on the Prohibition of Exports to Africa and on the Control of Transboundary Movements and on the Management of Hazardous Pollutants in Africa.

Protection against damage caused by nuclear accidents and radioactive emergencies is due to the coordination of international assistance in nuclear accidents or radioactive emergencies. In this regard, reference may be made to the Convention on Assistance in Nuclear Accidents or Radioactive Emergency Situations, the Convention on the Timely Notification of Nuclear Accidents, the NuclearSafety Convention and the Statute of the International Atomic Energy Agency. There are two indicators on the clear international law crisis; first; the area of cybersecurity is resistant to the development of laws implemented under a binding comprehensive multilateral treaty; second; countries have shown reluctance to do more to participate in the development of customary international cyber law. Also, countries' activity in this area has necessarily been on the shelf, and countries were reluctant to comment on nuclearsecurity laws (Nuclear Regulatory Commission, 2016). In some cases, this approach is certainly understandable and canbe the result of an internal political stalemate or even an intentional waiting strategy. Finally, this point addsto the pervasive ambiguity insofar as concerns are raised about the applicability of international law. This trend is evident even in the most recent developments. An example of the loss of opportunity to guide the development of cyber

mystics is provided by the new US law adopted in July 2015 on the law of war. However, the regulation contains a chapter on cyber operations, but it goes through all the nonsensical dilemmas including document standards, targeting rules, and cyber weapons review requirements. While the first two indicators are linked to the billions of countries creating new laws, the third one shows their actual behavior in relation to cyber governance.

Technologies not immune to incidents, errors, and common malfunctions

Nuclear energy has been viewed at different periods from different angles – both as a blessing and a tragedy. Concerns about health risks from radiation ionization have meant that the nuclear industry has put in place a wide range of security and safety expectations to prevent the catastrophic spread of radiation and to respond quickly and effectively to possible incidents of such incidents. However, no technology is safe from accidents, errors, or common malfunctions. The nuclear disaster at the [Fukushima Daiichi nuclear power plant] in 2011 following the "Great Earthquake and Tsunami of Tohoku" is a new example of what can happen when protocols and preventive upgrades are not implemented, and – or perhaps more importantly – when the [conditions] are unlikely to change and the planning task for the [confrontation] is severely disastrously neglected (Cortada, James ,2003).

Dangerous Consequences of Disrupting the Physical Activity of a Nuclear Power Plant

However, the role of nuclear power generation in many countries' energy ministries remains dramatic and is expanding in some areas. Vulnerability of critical infrastructure has been the subject of some research in recent years, but given Staxnet's digital virus revelations and the impact this virus appears to have had on the performance of Iran's nuclear program equipment, many experts have expressed concern that making similar efforts to disrupt the physical activity of a nuclear power plant may pose a serious risk. Admittedly, as this report notes, a number of incidents involving cyber interference in nuclear power plants have been reported – assuming that the nuclear industry operates in similar ways to other industries – we must assume that these examples are part of a much more serious problem (Rashidi,2011).

Scope of potential risks related to cybersecurity and nuclearsecurity intersections

Following these concerns, the Division of International Security of the Royal Chatham House – with the support of the “John Day Foundation. and Catherine. McArthur” – explored the scope of potential

risks related to cybersecurity and nuclear security intersections. The project oversight group consisted of expert experts in the areas of cybersecurity and nuclearsecurity. Caroline Bailon, a Research Associate in Science, Technology and Cyber Security at the Indexed Chatham House, led the research and analysis of the project – including conducting interviews with 30 industry experts. As well as Roger Brant and David Livingstone, both members of the Monitoring Group provided their extensive industrial expertise to the project and provided valuable input to [its] writing and analysis. This research showed that the nuclear industry is beginning to grapple with this new and insidious threat. The cyber threat against nuclear installations in particular due to the increasing reliance of the nuclear industry on digital systems, as well as the steady increase in cybercriminal activity, requires a sustained assessment and response (https://thehackernews.com/2019)

Countering the Cyber Threat Against Peaceful Nuclear Energy

Our goal is that the findings of this research and the recommendations made in this report to counter the cyber threat against peaceful nuclear energy should be considered in a spirit of cooperation and collaboration. The NuclearSecurity Summit process – with a view to the forthcoming summit in 2016 – and the role of the IAEA in addressing nuclearsafety and security in a coordinated way are mechanisms to ensure that this issue will receive greater attention. Nuclear industry, monitoring groups, securityagencies, governments, and international organizations should work with cybersecurity experts to develop decisive policy responses through coordinated action to address the technical, managerial, and cultural deficiencies identified in this report on a solid basis (https://www.reblaze.com).

The general belief that all nuclear facilities are separate and distinct from the Internet is a myth.The commercial benefits of internet connectivity mean that his communications are now. footstep.It Installed in some nuclear facilities where facility operators are sometimes unaware of [this issue].

– Search engines caneasily identify critical infrastructure components through such connections.

– This protection measure, even in well-equipped facilities, may be violated by a flash drive.

– Supply chain vulnerability means that equipment deployed in nuclear facilities is at risk atany stage.

– Lack of training alongside a disconnection between engineers and security personnel means that nuclear power plant employees are often not aware of key cybersecurity guidelines. [Adoption] A reactionary approach rather than a passive approach to [cybersecurity] helps to ensure that nuclear facilities may not be aware of a cyber attack until it is executed. The RFE/RL report draws broad lines

of the mix of policies and technical expectations that will be needed to address the threats and address the challenges of RFE/RL. Finally, as this research notes, many of the findings of this research canbe generalized toother industries and sectors. The wider critical infrastructure around the corner from communities – including power grids, transport networks, maritime transport and space-driven communication capital – is equally vulnerable to cyberattacks to varying degrees, but with potentially severe consequences. We hope that this research will benefit those responsible for the safety and security of this critical infrastructure and help build a culture of pragmatic negotiation between industry and cyber professionals for the benefit of all.

Conclusions

Finally, it should be said that shadow attacks on serious designers based on malicious software programs related to StaxNet are also smarter, stronger , more aggressive and more resilient. Therefore, it is not likely that I and the security of the CI&C nuclear power plants will be compromised by StaxNet-inspired shadow attacks, which may cause the reactor to shut down for dangerous incidents. Therefore, it must be said that peaceful nuclear facilities such as power plants and facilities linking organizations and houses have critical infrastructure. According to a recent study, cyber attacks targeting energy facilities and power plants in the United States rank third. Suburbs Europe, Australia and Japan have also reported increased threats to their critical infrastructure. All this shows that cyber threats against power plants and installations are global.This type of threat is exacerbated by the modernization of OT networks that control critical infrastructure. Previously, OT systems were far from internet space due to cybersecurity, which has been eroded by the convergence ofot and IT networks. The risk of a successful cyber attack on peaceful nuclear installations may be very high. For example, electric powertrains may be completely deactivated and the city may be left in absolute darkness, or even the lives of people at risk. And the good news is that senior executives at power plants and facilities are not dealing with cyberattacks on infrastructure and damage. A recent survey shows that 48% of senior executives believe that cyberattacks are imminent. Despite the lack of skilled labor and resources, 59% of senior managers of power plants and nuclear facilities consider cybersecurity professionals to be the most important role in their organization. The solutions that Fortnite provides for power plants and facilities support their technical team by providing integrated and automated protection in the evolving IT and OT environments. In this regard, implementing cybersecurity control measures such as placing HIDS in place of Hazardous Influence Syndrome

(HIDS)and using IDPS to deter infiltration (IDPS) with automated tools to back up nearby Anali Zaha in real time can be a good way to counter cyber-attacks against MFIS.

Suggestions for this research are as follows:

Guidelines should be developed for cybersecurity risk assessment in the nuclear industry, including a comprehensive risk assessment that takes into account security and safety expectations.

There should be a robust dialogue with engineers and contractors in orderto increase publicity about cybersecurity risk, including the risks of unauthorized internet communications.

Rules should be in place where they are not already in place to develop care. tea. Appropriate nuclear facilities (for example, toprohibit the use of personal instruments) come into force and laws are strengthened where they do not exist.

Disclosure should be improved by promoting sharing of information anonymously and establishing a 'Computer Rapid Response Task Force (CERTs)'.

The global adoption of regulatory standards should be promoted

References

[1] Baramzadeh, A and Adli, B. (2023). Tsai Tsai's safety studyonthe tightening of nuclear deterrents,the third National Conference on Cyber Defence.

[2] Bertrand, G. (1981) “Nuclear Non -Proliferation and Safeguards,” A

Conference Report, The Atlantic Institute for International Affairs, The American Nuclear Society, p.66.

[3] Cortada,W.(2003). The Digital Hand: How Computers Changed the Work of American Manufacturing, Transportation, and Retail Industries. Oxford University Press. 512/0 ISBN 978-0-19-516588-3.

[4] Deibert, R. and Rohozinski, R. (2010) ‘Risking Security: Policies and Paradoxes of Cyberspace Security’, International Political Sociology 4/1: 15–32. An intelligent account of the threat discourse that differentiates between risks to cyberspace and risks through cyberspace.

[5] Dunn Cavelty, M. (2008), Cyber Security and Threat Politics: US Efforts to Secure the Information Age, London: Routledge. Examines how, under what conditions, by whom, for what reasons, and with what impact cyber threats have been moved on to the political agenda in the United States.

[6] Little, R (2011). Transformation in equilibrium theories of force, Translation of Ghulam Ali Chagini Zadeh, Tehran:Institute of Contemporary Abhar.

[7] Nuclear Regulatory Commission, 2010. Regulation Guide 5.71: Cyber security programs for nuclear facilities. Nuclear Regulatory Commission, 2012.

[8] Nuclear Regulatory Commission, 2016. NRC Information Notice 2016-15: Effects of ethernet-based, non-Safety Related Controls on the Safe and Continued Operation of Nuclear Power Stations.

[9] Poreghdam,,M (2009),“ Comparison of the implementation of the process of nuclear disarmament in Rwanda,India and Pakistan ”, is the chapter paper.

[10] Rashidi, Amir(1399). What is a cyber attack?, BBC Persian Internet Access researcher.

[11] Wheeler, N (2009), “Beyond Waltz Nuclear World: More Trust May Be Better”, European Journal of International Relation, Vol.No.3, pp. 428-445.5.

[12] Waltz, K (2000), "Structural Realism after the Cold War," International Security, Vol. 25, No.1, pp. 5.41.

[13] Waltz, K and S, Sagan (1995), The Spread of Nuclear Weapons, A Debate. New York and London: Norton.

[14] Zagre, T. V. (2004), The Enduring Axioms of Balance of Power Theory, Stanford University Press.

[15] https://thehackernews.com/2019/12/web-application-cybersecurity.html.

[16] https://www.reblaze.com/product/ddos

[17] https://thehackernews.com/2019/12/web-application-cybersecurity.html

[18] https://www.reblaze.com

[19] https://www.reblaze.com.

ICNST 2024 International Conference on Nuclear Science and Technology
6- 8 MAY 2024 | Isfahan, Iran

Experimental and Monte Carlo Simulation Study of Diagnostic X-ray Shielding Performance by Micro- and Nano-PbO (Paper ID: 1272)

Nadia AsariShik [1*] and Payman Rafiepour [2]
[1] *Faculty of Physics, Yazd University, Yazd, Iran*
[2] *Department of Nuclear Engineering, School of Mechanical Engineering, Shiraz University, Shiraz, Iran*

Abstract

Diagnostic application is the main use of X-rays in medicine. According to known hazards of direct contact with X-rays as ionizing radiation, shielding against it is the most effective safety management method. The combination of nanoscience and radiation shielding is creating a new eyesight in radiation protection researchs. On the other hand, theoretical and simulation investigations assist experimental studies for validation of the results. In this study, the Geant4 Monte Carlo toolkit is used to investigate the diagnostic X-ray shielding properties besides the experimental work. Micro-PbO particles were purchased and nano-PbO particles were synthesized and the samples were prepared to be irradiated by kilovoltage X-rays of 40, 60, 80, and 100 keV cut-off energies. Comparing different parameters such as attenuation coefficient, half-value layer and attenuation percent in experimental and simulation sections showed that there is not a significant difference between shielding properties of nano- and micro-PbO particles for experimental investigations. The simulation and experimental results showed a greater agreement with each other in higher tube voltages. Generally, it could be said that the Geant4 Monte Carlo toolkit has an excellent performance for micro- and nano-scale shielding simulations.

Keywords: Diagnostic X-ray, Shielding, Simulation, Geant4, Nano-particle, Lead (II) Oxide.

Introduction:

The most practical parts of electromagnetic radiation in the field of medicine are ionizing radiation, focusing on X-rays for diagnostic applications. In that case, over 3 billion diagnostic exposures were reported in 2010 by the United Nations [1] which is increasing continuously. X-ray is an ionization radiation, so it can damage living tissues, cells, and even DNA structure as the most critical biological target of radiation. It is known that genetic information is saved and transferred by DNA, thus its malformation will cause genetic mutation or cancer [2,3]. Different safety managements were being established to reduce such damages: reduction of exposure time, increasing source-target distance, and

shielding. Among the above-mentioned methods, the most effective one was attention to the shielding performance [4]. According to physical concepts, high atomic number (Z) elements have a higher K-absorption edge and could be more effective for diagnostic X-ray shielding [5]. Different properties of lead (Pb, Z=28) such as flexibility, relative-low melting point (~330 ℃), abundance, and low cost, boosted choosing lead as the best choice of shielding for prolonged periods [5,6]. Several researches and applications of lead shielding have been published [5,7]. The discovery of nanotechnology affects different fields of science. The radiation protection field was also affected by the nanoscience revolution, leading numerous nano-material shielding researches [8-10] and investigations against ionizing radiation [11-13]. Most of these researches confirmed higher attenuation results by using nanomaterials [11,12].

Moreover, simulation and experimental studies are complementary to each other. Thus, simulation plays a main role in scientific research. The Monte Carlo N-Particle (MCNP) code and the Geant4 simulation toolkit are two examples of this purpose [14]. The Geant4 toolkit can simulate particle transport at nano- and micro-scales. Thus, It is used for simulation investigations in this study.

Materials and Methods

Experimental

Nano-PbO was prepared by a chemical method [15], and microparticles of PbO were purchased from Merck, USA. Morphological characteristic tests of nano- and micro-particles were obtained from scanning electron microscope (SEM) images and X-ray diffraction (XRD) spectra which showed below 10 µm and 70 nm particles of micro-PbO and nano-PbO, respectively. Figures1 and 2 show SEM pictures and XRD spectra, respectively[16].

Fig1. SEM of PbO (a) Micro-PbO and (b) Nano-PbO.

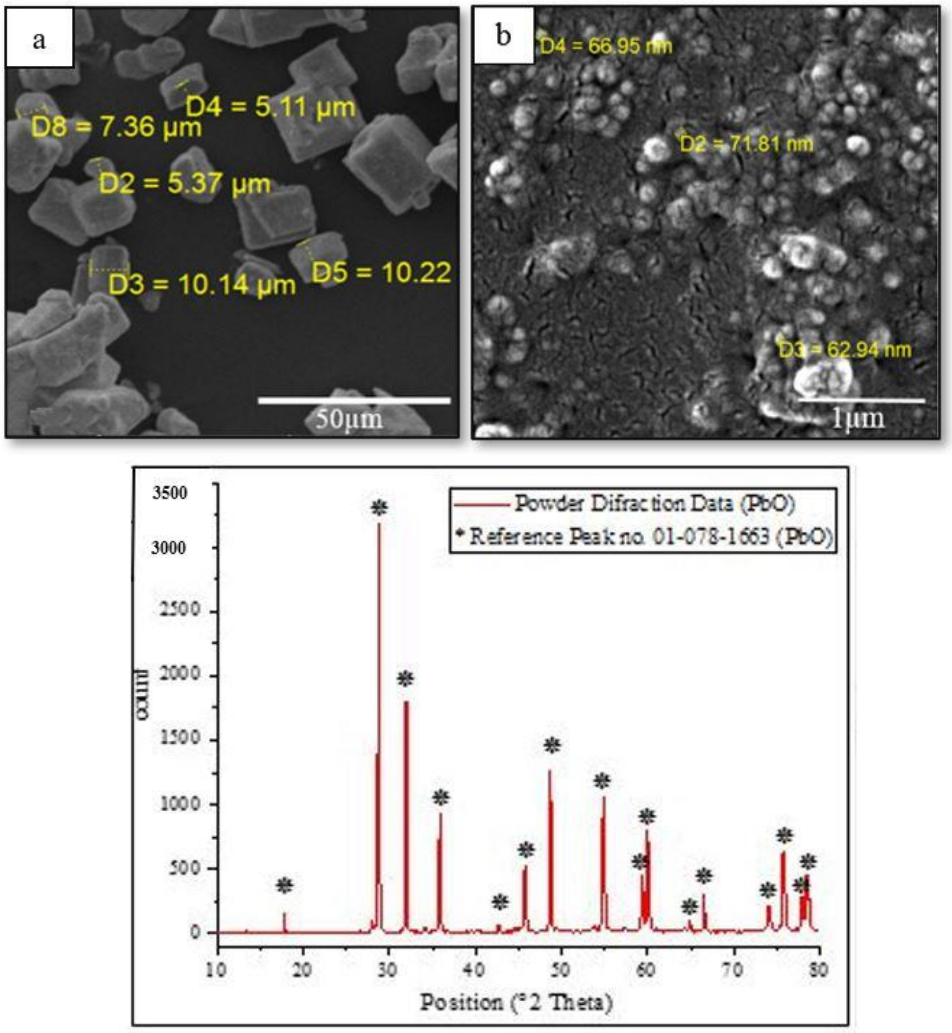

Fig2. XRD spectra of nano-PbO.

Matrix embedding consisted of 40 weight percentages (wt.%) of Polyvinyl Chloride (PVC, Arvand Petrochemical Co., Iran) and 40 wt.% di-sec octyl phthalate oil (DOP oil, Jahan Granule Co., Iran) which 20 wt.% of prepared nano- or micro-particles was added into the matrix to obtain shielding sheets with a thickness of ~1 mm. Experimental exposures were applied by an X-ray tube (Varian, USA) at four kilovoltages, i.e. 40, 60, 80, and 100 cut-off energies and 10 mAs, using a 3-mm Aluminum filter for eliminating low-energy photons of X-ray. Dosimetry was recorded by a calibrated Piranha detector (Sweden), and the Ocean software [16]. Figure 3 shows the exposure setup.

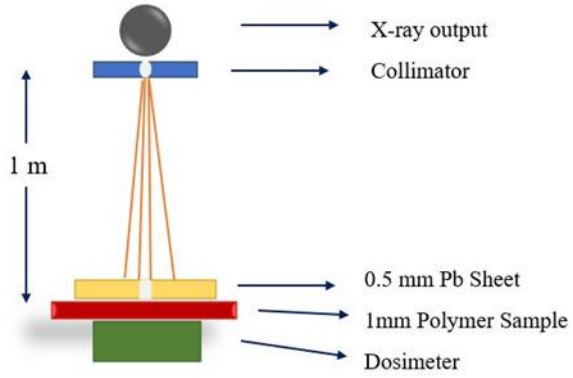

Fig3. Exposure setup.

Simulation

The simulation study was performed by the Geant4 Monte Carlo toolkit [17]. To converge the experimental and simulation conditions, the main parameters of the experimental section such as PbO particle size, the density of the samples, matrix embedding wt.%, and source-to-sample distance were determined in the simulation. PbO micro- and nano-particles were defined as a simple sphere, as the filler, inside a cube of the matrix (Fig. 4-a). The radius of the sphere and the side of the cube are varying depending on the desired concentration. Equation 1 is used to define the concentration of PbO fillers in terms of wt.% of the matrix:

$$Con.(wt.\%) = \frac{\rho_f \times V_f}{\rho_m \times V_m} \times 100 \qquad (1)$$

in which ρ and V are density and volume, respectively (for both filler (*f*) and matrix (*m*)). By setting the concentration percentage equal to 20%, the volume ratio of the filler to the matrix is obtained, according to equation 1. Finally, the matrix was reproduced in a grid in three directions to complete the sample size of 1 mm. Fig. 4-a shows the sample lattice structure for a small cube with a side of 1 mm and a filler concentration of 20%. Fig. 4-b shows the transport of photons through the sample.

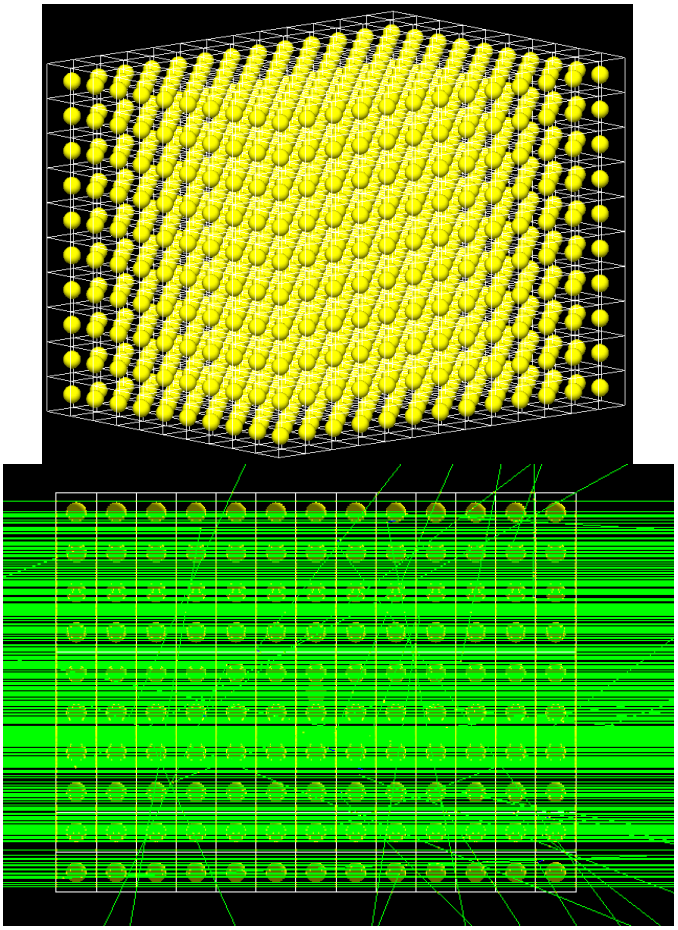

Fig 4. (a) The PbO fillers (yellow spheres) inside the matrix. (b) The transport of photons through the sample.

Theory

According to Lambert-Beer's law, X-ray attenuation depends on different parameters such as initial intensity (I_0), linear attenuation coefficient (μ), and shield thickness (x). Thus, the measured intensity (I) could be obtained by Lambert-Beer's formula [16]:

$$I = I_0 e^{-\mu x} \quad (2)$$

The linear attenuation coefficient is an appropriate parameter to show the shielding capability of a matter, especially for comparing the samples with approximately the same density. Using Archimedes' principle, the density of the samples was determined experimentally which were 1.28 $^{gr}/_{Cm^3}$ and 1.32 $^{gr}/_{Cm^3}$ for nano-PbO and micro-PbO samples, respectively [16]. According to equation 1, the linear attenuation coefficient is calculated by the following equation [16]:

$$\mu\ (cm^{-1}) = -\frac{I}{x}\ Ln(\frac{I}{I_0}) \quad (3)$$

Half-value layer (HVL) is a factor that gives the thickness of a shield to reduce the intensity of radiation by half. According to the equation 2, it could be calculated by:

$$HVL(cm) = \frac{0.693}{\mu} \quad (4)$$

The attenuation percentage (AP) of a sample is calculated by the equation 5:

$$AP(\%) = \frac{D_0 - D}{D_0} * 100 \quad (5)$$

Results and Discussion

Table 1 shows the linear attenuation coefficients of the samples in different kilovoltages cut-off energies.

Table 1. Experimental and simulation linear attenuation coefficient (cm^{-1}) of the samples. *

		40 kV	60 kV	80 kV	100 kV
Experimental	Nano-PbO	14.08	10.02	7.99	6.63
	Micro-PbO	16.17	11.56	9.32	7.68
Simulation	Nano-PbO	11.86	9.26	7.95	7.14
	Micro-PbO	15.99	12.56	10.84	9.83

*The differential uncertainty of the samples in the experimental and simulation sections are below 5%.

Figures 5 and 6 show the HVL values and attenuation percentage of the samples, respectively.

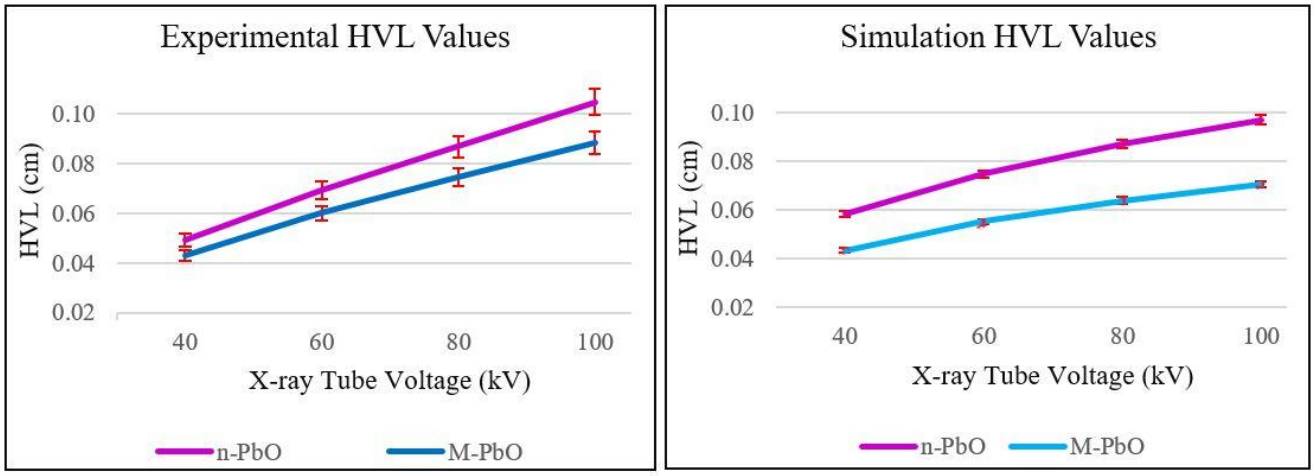

Fig 5. Experimental and simulation HVL values of the samples. Differential uncertainties of the experimental and simulation were 5% and 2%, respectivley.

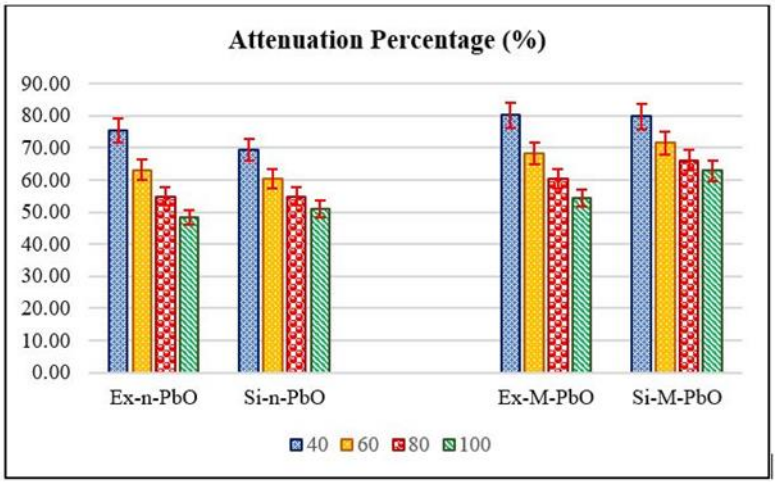

Fig6. Attenuation percentage of the experimental (Ex) and simulation (Si) studies. Maximum differential uncertainty was approximately 5%.

According to Table 1, it is obvious that the attenuation coefficient decreases by increasing the applied voltage which confirms the results obtained in the literature [11, 14, 18]. Also, it is seen that micro-PbO samples have higher attenuation coefficients. It might be related to the particle dispersion in the polymer matrix and needs to be checked in detail.

As seen in Figure 5, the experimental HVL values of the samples containing micro-PbO particles show better results, i.e., less thickness of such samples leads to a 50% reduction in the intensity of X-rays. Although HVL values of simulation shields are 0.04 and 0.06 cm for micro- and nano- PbO samples at 40 kV, respectively, increasing applied voltage, increases the HVL values of the samples in such a way that at 100 kV, HVL becomes 0.07 and 0.10 cm for micro- and nano- PbO samples, respectively. Thus, increasing voltage increases the HVL values. This result is in agreement with the total reports of [15].

Comparing the experimental and simulation sections shows that for nano-PbO samples, HVL has the same values. It could mean that the Geant4 simulation has excellent conformity with the experimental situation. Therefore, this simulation method could be developed for the excess nanoparticle studies. In addition, for micro-PbO, the HVL values of both of the sections are approximately the same.

In the case of AP (Figure 6), it is seen that for low-energy cut-off kilovoltage the experimental section has more AP, however, by increasing the voltage, the AP of the simulation section overtakes from the experimental section. Nevertheless, the relative difference is not statistically significant. Also, by increasing the voltage, the AP of the simulation section decreases smoothly with respect to the experimental section. Totally, it could be said that micro-PbO samples show more AP for both of the sections and different energies.

Conclusion

In this study, the shielding properties of nano- and micro-PbO matrices were investigated and compared in experimental and simulation sections by the Geant4 Monte Carlo simulation toolkit. The same conditions were established for both sections, and different parameters such as attenuation coefficient, half value layer, and attenuation percent were calculated. The results show that although the studied parameters of micro-PbO samples were higher than nano-PbO samples, no significant difference was seen. Furthermore, we show that the Geant4 Monte Carlo toolkit has a very good capability for the simuation of particle transport at micro- and nano-scales.

References

[1] United Nations Scientific Committee on the Effects of Atomic Radiation, (2010), "Sources and effects of ionising radiation". New York: United Nations Publications.

[2] Niu Sh et al. (2022), "Diagnostic and exposure criteria for occupational diseases", International Labour Organization, pp 558-566.

[3] Friedberg E.C. (2003), "DNA damage and repair", Nature, vol 421, pp 436–440.

[4] Storm D. (1996), "Ten Principles and Ten Commandments of Radiation Protection", Health Phys 70(3): 88–93.

[5] McCaffrey JP, Shen H, Downton B, Mainegra-Hing E. (2007), "Radiation attenuation by lead and nonlead materials used in radiation shielding garments", Med Phys, 34, pp 530–7. doi:10.1118/1.2426404.

[6] Storm D. (1996), "Ten Principles and Ten Commandments of Radiation Protection", Health Phys 70(3): 88–93.

[7] M. R. Aghamiri et al. (2011), "A Novel Design for Production of Efficient Flexible Lead-Free Shields against X-ray Photons in Diagnostic Energy Range," J. Biomed. Phys. Eng., vol. 1(1), pp. 17-21.

[8] Kim J. et al.,(2014), "Nano-W dispersed gamma radiation shielding materials", Adv. Eng. Mater. 16 (9).pp 1083–1089.

[9] Thibeault S.A. et al. (2015) "Nanomaterials for radiation shielding", MSR Bulletin, vol. 40, pp 836-841.

[10] Reddy B.C. et al. (2021), "Synthesis and characterization of multi functional nickel ferrite nano-particles for X-ray/gamma radiation shielding, display and antimicrobial applications", Journal of Physics and Chemistry of Solids 159, 110260.

[11] Mesbahi. A. and Ghiasi.H., (2018), "Shielding properties of the ordinary concrete loaded with micro- and nano-particles against neutron and gamma radiations," Applied Radiation and Isotopes 139, pp 27-31.

[12] Nikeghbal K. et al, (2020), "Designing and Fabricating Nano-Structured and Micro-Structured Radiation Shields for Protection against CBCT Exposure". *Materials 13*(19), 4371.

[13] Mesbahi A., Robatjazi M., et al, (2023), "Comparison of MCNPX and EGSnrc Monte Carlo Codes in the Calculation of Nano-Scaled Absorbed Doses and Secondary Electron Spectra around Clinically Relevant Nanoparticles", Frontiers in biomedical technologies, vol 10(3), pp 248-258.

[14] Asadpour N. et al.(2023), "Shielding performance of multi-metal nanoparticle composits for diagnostic radiology: an MCNPX and Geant4 study", Radiological Physics and Technology, Vol 12, pp 57-68.

[15] Mythili N., Arulmozhi K.T., (2015), "Studies on the electrical and dielectric properties of chemically synthesized α-PbO nanoparticles", Appl. Phys. A 118 (1),pp 261–267.

[16] Asari-Shik N., Gholamzadeh L., (2018), "X-ray shielding performance of the EPVC composites with micro- or nanoparticles of WO3, PbO or Bi2O3", Appl. Radiat. Isot. 139, pp 61–65.

[17] Agostinelli, S., Allison, J. et al. (2003). „GEANT4—a simulation toolkit", Nuclear instruments and methods in physics research section A: Accelerators, Spectrometers, Detectors and Associated Equipment, 506(3), pp 250-303.

[18] Al-HadeethiY., Sayyed M.I., Nune M., (2020), "Radiation shielding study of WO3–ZnO–PbO–B2O3 glasses using Geant4 and Phys-X: A comparative study", Ceramics International, 47(3).

ICNST 2024 International Conference on Nuclear Science and Technology
6- 8 MAY 2024 | Isfahan, Iran

An Investigation into the Tensile Properties of Irradiated Shields Based on High-Density Polyethylene Filled with Boron Nitride: Compatibilizer Effect (Paper ID: 1307)

Rafiei-Sarmazdeh. Z[1*], Zahedi-Dizaji, S. M[2], Karimi. M[3]

[1] Nuclear Fuel Cycle School, Nuclear Science and Technology Research Institute, Po. Box: 14399-51113, Tehran, Iran

[2]Plasma and Nuclear Fusion Research School, Nuclear Science and Technology Research Institute, P.O. Box: 14399-51113, Tehran, Iran

[3]Physics and Accelerators Research School, Nuclear Science and Technology Research Institute (NSTRI), Tehran, Iran

Abstract

Maintaining the mechanical properties of the shield is crucial to ensure its effectiveness in protecting against radiation. Effective neutron shields for use in nuclear power plants and space exploration require an understanding of materials' radiation resistance through the analysis of their properties. In this study, the influence of a compatibilizer on the tensile properties of high-density polyethylene (HDPE) composites filled with boron nitride (BN) as a neutron absorber was examined. HDPE and BN (1 wt.%) composites were prepared using the melt mixing technique, with or without the compatibilizer maleic anhydride-grafted-polyethylene (MA-g-PE). The effects of compatibilizer and gamma doses (0, 25, and 100 kGy) on mechanical properties were studied experimentally. Findings indicated that uncompatibilized composites irradiated at 25 kGy demonstrated the best mechanical properties. A significant decrease in the tensile properties of irradiated compatibilized composites can be effectively explained by the degradation effect. In addition, the gamma-irradiated compatibilized composite exhibited the highest modulus at 100 kGy, and a decrease in elongation at break (El@Br) was also observed at 25 and 100 kGy.

Keywords: Shield, Mechanical properties, Radiation effect, Composite, Boron nitride

Introduction

The development and optimization of advanced nuclear shielding materials are crucial for ensuring safe operation and minimizing radiation exposure within the nuclear industry. In this context, high-density polyethylene (HDPE), a versatile thermoplastic, has emerged as a promising candidate for irradiated shield applications due to its excellent mechanical properties, its low cost, ease of processing, and good radiation resistance [1, 2].

The use of boron nitride in materials science has garnered significant attention due to its exceptional properties and diverse applications. Boron nitride's remarkable ability to absorb neutrons makes it an

ideal candidate for neutron shielding applications, thereby contributing to the safety and efficiency of nuclear and space facilities. In particular, incorporating boron nitride into high-density polyethylene for the development of irradiated shields holds great promise, as it offers a unique compatible effect that can enhance the neutron shielding properties of the polyethylene [3, 4]. This is of significant interest in the nuclear industry, where such shields play a crucial role in mitigating radiation exposure. However, its poor compatibility with high-density polyethylene can lead to reduction in mechanical properties.

The performance of composites can be significantly affected by the compatibility between the different components used in their fabrication. In particular, the use of fillers and additives can lead to poor interfacial adhesion, resulting in reduced mechanical properties [5]. One approach to enhancing the compatibility of composite materials is by using compatibilizers. They work by modifying the interfacial properties of the composite, reducing the interfacial tension, and promoting adhesion between the different components. Compatibilizers are compounds that can improve the adhesion between the various components of a composite material, resulting in improved mechanical properties [6].

In this study, we are investigating the impact of a compatibilizer on enhancing the interfacial adhesion between the high-density polyethylene and boron nitride on the tensile strength of irradiated shields. The results of this study have important implications for the development of high-performance composite materials for use in radiation shielding applications. By recognizing of the compatibility between the different components of a composite material, we can improve its mechanical properties and overall performance. This can lead to the development of more efficient and effective radiation shielding materials, with potential applications in the nuclear industry, space exploration, and medical imaging.

Experimental

Materials and Characterization

The high-density polyethylene (PE) used in this study was obtained from Jam Company, HM 5010 T2N, EX3. It has a density of 0.945 g/cm³ and a melt flow index of 0.45 g/10 min. At 190°C, hexagonal boron nitride (BN) with lateral dimensions of 3-5 μm, which was required the investigation, was supplied by Aldrich. Maleic anhydride-grafted-polyethylene (MA-g-PE) was used as a compatibilizer in this study and was obtained from Kimia Baspar Asia in Iran. The processing equipment used includes

an internal mixer (Brabender, Germany), an injection molding machine (Laboratory Platen Press, model: P200P, Germany), a tensile machine (HIWA/Material Testing, Hiwa-200, Iran) to create dumbbell samples (ASTM D-638), and a 60Co source with a gamma cell 220 (activity: 8775 Ci).

Preparation of Composites

Melt-mixing specimen preparation was conducted using an internal mixer. In this experiment, two distinct systems are created using HDPE/BN (1 wt.%) composites with or without a compatibilizer, and 3 wt.% of MA-g-PE is also considered.

Irradiation of Composites

Dumbbell samples were irradiated in Gamma Cell 220 with absorbed doses of 0, 25, and 100 kGy.

Results and Discussion

Effect of Compatibilizer on Tensile Strength of Irradiated Composites

Fig. 1 illustrates the variations in tensile strength based on the received dose of gamma radiation for neat PE, composites containing 1 wt.% of BN, namely HD/BN, and HD/BN/HD-g-MA. As the received dose increases, the tensile strength of all samples decreases. However, for neat HD and HD/BN, the strength changes are much more pronounced in the high dose compared to the low dose. On the other hand, HD/BN/HD-g-MA exhibits the most significant decrease in tensile strength at 25 kGy, and the rate of decrease slows down at higher doses. The tensile strength of this material decreases by 31% and 54% at doses of 25 kGy and 100 kGy, respectively, while the tensile strength of HD/BN decreases by 6% and 44%.

The noteworthy point in the investigation of this parameter is that the addition of a compatibilizer increases the slope of tensile strength reduction. Due to the presence of type 3 carbon and carbonyl groups, the samples containing HD-g-MA exhibit a significant decrease in tensile strength. During the irradiation of samples containing polyethylene, processes such as the formation of crosslinks, chain scission, and branching occur. However, at the same time as the formation of crosslinks that enhance the mechanical properties, random branching and chain scission also occur, which have a negative effect on the properties. The speed at which these processes occur determines the final behavior of the composite.

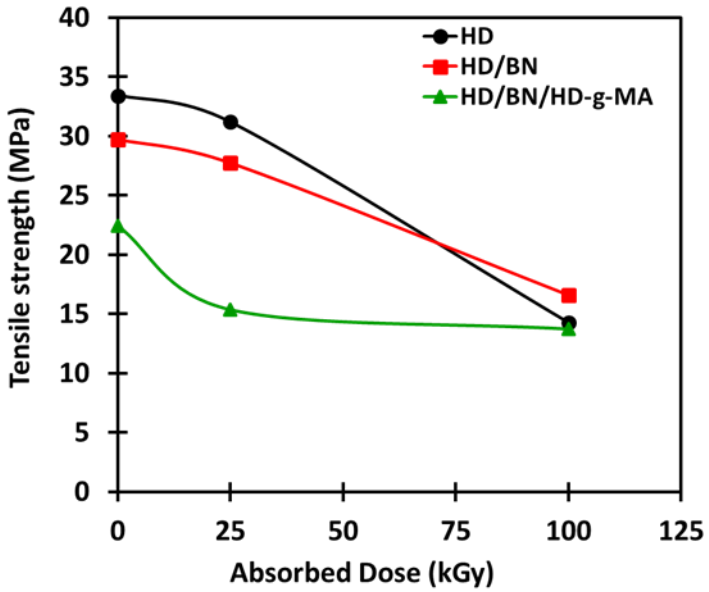

Fig. 1. Changes of the tensile strength of neat PE, BN/PE and HD/BN/HD-g-MA versus absorbed dose (0, 25 and 100 kGy)

Effect of Compatibilizer on Tensile Modulus of Composites

The tensile modulus of specimens using HD, HD/BN, and HD/BN/PE-g-MA are shown in Fig. 2. Tensile modulus is a measure of the stiffness of a material. Theoretically, the tensile modulus depends on the tensile stress and tensile strain of the material. Materials that are relatively brittle and fracture at low tensile stress and very low tensile strain will also exhibit a high tensile modulus value.

For non-irradiated samples, the neat HD sample has the lowest modulus, and the presence of BN in the structure increases the modulus of the composite samples due to the higher modulus of BN. By irradiation, the tensile modulus of the HD/BN specimen was lower than that of the HD and the compatibilized HD/BN/HD-g-MA specimen. Due to improper adaptation and the presence of HG-g-MA, the compatibilized HD-g-MA specimens contained voids.

The presence of voids may cause premature failure of the specimen. When the specimen fails at a relatively low strain, the result might indicate a higher tensile modulus as well. The increase in absorbed dose led to an increase in the tensile modulus of the specimens, with the highest tensile modulus observed at 100 kGy.

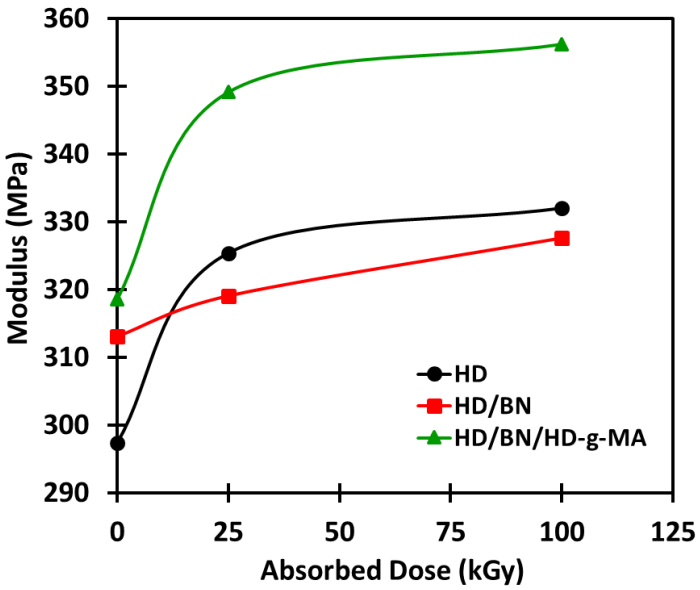

Fig. 2. Changes of the modulus of neat PE, BN/PE and HD/BN/HD-g-MA versus absorbed dose (0, 25 and 100 kGy)

Effect of Compatibilizer on Elongation at Break of Composites

Since brittleness is one of the significant outcomes of polymer degradation due to radiation, El@Br is considered a sensitive parameter for degradation analysis. Fig. 3 illustrates the variations in this parameter concerning gamma radiation dose for pure HD, HD/BN, and HD/BN/HD-g-MA. As the absorbed dose of radiation increases, the structure of the HD matrix becomes more fragile. The El@Br for HD/BN composite increases at a low received dose compared to the non-irradiated HD/BN. However, at a high dose, a decrease in El@Br is observed. According to the tensile strength of the studied sample, this trend can be attributed to the effect of radiation in creating crosslinking at low doses. The decreasing trend of El@Br with increasing absorbed dose for HD/BN/HD-g-MA indicates more destruction of the matrix due to the presence of type 3 carbon and carbonyl groups. However, the samples still possess sufficient toughness to be utilized in industry and potential applications.

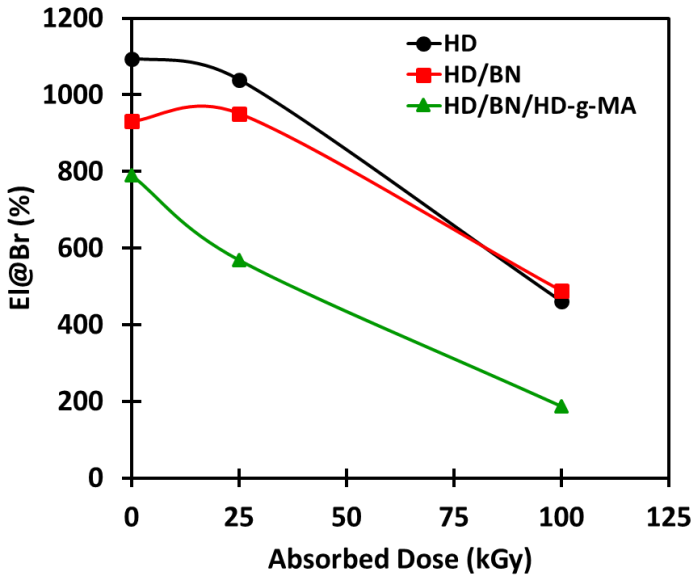

Fig. 3. Changes of the El@Br of neat PE, BN/PE and HD/BN/HD-g-MA versus absorbed dose (0, 25 and 100 kGy)

Conclusions

Polyethylene/boron nitride composites with a 1 wt.% filler content were prepared using a melt mixer. To enhance the properties, interfacial treatments using HD-g-MA compatibilizer were proposed to improve the interfacial adhesion between BN and HD. The effect of gamma irradiation, with and without a compatibilizer, on the tensile properties of the composites was determined. When only irradiation was applied at a low dose, improvements in tensile properties were observed at a radiation dose of 25 kGy. When both gamma irradiation and a compatibilizer were applied, a negative effect on the properties of HD/BN/HD-g-MA composite was observed. The treatment with a compatibilizer at low and high radiation doses resulted in a decrease in all tensile parameters due to degradation. In the dose of 25 kGy, the HD/BN specimen exhibits acceptable properties attributed to the formation of a crosslink bonds.

References

[1] More, C. V., Alsayed, Z., Badawi, M. S., Thabet, A. A., & Pawar, P. P. (2021). Polymeric composite materials for radiation shielding: a review. Environmental Chemistry Letters, 19(3), 2057-2090.

[2] Li, X., Yu, M., Xu, X., & Wu, R. (2021). Optimization design and application study on a high temperature resistant borated polyethylene shielding material. IOP Conference Series: Earth and Environmental Science, 675(1), 012215.

[3] Vira, A. D., Mone, E. M., Ryan, E. A., Connolly, P. T., Smith, K.,. Roecker, C. D., Mesick, K. E., Orlando, T. M., Jiang, Z., First ,P. N. (2023) Designing a boron nitride polyethylene composite for shielding neutrons. APL Materials, 11 (10), 101104.

[4] Hamisu, A., Khiter, O., Al-Zhrani, S., Haridh, W. S. B., Al-Hadeethi, Y., Sayyed, M. I., Tijani, S. A., The use of nanomaterial polymeric materials as ionizing radiation shields, Radiation Physics and Chemistry (2023) 216, 111448.

[5] Periasamy, K., Kandare, E., Das, R., Darouie, M., Khatibi, A.A. Interfacial Engineering Methods in Thermoplastic Composites: An Overview. Polymers (2023) 15, 415.

[6] Song, W., Guo, K., Li, Z., Zhao, Y., Zhu, K., Yuan, X., Polymer Composites (2022), 43(2), 1136.

ICNST 2024
International Conference on Nuclear Science and Technology
6- 8 MAY 2024 | Isfahan, Iran

Examination of the effect of BTO particles on the radiation shielding properties in low-density polyethylene; Monte Carlo study (Paper ID: 1333)

Nikrah A.[2], Taherparvar P.[1*], Sadremomtaz A
[1]Department of Physics, Faculty of Science, University of Guilan, Guilan, Iran
[2]Department of Physics, Campus faculty, University of Guilan, Guilan, Iran

Abstract:

Today, Metal Polymer Composites (MPCs) are a newly popular non-toxic shield that contains no lead. This study investigated the role of $Bi_4Ti_3O_{12}$ (BTO) particles with proportions of 10, 15, 20, and 25 wt% in the Light-density Polyethylene (LDPE) Matrix as a novel material for gamma-ray shielding applications using the Monte Carlo code MCNPX. The mass attenuation coefficient, half-value layer (HVL), mean free path (MFP), and transmission factor (TF) were evaluated for 0.015, 0.1, 0.5, 1, 2, 5, 8, 10, and 15MeV. In the verification process, the results show a good agreement - with a difference of less than 1% - between the NISTXCOM library and the simulation results in the present study. Our results show that increasing the weight percentage of BTO in the LDPE medium increases μ_m and decreases HVL, MFP, and TF parameters. Therefore, composite with the highest weight percent of BTO have the highest μ_m values and lowest HVL and MFP. Furthermore, LDPE with 25 wt% of BTO particles has the best radiation shielding characteristics among all simulated composites.

Keywords: MCNPX, Bismuth Titanate, Metal Polymer Composite, LDPE

Introduction:

Ionizing radiation can cause a considerable threat to ecological systems and human health, inducing cellular mutagenesis, organ dysfunction, systemic failures, and a spectrum of deleterious outcomes [1]. Ensuring that radiation exposure remains below the occupational exposure limit necessitates advancing research in the fabrication and deployment of diverse radiation shielding modalities, which are capable of effectively attenuating gamma radiation. Historically, lead (Pb), because of its high atomic number and density, has been considered the material of choice for stopping the penetration of gamma and X-ray photons [2]. Nevertheless, Pb's toxicity and environmental hazards present significant drawbacks [3-5].

In response to such challenges, different investigations have increasingly concentrated on pioneering non-Pb, lightweight, and flexible alternatives for X-ray shielding materials. For example, a shielding composite made of bismuth titanate ($Bi_4Ti_3O_{12}$, BTO) has been developed using bismuth oxide (Bi_2O_3) and titanium dioxide (TiO_2) as precursors [6,7]. This composite material combines the beneficial properties of Bi_2O_3, a high atomic number metal compound, and TiO_2, known for its excellent thermal stability and chemical inertness, to enhance its efficacy in X-ray shielding. Bismuth titanate (BTO) has been utilized as an effective X-ray attenuating agent. Moreover, light-density polyethylene (LDPE) has been elected as the foundational matrix for radiation shielding fabrication due to its thermoset properties, non-toxicity, economic viability, lightweight characteristics, and compatibility with surface adhesion to textiles [8].

Hereby, in this work, the shielding efficacy of six LDPE/BTO composite samples has been evaluated by some criteria such as mass attenuation coefficient (μ_m), half-value layer (HVL), and transmission factor (TF) for energies ranging from 0.015 to 15 MeV, which commonly used in photon calculations by the ANSI/American National Standard (ANS) standards. The evaluation was performed using Monte Carlo N-Particle Extended (MCNPX) codes and WinXCOM computational platforms.

Materials And Methods:

Research Theories:

The interaction probability of the incident gamma ray with a shield with a thickness of x (cm) is defined as the linear attenuation coefficient of the gamma-ray (μ), described by the Beer-Lambert law**:**

$$\mu(cm^{-1}) = \frac{1}{x} Ln(\frac{I_0}{I}) \quad (1)$$

where I and I_0 are transmitted and incident photon intensity, respectively. One of the essential protective parameters in shielding terminology is the mass attenuation coefficient (μ_m). The μ_m for a specific material can be described by equation (2):

$$\mu(cm^2 \times g^{-1}) = \frac{\mu(cm^{-1})}{\rho(g \times cm^{-3})} \quad (2)$$

where ρ is the density of the studied material during the gamma-ray interaction. The distance between the following two collisions is defined as the mean free path (MFP), as follows:

$$\mathrm{MFP(cm)} = \frac{1}{\mu(\mathrm{cm^{-1}})} \quad (3)$$

the thickness required to reduce the gamma-ray intensity to half its initial value is called the half-value layer (HVL):

$$HVL(cm) = \frac{\log 2}{\mu(cm^{-1})} \quad (4)$$

the transmission factor (TF) is the ratio of the photons transmitted in the presence of the filler in the matrix (BTO/LDPE) to the photons that pass through the LDPE sample, which is shown by the equation (5).

$$\mathrm{TF} = \frac{(\mathrm{BTO/LDPE})}{\mathrm{LDPE}} \quad (5)$$

Simulation Methods:

This work uses MCNPX Code (version 2.6.0) as a simulation program. The MCNPX is the Monte Carlo N-Particle extended, which can be used for transport simulations of the different types of particles such as neutron, photon, electron, and coupled neutron/photon/electron. The geometry implemented in the MCNPX code for the assessment of different shield properties can be seen in Figure 1.

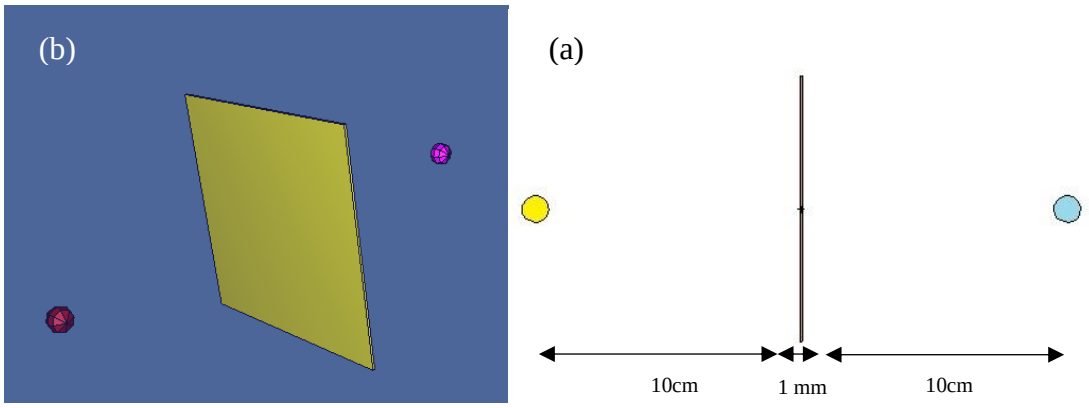

Fig.1. General-view of designed simulation setup (a), 3-D setup obtained from MCNPX (b)

In order to simulate a narrow beam configuration, based on the Beer-Lambert law, a photon point source with an energy of 0.015 to 15MeV was placed, and at a distance of 10 cm from the source, an LDPE/BTO sample with dimensions of 1 mm was placed. Also, a spherical detector with dimensions of 1 cm is located in front of the source. Tally F4 is used to investigate the flux of a particle through a

cell in the MCNPX code using the library of Evaluated Nuclear Data Files (ENDF)/B-VI-Released 8.Since the geometry is ideal, the condition of equation 1 is satisfied.

Results and discussion:

At first, the geometry designed for the LDPE shield was compared to the XCOM library data for validation purposes. Our simulation results and standard XCOM output are shown in Figure 2.

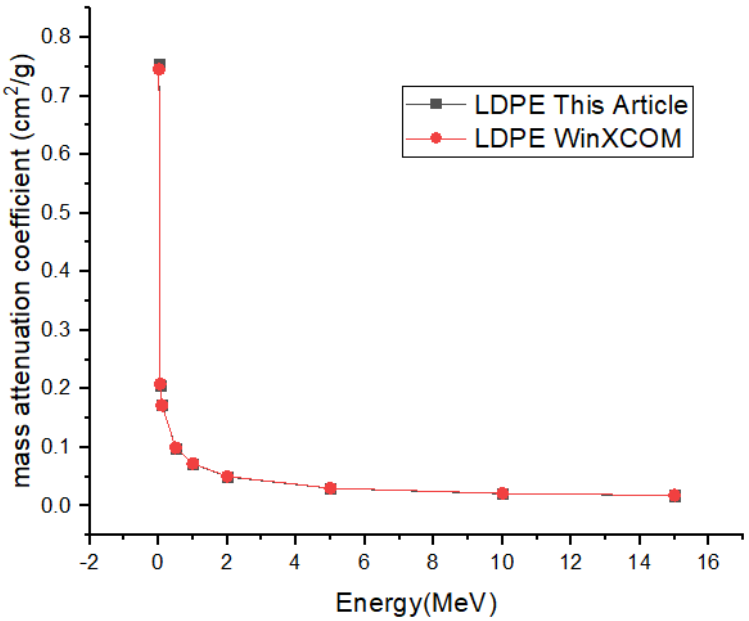

Figure 2. Comparison of Results in this Article with XCOM Data

According to Figure 2, there is a good agreement between the simulation results and the WinXCOM data, and the deviation of our results to the XCOM data is less than 1%.

After the validation process, the same geometry as Figure 1 was used to evaluate the effects of adding different BTO on the μ_m of LDPE. The concentrations of 10%, 15%, 20%, and 25 %wt of $Bi_4Ti_3O_{12}$ in the LDPE matrix were used to evaluate the effect of increasing $Bi_4Ti_3O_{12}$ concentration on the shielding properties of the LDPE. The variation of the μ_m in terms of photon energy is shown in Figure 3.

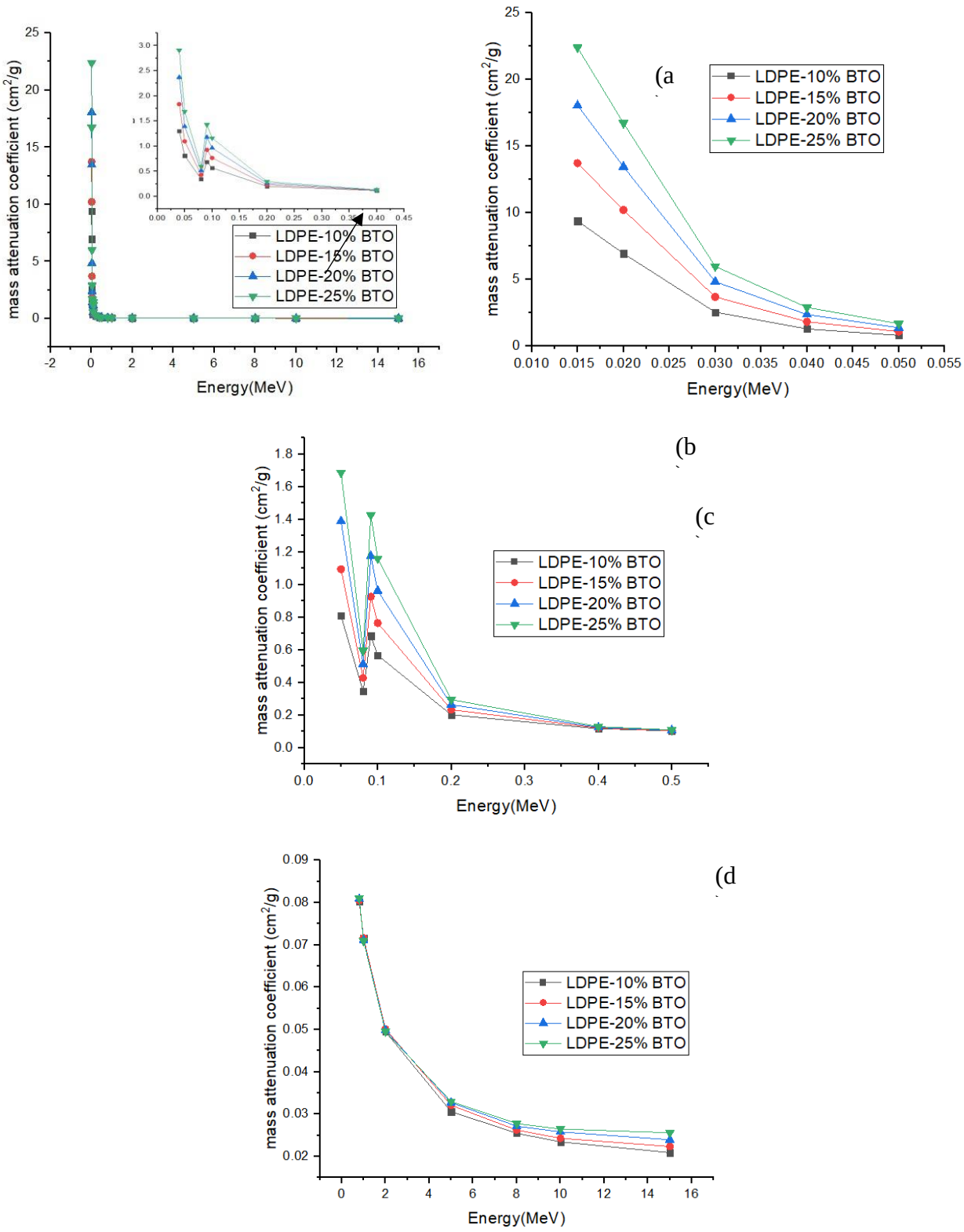

Figure 3. Variations of μ_m obtained with MCNPX versus gamma energy for the LDPE/BTO in the energy region of 0-15 MeV (a), 0.015-0.05 MeV (b), 0.05 MeV - 0.5 MeV (c), 0.8 MeV - 15MeV (d).

According to Figure 2 and 3, because of the photoelectric effect is dominant at low energy regions, a substantial increase is seen in the μ_m curves by adding BTO, which has a higher atomic number. This is due to the relationship between the probability of occurrence of the photoelectric effect with the atomic number (Z) in the form of Z^3 [9].

Furthermore, due to the presence of Bi in this filler, the k absorption edge (related to the Bi) is created in the composite in an energy of 90.53 keV, by adding BTO to the LDPE. It causes the μ_m of the composite is greatly increased in this energy of incident photons.

On the other hand, in the intermediate energy regions (0.5 to 1MeV), the effect of BTO grinding is negligible. It is because of dominant interaction in this region of energy is Compton scattering, which its probability occurrence is no strong dependence on atomic number of medium. Hence, the effect of adding BTO is negligible. At high energies, the dominant interaction is pair production. The cross-section strongly depends on the atomic number as Z^2 [9] explains the behavior of μ_m values in this region. Therefore, it can be said that the μ_m ability of composites increases with the increase of BTO concentration. Also, the best composite type for shields contains 25% of BTO.

Investigating the Half Value Layer for LDPE/BTO composites

Figure 4 shows another vital quantity called HVL, which shows the shield's ability to reduce the radiation flux by half its initial value.

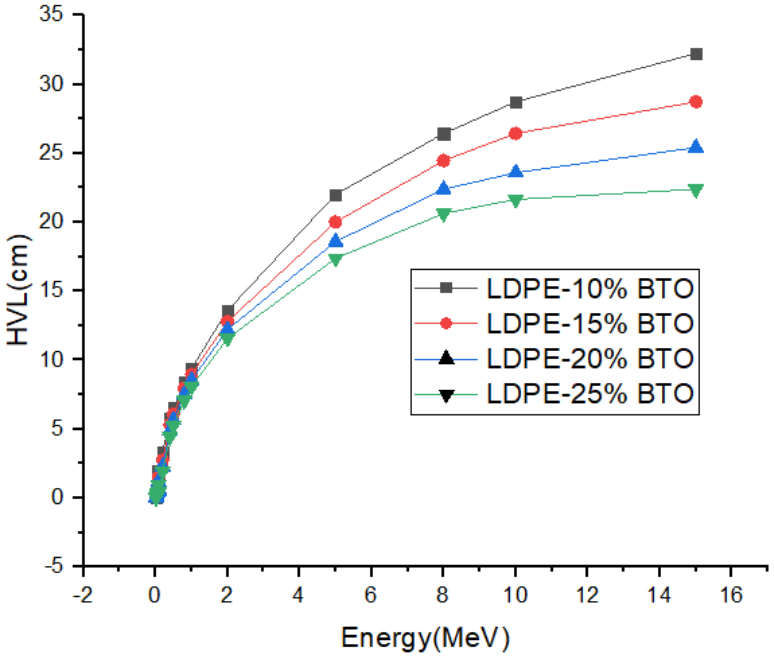

Figure 4. Variations of HVL obtained with MCNPX versus gamma photon energy for the LDPE/BTO

According to Figure 4, compared to LDPE and LDPE/BTO shields, the shields containing BTO have lower HVL. With the increase of BTO in the LDPE composite, HVL decreases; as a result, by increasing the percentage of BTO in the composite from 10% to 25%, shielding properties improvement is also observed, as well as the need for less shield thickness.

Mean Free Path for LDPE/BTO Composites

The MFP represents the average distance traveled between successive photon collisions with matter particles; therefore, with the increase of this parameter, more photons are expected to penetrate. As a result, the lower the values of this parameter, the more influential the protection capability of it from gamma photons irradiation.

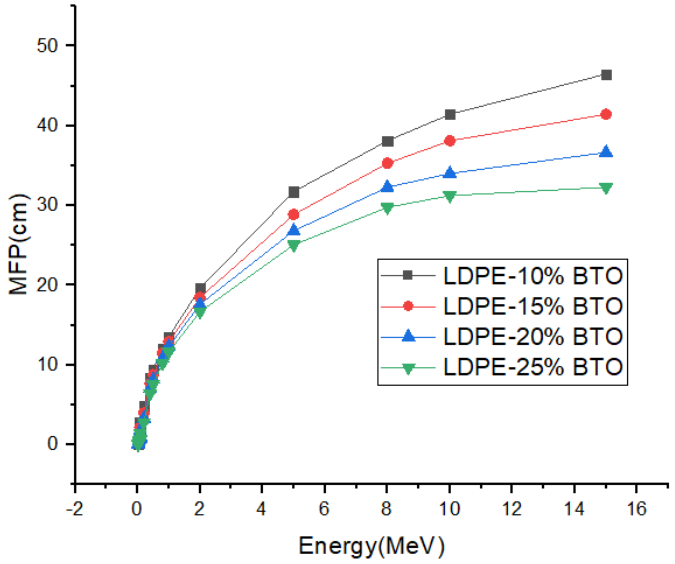

Figure 5. Variations of MFP obtained with MCNPX versus gamma photon energy for the LDPE/BTO

According to Figure 5, the MFP (cm) increases from a lower to a higher value concerning an increase in energy and becomes saturated and constant for all four samples. Increasing the percentage of BTO in the composite shield from 10% to 25%, decrease MFP values related to the sample. The samples with highest BTO concentration, which has higher Z-number with the highest density, indicating an improvement in shielding against radiation, as MFP criteria.

Transmission Factor for composites containing BTO

Figure 6 shows the transmission factor (TF), calculated by dividing photon flux passed through LDPE/BTO by that through the LDPE sample.

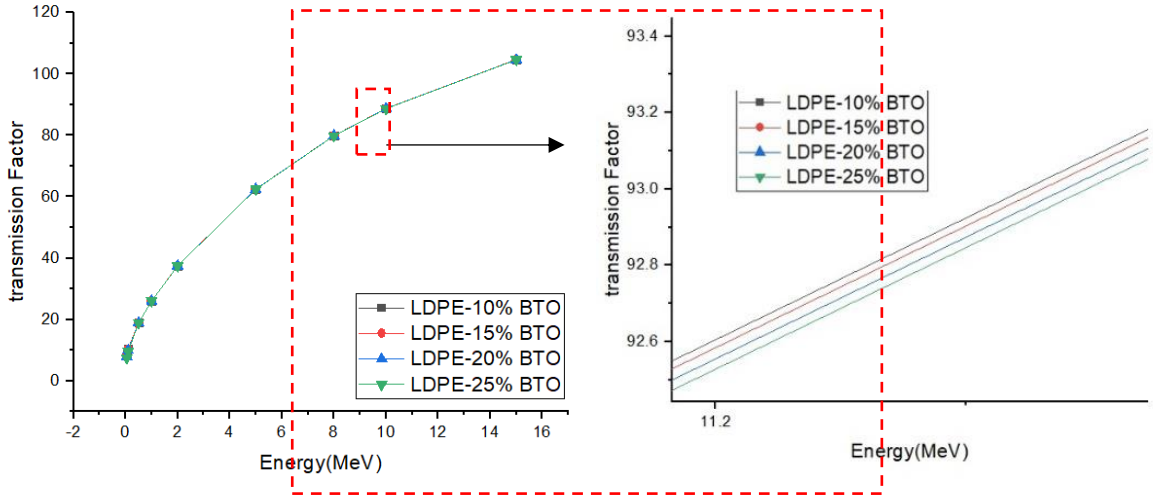

Figure 6. Photon transmission factor of LDPE/BTO composites calculated by MCNP code

According to Figure 6, the amount of TF for shields containing LDPE/BTO compared to LDPE decreases to some extent, with the increase of the percentage of weight percent from 10% to 25%. This is because of the reduction of photons passing through composites containing BTO as a result of shields containing more BTO, result in the improvement of shielding properties of it. With increasing energy, the ability of the shields decreases, resulting in the transmission factor gradually increasing for all composites.

Conclusions

The current study used the MCNPX code to simulate the properties of different radiation shields based on the LDPE/BTO composites at energies of 0.015 to 15 MeV. The results were validated with the data of the XCOM library. By that, the quantities μ_m, HVL, MFP, and TF, which were used to investigation of the radiation shielding properties, were calculated for composites containing BTO. According to the results, increasing the amount of BTO in the composite improves μ_m of all the investigated energies. The effect of the K-edge absorption of BTO in the LDPE in all simulation diagrams are seen, which leads to an increase in the μ_m.

In addition to, by increasing the BTO into the LDPE sample, the HVL, and MFP decreased, which indicates that shields containing BTO more facilitate the ability to create shields with less thickness to achieve acceptable protective properties. The reduction of TF by increasing the amount of BTO applied to primary LDPE improved the shielding properties of samples. As a result of this investigation, the

composite containing 25% of BTO in LDPE has the most radiation-shielding properties, and this investigation showed that using BTO in radiation-shielding compounds is very feasible.

Reference

[1] Basu, P., et al. (2019). Gamma-ray buildup factors for conventional shielding materials and buildup factors computed for tungsten with a thickness beyond 40 mean free paths (Vol. 154), Article 108864.

[2] Oglat, A. A., & Shalbi, S. M. J. G. (2022). An alternative radiation shielding material based on barium-sulfate (BaSO4)-modified fly ash geopolymers (Vol. 8, p. 227), 4

[3] Ambika, M. R.; Nagaiah, N.; Suman, S. K. Role of bismuth oxide as a reinforcer on gamma shielding ability of unsaturated polyester based polymer composites. J. Appl. Polym. Sci. 2017, 134, 1.

[4] More, C. V.; Alsayed, Z.; Badawi, M. S.; Thabet, A. A.; Pawar, P. P. Polymeric composite materials for radiation shielding: a review. Environ. Chem. Lett. 2021, 19, 2057−2090

[5] Kadyrzhanov, K.K., Shlimas, D.I., Kozlovskiy, A.L., Zdorovets, M.V., 2020. Research of the shielding effect and radiation resistance of composite CuBi2O4 films and their practical applications. J. Mater. Sci. Mater. Electron. 31, 11729–11740.

[6] Gupta, N.; Kaur, A.; Khanna, A.; Gonzàlez, F.; Pesquera, C.; Iordanova, R.; Chen, B. Structure-property correlations in TiO2-Bi2O3-B2O3-TeO2 glasses. J. Non-Cryst. Solids 2017, 470, 168−177.

[7] Le Yu, Pei Lay Yap, Alexandre Santos, Diana Tran; Lightweight Bismuth Titanate (Bi4Ti3O12) Nanoparticle-Epoxy Composite for Advanced Lead-Free X-ray Radiation Shielding; ACS Appl. Nano Mater. 2021, 4, 7471−7478.

[8] Duffy, D.C., McDonald, J.C., Schueller, O.J., Whitesides, G.M., 1998. Rapid prototyping of microfluidic systems in poly(dimethylsiloxane). Anal. Chem. 70, 4974–4984.

[9] N. Tsoulfanidis, S. Landsberger, Measurement and Detection of Radiation, 3rd edn. (Taylor & Francis, London, 2010)

ICNST 2024 International Conference on Nuclear Science and Technology
6- 8 MAY 2024 | Isfahan, Iran

Evaluation of Lung Absorbed Dose due to Inhalation of Radon Short-lived Decay Products by Monte Carlo GATE Simulation Code (Paper ID: 1432)

Yousefi Tajani S., Zaki Dizaji H.*

Department of Physics, Imam Hossein University, Tehran, Iran

Abstract

Internal exposure to radon gas short-lived products causes a lot of damage to the human respiratory system, especially the lungs. Due to the fact that radon gas is produced in the soil and rocks underground and gradually comes to the earth surface and diffuse to it, people who work in closed underground environments such as mines are at greater risk. For this reason, in this research, we evaluated the absorbed dose of lung tissue in exposure to alpha decay of Radon-222 short-lived decay products, using Monte Carlo GATE code. For this purpose, we designed a lung equivalent phantom, with 125 air sacs, in 5 equal rows by Monte Carlo GATE. Each air sac is a spherical shell with a shell thickness of 0.01 cm, which is composed of lung tissue. Then, in each simulation, we placed the radon decay products inside these air sacs in both suspended and deposited states and calculated the lung tissue absorbed dose. The result of the simulations and calculations show that the received dose of the lung in the deposited state is significantly higher than that of in the suspended state. Also, Po-218, as one of the decay products of Radon-222, deposits a larger dose into the lungs tissue and therefore, causes more damage to the lung tissue.

Keywords: Internal Exposure, Monte Carlo GATE, Lung, Radon, Dosimetry.

Introduction

It has become recognized that the greatest fraction of the natural radiation exposure in humans results from inhalation of the short-lived Radon-222 progeny [1]. Radon-222 is a natural, non-flavor, non-odor and non-color radioactive gas, mainly derived from the day chain of Uranium series [2]. It can be produced inside the soil and rocks and gradually diffuse to the earth surface [3]. High radon concentrations in indoor air coupled with the prolonged exposure periods related to indoor habitation make indoor radon a potential health hazard and can lead to dangerous biologic effects. It is the second leading cause of cancer in the United States after smoking. Research in the United States shows that radon kills between 15,000 and 22,000 people a year [4]. The radioactive radon progeny can enter the lung through two different pathways. In the first case, the radon gas directly enters the respiratory

system through breathing and releases daughters of radionuclides remaining inside the lung air sacs as the dust particles (suspended state). In the second one, the daughter radionuclides of the radon gas are produced outside the body and enter the lung after attaching to the ambient aerosols and deposit on the air sacs of the inner walls of lungs (deposited state) [5]. After decay, radon progeny produce significant amounts of energetic alpha beams and low values of beta and gamma radiations from various energies. Despite their restricted tissue penetration potential, alpha particles can cause important biological damage in exposed tissue due to their high relative biological effectiveness (RBE). Beta and gamma-radiation is also emitted from the decay of radon derivatives, but the RBE is minimal in comparison. Each member of the body, according to its structure and dimensions, can absorb the fraction of energy beam emission. The alveoli in the lung, contain several small air sacs and are the last place of the gas exchange of the body, and in most studies, it has been introduced as the main deposition place [6]. The purpose of this research was to evaluate the absorbed dose of lung tissue as the most sensitive part of the body in exposure to alpha decay of Radon-222 short-lived decay products in both the suspended and deposited states, using Monte Carlo GATE code.

Material and Methods

The radon gas decays through a series of short-lived decay products and reaches Pb-210, a nuclide with a 20 year half-life, and finally stable Pb-206. The decay chain of Radon-222 is as below:

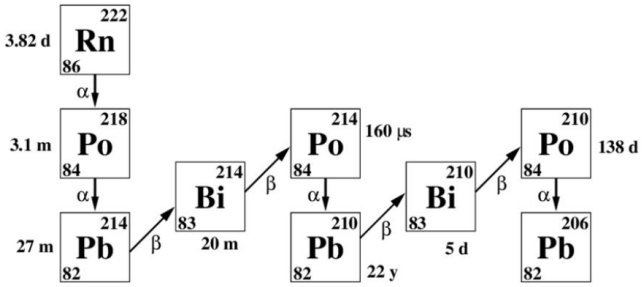

Fig. 1. The decay chain of Radon-222 [7]

The absorbed dose is given by: $\boldsymbol{D = \frac{dE}{dm}}$, where $\boldsymbol{dE}$ is the energy imparted by ionizing radiation to matter of mass $\boldsymbol{dm}$. The SI unit of absorbed dose is J/kg which is named gray (Gy). Also, The equivalent dose to a tissue or organ is defined as: $\boldsymbol{H = \sum_R w_R D_{RT}}$, where $\boldsymbol{w_R}$ is the radiation weighting

factor for radiation type R, and $\boldsymbol{D_{RT}}$ is the organ absorbed dose from radiation type R in a tissue or organ T [8].

Since the lung is the most sensitive organ of the body against inhalation of radioactive materials, in this study, we have investigated the effects of radon decay products on the lung. Since it is not possible to investigate the effects of this radioactive gas on a living organism, the simulation of this case based on the Monte Carlo method is an alternative way. There are about three hundred million alveolar air sacs in the lung and the simulation of all these air sacs in one simulation and attaching source to it is very hard and heavy and requires high computer systems. So, we simulated 125 air sacs and analyzed the results as representative.

The geometry of the lung phantom, which was simulated in this study, is a box with the total length of 0.115 cm, included 125 air sacs designed in 5 equal rows. The composition of the lung tissue is mentioned in Table 1. The wall of the air sacs is composed of soft tissue with a density of 1.04 g/cm^3. The composition of soft tissue is given in Table 2. The space inside the air sacs contains air with the density of 0.00129 g/cm^3. Each air sac was a spherical shell with outer radius of 0.01 cm and inner radius of 0.0098 cm.

Table 1. The composition of lung tissue

Element	Fraction
Hydrogen	0.103
Carbon	0.105
Nitrogen	0.031
Oxygen	0.749
Other elements	0.012

Table 2. The composition of soft tissue.

Element	Fraction
Hydrogen	0.104
Carbon	0.232
Nitrogen	0.025
Oxygen	0.63
Other elements	0.0082

The geometry of lung can be seen in Figure 2. In this Figure, the blue cubic is lung and the red spheres are air sacs.

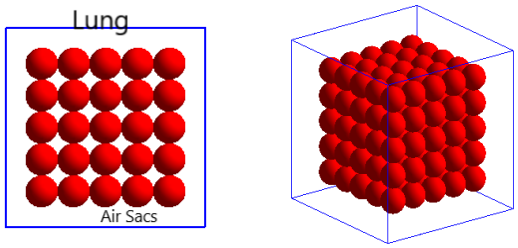

Fig. 2. The geometry of lung phantom

Since the beta and gamma dose due to radon progeny, including Pb-214 and Bi-214, inside the lung, has no significant contribution to the overall lung dose, we considered the dose from alpha-emitter progenies of radon [9]. In this study, radioactive products of radon were evaluated as two physical states. In the first state, the radon radioactive products were assumed as the suspended particles within the air sacs. In this state, there is always a probability for radon progenies to escape from the lung. So, there is a weighing factor for each daughter nuclide due to its half-life and its priority in radon decay chain, as mentioned below:

$$W_{218_{Po}} = 1 - e^{-\lambda_{218_{Po}} t}$$

$$W_{214_{Pb}} = (1 - e^{-\lambda_{218_{Po}} t})(1 - e^{-\lambda_{214_{Pb}} t})$$

$$W_{214_{Bi}} = (1 - e^{-\lambda_{218_{Po}} t})(1 - e^{-\lambda_{214_{Pb}} t})(1 - e^{-\lambda_{214_{Bi}} t})$$

$$W_{214_{Po}} = (1 - e^{-\lambda_{218_{Po}} t})(1 - e^{-\lambda_{214_{Pb}} t})(1 - e^{-\lambda_{214_{Bi}} t})(1 - e^{-\lambda_{214_{Po}} t})$$

By assuming an average time of 3 seconds for each respiratory cycle including inspiration and expiration [10] and the decay constant of Po-214 and Po-218, the weighing factor of these two progenies of radon is given in Table 3.

Table 3. The weighting factor of Po-218 and Po-214 in a radon decay chain.

Radon Progeny	Weight Factor in a decay chain (W)
Po-218	0.011
Po-214	2.5×10^{-8}

In the second state, the radioactive products of radon were considered as the deposited materials in the form of a spherical shell with 1 μm thickness. So, they have no chance to escape from the lung and therefore, all the emitted energy by daughter products would be deposited in the lung. In each state, an alpha homogeneous mono-energy source was defined by Monte Carlo Gate code based on NuDAT 3.0 [11] and attached to the intended volume. The source volume in the deposited state was a spherical shell with 1 μm thickness inside each air sac and in the suspended state, it was a sphere with the radius of 0.0098 cm inside each air sac. So, in both states, each air sac is a radioactive source. The energy of alpha particle for Po-218 was 6.11 MeV and for Po-214 was 7.83 MeV. Because of the long half-life of Pb-210 (22.3 years), this radioactive product and its subsequent products are not assumed in the simulations. The physics list which used in these simulations was G4Elastic.

After definition of geometry and sources, we attached Dose Actor to each air sac to accumulate data about the amount of energy that was deposited in that air sac. In order to optimize the error in the calculations, we executed the code using 5 million particles. The code ran for two alpha-emitter radon progeny (Po-214 and Po-218) and in two physical states. After running the code, we collected the energy deposited data and calculate the absorbed dose due to the mass (volume and density) of each air sac.

Results and Discussion

After running the program and collecting the results as energy deposited in the unit of MeV, we averaged these results and divided it by the mass of each air sac to obtain the average absorbed dose to air sacs. Then, to obtain the equivalent dose, we multiplied this value by the weight factor, which is equal to 20 for alpha particles. We should consider and multiply the weighting factor of Po-218 and Po-214 in a radon decay chain in the suspended state.

In the deposited state, by considering the mass of each air sac as 2.56×10^{-10} kg, the amount of average deposited energy, average absorbed dose and equivalent dose in each air sac is given in Table 4. The weight factor of alpha radiation is taken from ICRP 103 [12].

Table 4. The values of average deposited energy, average absorbed dose per decay and equivalent dose per decay for Po-218 and Po-214 in the deposited state.

Radon Progeny	Average Deposited Energy (MeV)	Average Absorbed Dose (Gy) per Decay	Average Equivalent Dose (Sv) per Decay
Po-218	7.44×10^{5}	9.3×10^{-5}	1.86×10^{-3}
Po-214	6.71×10^{5}	8.38×10^{-5}	1.68×10^{-3}

Also, In the suspended state, by considering the weighing factors and the mass of each air sac as 2.56×10^{-10} kg, the amount of average deposited energy, average absorbed dose and equivalent dose in each air sac is given in Table 5.

Table 5. The values of average deposited energy, average absorbed dose per decay and average equivalent dose per decay for Po-218 and Po-214 in the suspended state.

Radon Progeny	Average Deposited Energy (MeV)	Average Absorbed Dose (Gy) per Decay	Average Equivalent Dose (Sv) per Decay
Po-218	6.99×10^{5}	9.61×10^{-7}	1.92×10^{-5}
Po-214	6.2×10^{5}	1.94×10^{-12}	3.88×10^{-11}

After the calculation, the maximum relative difference between the average energy deposited and the values of energy deposited in each air sac was equal to 3.1 percent. This shows that the value of energy deposited and absorbed dose is almost same in all air sacs and therefore, it indicates that the dose of each air sac is due to its adjacent air sacs, because otherwise, the dose of some air sacs should be higher than others. Also, it indicates that the effect of the radioactive elements in these air sacs on the rest of the respiratory system outside the lung well be negligible.

As can be seen in Table 4, in the deposited state, the average absorbed dose per decay for Po-218 and Po-214 was approximately the same and its value was about 9 μGy. Also, the average equivalent dose was of order of 1 mSv. So, in the deposited state, the Po-218 and Po-214 radionuclides has approximately the same contribution in the overall lung dose. As shown in Table 5, in the suspended state, the value of the average absorbed dose for Po-218 was 5 orders of magnitude greater than the average absorbed dose of Po-214. Also, the value of the average equivalent dose for Po-218 was 6 orders of magnitude greater than the average equivalent dose of Po-214. It demonstrates that in the suspended state, Po-218 due to priority in the radon decay chain, has more contribution in lung dose.

The comparison of the values of Table 4 and Table 5, indicates that the average absorbed and equivalent dose received by lung in the deposited state is more than suspended state. It also can be seen in Table 6. According to ICRP recommendations, the maximum annual permissible dose for radon and its progenies is 200 Bq/m^3 [13]. On the other hand, the annual equivalent dose to the whole lung caused by inhalation of 1 Bq/m^3 concentration of radon gas should be considered $7 \times 10^{-6}\ Sv/year$ [14]. Therefore, the maximum permissible equivalent dose caused by inhalation of radon gas in the lung is 1.4 $Sv/year$. As can be seen in Table 6, the equivalent dose in the deposited state is greater than the maximum permissible dose. On the other hand, the equivalent dose in the suspended state is smaller than the permissible dose. Therefore, if in similar conditions, radioactive materials are deposited in the lung, the equivalent dose will exceed the annual permissible dose. It can cause damage to the lungs and the delicate structure of the air cavities and serious damage to them. Considering that these air sacs have the task of air exchange with blood vessels, damage to them can eventually lead to death.

Table 6. Comparison of the average absorbed dose and average equivalent dose in the deposited state and suspended state.

Physical State	Average Absorbed Dose (Gy) per Decay	Average Equivalent Dose (Sv) per Decay
Deposited State	1.77×10^{-4}	3.54×10^{-3}
Suspended State	9.61×10^{-7}	1.92×10^{-5}

Conclusions

In this research, we evaluated the dose received by lung tissue in exposure to alpha decay of Radon-222 short-lived decay products, using Monte Carlo GATE code. The results showed that the contribution of Po-214 and Po-218 in the lung dose in the deposited state was the same, But in the suspended state, Po-218 has more contribution in the lung received dose. Also, the overall received dose by lung in the deposited state was higher than the suspended state. In other words, when the radioactive products of radon are deposited inside the lung, they deliver more dose to the lung tissue. Therefore, they are more dangerous when they are deposited within the lung. On the other hand, inhaling radon radioactive products is more dangerous than inhaling radon gas itself. Because radon has a half-life of 3.8 days and after inhalation, without any special effect, it leaves the respiratory system through exhalation, but the radioactive daughters of radon, Especially its alpha-emitter

products, including Po-218 and Po-214, have relatively very shorter half-lives and can enter the respiratory tract and also, can be deposited in the lung by sticking to other particles of atmosphere.

References

[1] El-Hussein, A. Ahmed, A. Mohammed, A. (1998). Radiation Tract from Dose to the Human Respiratory Inhalation of Radon-222 and its Progeny, Pergamon. 49(7):783-790.
[2] Pinti LD, Retailleau S, Barnetche D, Moreira F, Moritz MA, Larocque M, et al. (2014) Rn-222 activity in groundwater of the St. Lawrence Lowlands, Quebec, eastern Canada: relation with local geology and health hazard. J Environ Radioact. 136: 206-217.
[3] Tsapalov A, Kovler K. (2016) Revisiting the concept for evaluation of radon protective properties of building insulation materials. Building Environ. 95: 182-188.
[4] Hahn ,EJ. Gokun, Y. Andrews, JW. Overfield, BL. Robertson, H. Wiggins, A. Et al. (2015). Radon potential, geologic formations, and lung cancer risk. Preventive medicine reports. 2:342-3466.
[5] Danaei Z, Baghani HR, Mowlavi AA. (2020) Absorbed Dose Assessment from Short-Lived Radionuclides of Radon (Rn-222) Decay Chain in Lung Tissue: A Monte Carlo Study. Iranian Journal of Medical Physics. 17(2):66-74.
[6] Mohammad Jafari, F. Bahmani, J. (2021). Determining the Absorbed Dose of Alpha Radiation due to Inhalation Radon Gas and Its Derivatives in Human Lung Using MCNPX 2.6.0 Simulation Model. Journal of Advanced Biomedical Sciences. 11(4):4077-4087
[7] Guiseppe, V. Elliott, S. Hime, A. Rielage, K. Westerdale, S. (2010). A Radon Progeny Deposition Model. AIP Conference Proceedings. 1338. 10.1063/1.3579565.
[8]] ICRP. The 2015 Recommendations of the International Commission on Radiological Protection. ICRP Publication 130. Ann ICRP. 2015.
[9] Hofmann W, Li WB, Friedland W, Miller BW, Madas B, Bardiès M, et al. (2020). Internal micro dosimetry of alpha-emitting radionuclides. Radiation and environmental biophysics. 59(1):29-62
[10] Warliah L, Rohman AS, Rusmin PH. (2012) Model development of air volume and breathing frequency in human respiratory system simulation. Procedia Soc Behav Sci. 67: 260-268.
[11] https://www.nndc.bnl.gov/nudat3
[12] ICRP. The 2007 Recommendations of the International Commission on Radiological Protection. ICRP Publication 103. Ann ICRP. 2007.
[13] ICRP. The 1993 Recommendations of the International Commission on Radiological Protection. ICRP Publication 65. Ann ICRP. 1993.
[14] Vennart J. Limits for intakes of radionuclides by workers: ICRP publication 30. Health physics. 1981; 40: 477-84

ICNST 2024
International Conference on Nuclear Science and Technology
6- 8 MAY 2024 | Isfahan, Iran

Nuclear security innovations in nuclear facilities: approaches and challenges (Paper ID: 1508)

Nili F. Correspondent1*, Shafeie S. Co-Author2

[1&2] Iran Nuclear Regulatory Authority (INRA), National Nuclear Safeguards Department, Tehran, Iran

Abstract

Nowadays, the use of nuclear energy in various areas around the world has been noticed. Energy production and peaceful use of nuclear technology, considering its diverse applications in various industries and scientific and specialized fields, requires the adoption of policies and adherence to special requirements that lead to the safe and secure use of this technology away from potential accidents and threats, at the level of nuclear facilities and national and international dimensions. From this standpoint, this study tries to consider the innovations in this field while examining the scientific and technical achievements in the area of nuclear security and analyzing both approaches and challenges in this direction. From this point of view, present research examines nuclear security innovations to gradually achieve deterrence, prevention, detection and response to threats in nuclear facilities, for instance, analyzing logical and programming methods, accountancy and control of nuclear materials (NMAC), computer modeling to identify malicious acts, researches in the field of using blockchain in nuclear security, creating and strengthening security culture, development of the nuclear security training network, providing an effective framework for international response to the threat of nuclear terrorism in order to strengthen nuclear security, relation and cross section between safety and security, and finally the interaction between 3S (Nuclear Safety, Security and Safeguards)with the aim of optimized, safe, secure and peaceful use of nuclear technology. Obviously, this research can be useful for policy makers, activists and researchers in the process of policy making and operating in the nuclear industry by drawing a general overview of the status and perspective of nuclear security.

Keywords: Nuclear Security, Nuclear Safety, Innovations, Nuclear Energy

Introduction

Considering the importance of using new science and technologies in various industries, all around the world, nuclear energy as a useful source with numerous usages, can benefit from wide range of them. According to the sensitivity of working with radioactive material, it is crucial to manage all activities in this field in a safe and secure manner. Based on IAEA definitions, both nuclear safety and security

try to protect society, properties and environment from harmful hazards and consequences of nuclear and radioactive material and related areas. However, nuclear security is all rules, laws, measures and inspections on the way of prevention, detection and response to any unauthorized access, malicious acts or other intended events involving radioactive material and facilities. Innovations in nuclear security is valuable step toward operating safe and secure in nuclear facilities. In this article, after reviewing studies in the field of nuclear security, these researches have been divided into three sections: Instruments, Strategies, and Infrastructures, therefore the trends and types of innovations in all three parts can be examined separately considering challenges and recommended approaches.

Nuclear Security Innovations

Reviewing studies shows that in order to increase the accuracy and speed of prevention, detection and response, as essential elements of nuclear security, the use of surveillance and monitoring systems, artificial intelligence, remote sensing, data mining, assistance in detection, prevention and countermeasures, improvements in physical protection, improvement of alarm and response systems, systems based on mobile, hand-held and portable devices, the ones which can be mounted on vehicles, 3D sensors, use of new methods of risk assessment, non-destructive assessment, improvement of access control status with the help of new detection technologies are of interest to researchers in this field [3]. Table1. summarizes and categorizes a brief review of some of studies in this field and categorized them into three above mentioned groups.

Table1. Researches Review based on three main categories

Researches Review				
Title	Author	Year	Objective/Result	Category
Data, language and graphbased reasoning methods for identification of human malicious behaviors in nuclear security	Li & et al.	2024	Proposing a computer vision module and a reasoning module both evaluating by using 4 event scenarios for identification of human malicious behaviors	Instrument
Strengthening Nuclear Material Accountability & Control (NMAC) Against Terrorism in Norther Nigeria: A Progressive Global Training Approach	Onyeanu & et al.	2023	Proposing a global training approach for NMAC (workshops, webinars, learning exchanges and etc.)	Infrastructure
Malicious behaviors identification in nuclear security based on visual relationships extraction and knowledge reasoning	Li & et al.	2023	Proposing a visual relationships extraction (computer vision module) and a knowledge reasoning method for behavior identification	Instrument
The Trust Machine: Blockchain Technology in Nuclear Security and Prospects for Application in the Middle East	Auda	2023	Examining the role of blockchain in nuclear security	Instrument
Emergence of Technological Threats and Opportunities for Nuclear Security in the Digital Age	Kalinichenko	2019	Recognizing opportunities and threats and determining the appropriate approach	Strategies

Results and Discussion

According to the logic described for the classification of studies in the field of innovations in nuclear security, these innovations are examined in three sectors, and in the following, the interaction of security with safety and safeguards is discussed.

A: Instruments

Like all sciences and industries, nuclear energy also seeks the correct use of today's technologies in order to improve its status, including nuclear security. Thus, choosing appropriate instrument is crucial. For instance, identifying malicious acts is one of the priorities in managing and establishing security in nuclear facilities. The use of deep learning technology and computer modeling to investigate people's behavior in order to identify malicious behaviors is one of the topics of interest in this field. Among these, logical models such as data-based reasoning method, graph-based reasoning method, pose estimation, object detection, and action recognition can be mentioned [5]. Based on the goals of the fourth industrial revolution and considering the increasing role and importance of blockchain in all scientific and industrial sectors, its use in nuclear industry and specifically nuclear security is considered in various studies. Furthermore, it is worth mentioning, the use of blockchain-based monitoring system for improving security of materials through providing a secure network [9]. The pervasive use of artificial intelligence has also entered the field of nuclear security: using AI based on machine learning for surveillance or for detection of dangers, people and objects [10].

B: Strategies

In reviewing nuclear security management strategies, it is important to consider the global, regional and national situation and conditions. For example, in studies in the field of nuclear security in Asia, the strong role of India and Pakistan and the movement of China in the progress of benefiting from nuclear knowledge in all practical levels are taken into account [7]. Obviously, considering the cons and pros of nuclear energy, IAEA and states, try their best to follow plans and roadmaps which can be helpful in order to optimize using this energy simultaneously with its risk reduction. Following the principles and measures of Nuclear Material Accounting and Control (NMAC) is one of these solutions. The innovation and training of NMAC is a defense strategy against nuclear terrorism by creating a system for tracing, auditing and safeguarding nuclear materials by promoting prevention, detection, reducing insider risk, strengthening physical

protection measures, increasing international interaction and creating deterrence which can reduce the risk of deviation from peaceful objectives and nuclear security incidents [6].

C: Infrastructures

Some researchers focus on training role to strengthen the foundations of nuclear security. Holding events and meetings in the field of nuclear security has accomplished in order to increase the participation of all related institutions in the field of nuclear security such as Agency, the United Nations, Interpol, the Global Initiative to Combat Nuclear Terrorism and so on [4]. In basic nuclear security reviews, it is important to consider up-to-date threats based on technological advances. These technologies may facilitate or increase access to facilities and nuclear and radioactive materials, as well as the possibility of sabotaging them. Among the technological threats in this field, it should be noted the drone threat and cyberattack [10].

Challenges

Alongside all advantages, advancements in nuclear energy, reactors and weapons have created challenges for the security of countries [2]. According to NSS20[1], state is responsible for ensuring the security of nuclear material, other radioactive material, associated facilities and activities, within the state. Therefore, they must be aware of threats and challenges in this regard [16]. Among the security threats investigated in the studies regarding the relationship and type, the threats of cyber-attacks and related to artificial intelligence as well as the threats of information dissemination in nuclear security are important [1]. However, the growth and development of technologies also brings challenges. For instance, facilitating access to information, problems arising from free access to the Internet may cause problems [6]. Moreover, drone threat might be the possibility of stealth smuggling, stealth reconnaissance and sabotage or for cybersecurity concerns arias from the diversity of different digital systems in nuclear facilities, which leads to variety in cyber risks [10].

Approaches

According to numerous applications of new technologies, they can be used as new methods to improve nuclear security. Along with that, it is important to adopt a suitable approach to reduce risks and catch up the maximum benefits. One of these practical approaches is taking advantage of drones to strengthen nuclear security and aerial surveillance and dealing with drone risks, with combination of detection systems and countermeasures. Plus, dealing with cybersecurity risks can be performed by access control management, prohibiting receiving information from external networks and data storages, cybersecurity training, etc. [10].

Safety and Security Interface

Examining the interface between safety and security in nuclear power plants, nuclear facilities and activities is done with the aim of improving their performance and reaching resistance against cyberattacks, high flexibility against digital systems and networks [11]. In line with the development of technologies, resolving conflicts between safety and security in physical protection, cybersecurity and emergency preparedness is necessary for safe and secure operation of facilities [12]. Meanwhile, constructive interaction between safety and security in nuclear facilities requires structural support, organizational culture and proactive management (structural, functional and cultural) [13].

3S and Innovation

Improvement and development at the points where there is interaction of different fields, should be done keeping in mind the ultimate goal of optimal performance. Therefore, in the nuclear field, progress in all three sectors of safety, security and safeguards should be performed in an interactive way in order to achieve the appropriate operation in nuclear facilities [15]. Table2. explains the differences of goals and approaches of 3S.

Table2. 3S goals and approaches [16&17]

Interaction between 3S			
Concept	Goal in Normal Situation	Goal in Event Situation	Responsiveness
Safety	Unintended Events	Accident control to mitigate human and environmental harm	Society
Security	Advertent Events	Security analysis and security control of event	State Security Entities
Safeguards	Preventing the diversion of nuclear materials and activities from civil usages to military applications	Responding to IAEA	IAEA

[1] Nuclear Security Series No.20

Conclusions

Due to the increasing importance of nuclear energy and the growth of technologies, the role of new technologies in nuclear security was considered in this research. By examining the studies, it was tried to examine the innovations in this sector in three categories of instruments, strategies and infrastructures, as well as the interaction of nuclear security with safety and safeguards, considering the role of innovations. Ultimately, it is clear that innovations and measures in the field of nuclear security in all three sectors of instrumrnts, strategies and infrastructure must be carried out in sync with each other, with appropriate policies, targeted and accurate tools and strong infrastructure, to obtain nuclear security goals globally in nuclear facilities, countries and societies.

References

[1] Rolenc, J. M. (2020). Technological change and innovation as security threats. In SHS Web of Conferences (Vol. 74, p. 02015). EDP Sciences.

[2] Crowe, S. D. (2018). Nuclear innovation and national security (Doctoral dissertation).

[3] Shubayr, N. (2024). Nuclear security measures: A review of selected emerging technologies and strategies. Journal of Radiation Research and Applied Sciences, 17(1), 100814.

[4] Bufford, J. (2023). Fostering Nuclear Security Leadership and Innovation-Lessons Learned from 10 Years of Global Dialogue.

[5] Li, Z., Song, X., Chen, S., & Demachi, K. (2024). Data, language and graph-based reasoning methods for identification of human malicious behaviors in nuclear security. Expert Systems with Applications, 236, 121367.

[6] Onyeanu, E. O., Ikechukwu, E. M., Ahmed, A. T., & Bamanga, B. (2023) Strengthening Nuclear Material Accountability & Control (Nmac) Against Terrorism in Norther Nigeria: A Progressive Global Training Approach.

[7] Mohan, A. Nuclear Security Architecture of South Asia.

[8] Li, Z., Song, X., Chen, S., & Demachi, K. Malicious behaviors identification in nuclear security based on visual relationships extraction and knowledge reasoning.

[9] Auda, J. (2023). The Trust Machine: Blockchain Technology in Nuclear Security and Prospects for Application in the Middle East. In International Conference on Nuclear Security: Sustaining and Strengthening Efforts. Proceedings of an International Conference.

[10] Kalinichenko, Y. E. V. H. E. N. (2019). Emergence of Technological Threats and Opportunities for Nuclear Security in the Digital Age. Published online.

[11] e Silva, R. B., Piqueira, J. R. C., Cruz, J. J., & Marques, R. P. (2021). Cybersecurity assessment framework for digital interface between safety and security at nuclear power plants. International Journal of Critical Infrastructure Protection, 34, 100453.

[12] Baek, M., & Oh, S. (2021, May). A Study on the Improvement of Nuclear Safety-Security Interface Management. In Transactions of the KNS Spring Meeting.

[13] Ylönen, M., & Björkman, K. (2023). Integrated management of safety and security (IMSS) in the nuclear industry–Organizational culture perspective. Safety science, 166, 106236

[14] Physical protection of nuclear material and nuclear facilities (implementation of INFCIRC 225),

[15] IAEA, 2018

[16] Nuclear power for sustainable development, IAEA, 2017

[17] Objective and essential elements of a state's nuclear security regime (NSS20), IAEA, 2014

[18] Establishing the Nuclear Security Infrastructure for a nuclear power program (NSS 19), IAEA, 2013

[19] Fundamental safety principles, IAEA, 2006

[20] INFCIRC/153, 1972

[21] INFCIRC/214, IAEA, 1974

ICNST 2024 International Conference on Nuclear Science and Technology
6- 8 MAY 2024 | Isfahan, Iran

Designing a wide field of view gamma camera to imaging nuclear contamination (Paper ID: 1517)

Mohammadreza Hosseini Safa, Hamidreza Shakur*, Seyyed Mohammadreza Hashemi[3]

Science and technology center of physics, Faculty of basic science, Imam Hossein comprehensive university, Tehran, Iran

Abstract

Today, nuclear imaging is considered an important issue because it has been applied in many fields, including nuclear medicine, industrial surveys, environment monitoring, and homeland security. Coded Aperture Imaging (CAI) has been proposed as an alternative collimation technique in nuclear imaging. In this paper, we've designed a Modified Uniformly Redundant Array (MURA) Coded Aperture Imaging (CAI) system which is predicted to have good properties and sensitivity. The CAI system is designed to be a NaI(Tl) detector with dimensions of 27×27×2 cm3 and a rank 19 tungsten musk with hole dimensions of 0.73×0.73 cm2 and thickness of 0.6 cm enlarged with the "mosaic" method (2×2 mosaic structure and 37 mosaic rank) to increase the Fully Coded Field of View (FCFV) which is placed at a distance of 3 cm from the detector. In order to demonstrate the performance of the designed coded aperture, Monte-Carlo simulations of the encoding process have been performed using Gate code and the encoded images have been reconstructed with the Maximum-Likelihood, Expectation-Maximization (MLEM) algorithm. The results showed that the designed coded aperture could clearly identify the location of the 241Am surface source at a distance of 10 meters from the system and at an angle of 50 degrees to the line perpendicular to the system along the horizon. Also, the results showed that the minimum detectable activity (MDA) of the proposed coded aperture under the aforementioned geometry is equal to 5 μCi.

Keywords: Gamma camera, nuclear imaging, coded aperture, Gate code.

Introduction

Technology and the ever-increasing use of radioactive source by mankind, in industry, agriculture, research, medicine and pharmaceuticals, have made the use of radioisotopes increasingly inevitable. Nuclear threats have expanded in parallel with this wide range of applications. In addition to the threats of nuclear war due to the large number of nuclear weapons, another important threat is related to the leakage of radioactive materials or the destruction of nuclear facilities due to natural disasters or human

accidents. Perhaps the most important nuclear threat is the threat related to radiation terrorism [1]. The risk of the use of nuclear weapons or of nuclear or radioactive material by terrorists only began to be acknowledged as a real threat at the beginning of the ^{21}st century [2]. While the human and environmental consequences of a terrorist attack with nuclear or radiological materials are barely imaginable, the threat of nuclear terrorism is real [3]. Today, nuclear imaging is considered an important issue because it has been applied in many fields, including nuclear medicine, industrial surveys, environment monitoring, and homeland security [4]. In security applications, coded-aperture-based gamma cameras can provide spatial and spectral maps of the radioactive elements in the environment [5]. Coded-aperture imaging technology has been successfully applied to arms control and nonproliferation applications. Compared with Compton cameras, radiation imagers based on coded-aperture designs can have superior angular resolution, a wider measurable energy range, simultaneous multinuclide identification, dose linearity and sensitivity [6]. Another motivation arises from the fact that many times large volumes of radioactive waste are concentrated in one single isolated region of that large volume. By quickly identifying such scenarios, it would become possible to optimize the classification procedures, and eventually reduce the total amount and costs for nuclear waste disposal [7]-[9].

Well-established means for gamma-ray imaging consist of a collimator in front of a gamma-ray detector for uncorrelated emissions of gamma rays [10]. A collimator is required to define the incident direction of the photon since it is not possible to focus gamma rays as in optical lens systems effectively and with large field-of-view. Collimator-based systems are realized as tungsten or lead plates with parallel hole, fan-in or fan-out, single, or multiple pinholes or spatially or temporarily modulated aperture geometries. Alternatively, coded appertures can be used instead collimator of parallel cavity beamformers [11]. The main advantage of coded apperture imaging (CAI) system is increasing light collection efficiency compared to other imaging methods [13]. In this article, we've developed a Modified Uniformly Redundant Array (MURA) Coded Aperture Imaging (CAI) system which is predicted to have good properties and sensitivity. In order to demonstrate the performance of the designed coded aperture, Monte-Carlo simulations of the encoding process have been performed using Gate code and the encoded images have been reconstructed with the Maximum-Likelihood, Expectation-Maximization (MLEM) algorithm. Peak signal-to-noise ratio (SNR) was used to evaluate of the quality of reconstructed images. Also, the minimum detectable activity (MDA) of the proposed

coded aperture was determined using the ^{241}Am surface source at a distance of 10 meters from the system and at an angle of 50 degrees to the line perpendicular to the system along the horizon. The importance of this research relies on the study of radioactive source localization, especially in security cases such as preventing nuclear terrorism, nuclear disarmament, border monitoring and decontamination; Because often the actual location of the radioactive source is unknown.

Research Theories

In this study, the coded aperture MURA mask performance and minimum activity are derived through computational simulations. GATE software, which is a framework based on GEANT4, is used to ascertain the detector response when the source location, activity and other related parameters. The detector and mask parameters input to GATE software for the coded-aperture imaging (CAI) system simulation is shown in Table 1. The CAI system is designed to be a NaI(Tl) detector with dimensions of 27×27×2 cm^3 and a rank 19 tungsten musk with hole dimensions of 0.73×0.73 cm^2 and thickness of 0.6 cm enlarged with the "mosaic" method (2×2 mosaic structure and 37 mosaic rank) to increase the Fully Coded Field of View (FCFV) which is placed at a distance of 3 cm from the detector. As shown in Fig. 1, a tungsten-based coded aperture with an 19×19 normal MURA pattern and a centered-mosaic MURA pattern was designed, and demodulation pattern were obtained and used for the radiation source image reconstruction.

Table 1
Monte Carlo simulation conditions for the mask to find minimum detectable activity

Mask material	Tungsten (W.p = 19.3 g/cm^3)
Rank	19
Mask cell size	0.73×0.73 cm^2
Detector size	0.73×0.73 cm^2
Mask pattern	MURA
Scintillator pixel size	7×7×20 mm^3
Source energy	59.5 keV

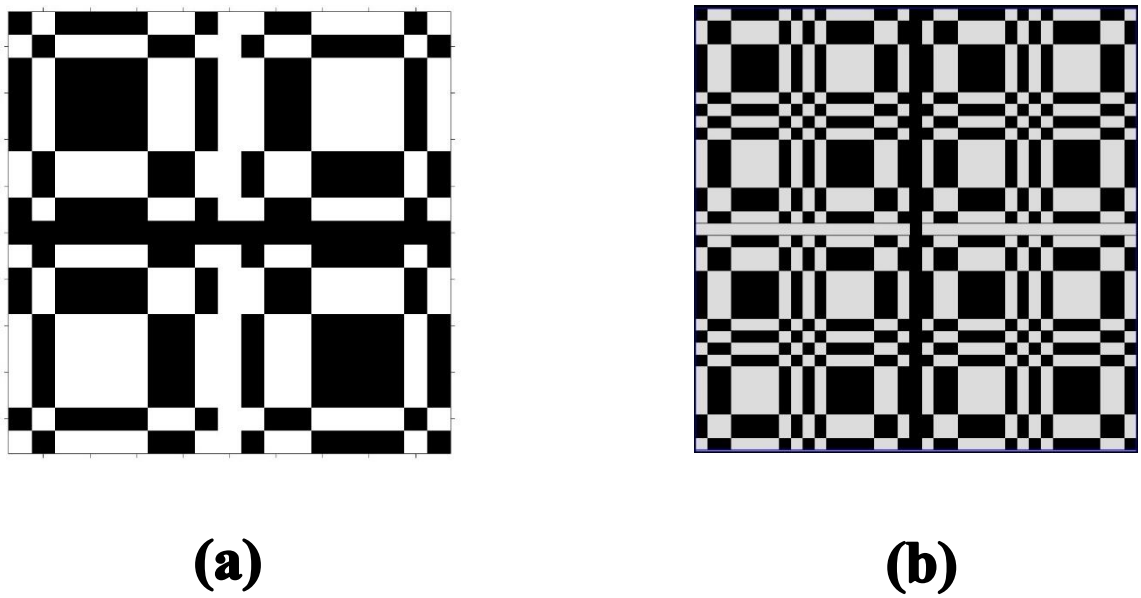

Fig. 1. (a) Normal MURA (rank 19) pattern and (b) centered mosaic MURA pattern (37×37) for the Gate simulation

The quantity of signal-to-noise ratio obtained from equation 1 was used to evaluate the images. This ratio for each image is defined as the difference between the maximum value of the image and the average value of the image, divided by the standard deviation of the image:

$$\mathrm{SNR} = \frac{(max(I) - mean(I))}{\sigma(I)} \quad (1)$$

The reconstruction of the image as well as the MLEM statistical repeatability method in this study is the same as the method presented in the authors' previous work [12].

Results and Discussion

Evaluation of the performance of the designed system was done using the ^{241}Am surface source at a distance of 10 meters from the system and at an angle of 50 degrees to the line perpendicular to the system along the horizon. The imaging time was selected as 60 seconds. Fig. 2 shows the schematic diagram of simulated setup used to evaluate the performance of the designed system. In order to derive the MDA, qualities of the reconstructed images were assessed using the SNR quantity when increasing the ^{241}Am source activity ranging from 0.2 mCi to 0.005mCi.

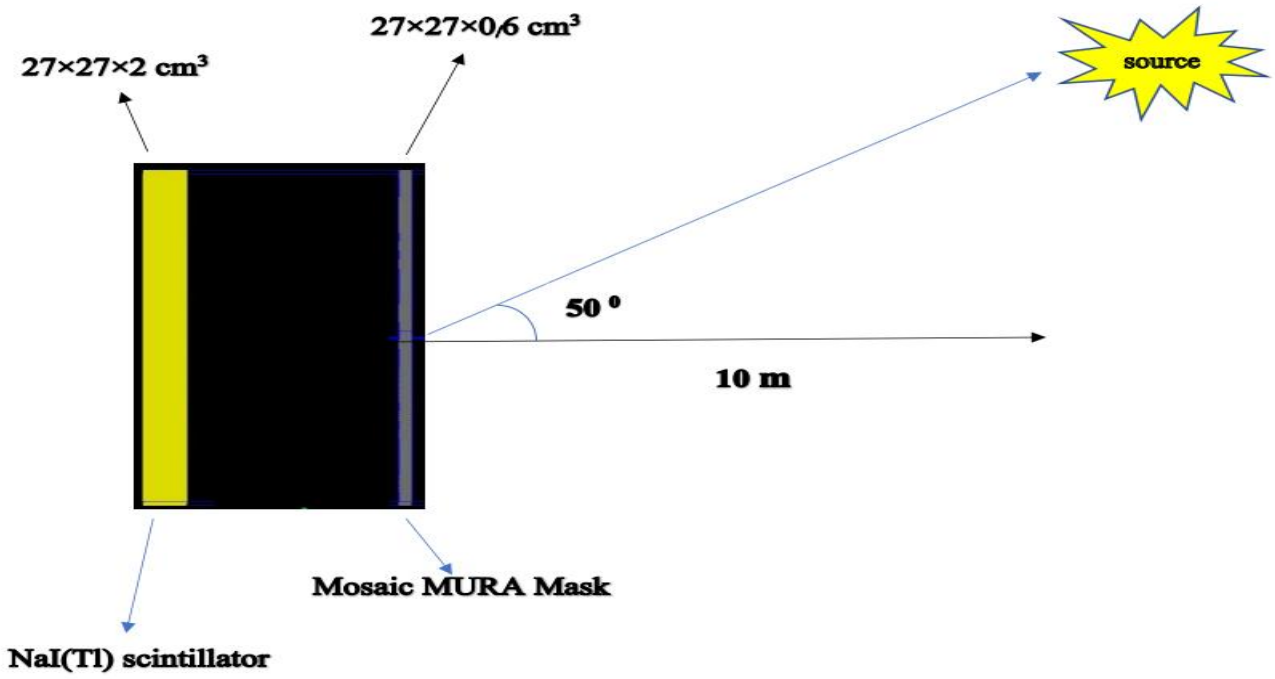

Fig. 2. Schematic diagram of experimental setup used to gamma camera with the MURA mask to find minimum detectable activity

Figure 3 shows the raw and denoised image after 10 iterations of MLEM algorithm for 0.2 millicury ^{241}Am source. It clear from this image that the location of the ^{241}Am source was correctly identified and located. the signal-to-noise ratio of the raw image was 6.66, which is a large and suitable value for image reconstruction so that the source can be recognized without denoising.

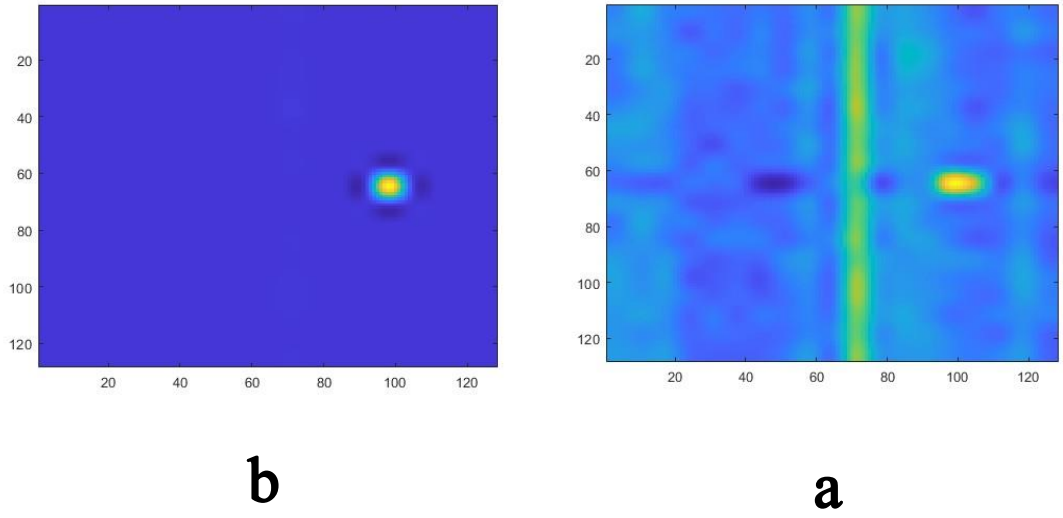

Figure. 3. a) raw image b) denoised image after 10 iterations of MLEM algorithm

In the next step, the source activity of ^{241}Am was decreaced to 0.02 mCi while other parameters of set up was kept unchanged. Figure 4 shows the raw and denoised image after 10 iterations of MLEM algorithm for 0.02 millicury ^{241}Am source. It clear from this image that the location of the ^{241}Am source was correctly identified and located again but the signal-to-noise ratio of the raw image was decreased to 5.29. However, this signal-to-noise ratio value is adequate for image reconstruction so that the source can be recognized without denoising.

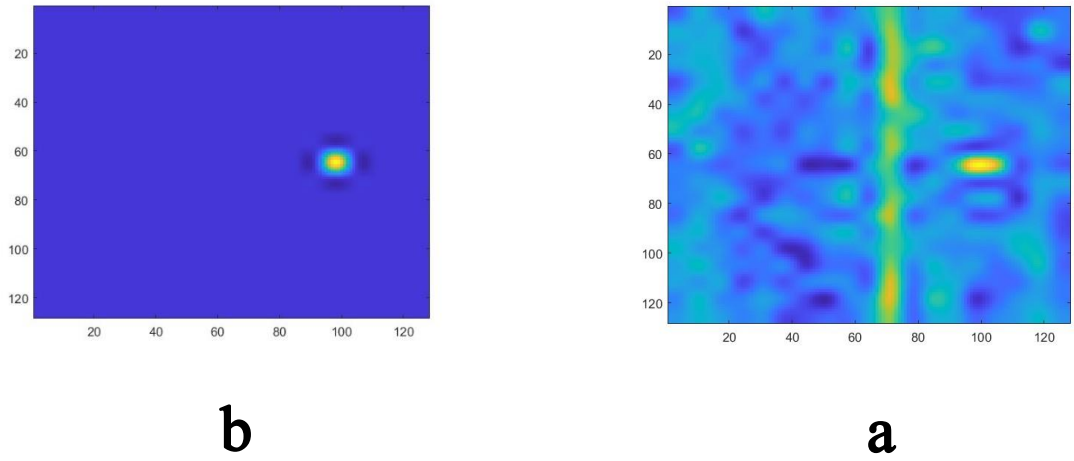

Figure. 4. a) raw image b) denoised image after 10 iterations of MLEM algorithm

In the next step, the source activity of ^{241}Am was decreaced to 0.005 mCi while other parameters of set up was kept unchanged. Figure 5 shows the raw and denoised image after 10 and 100 iterations of MLEM algorithm for 0.005 millicury ^{241}Am source. It clear from this image that the raw captured image is so blurry that location of the ^{241}Am source was not correctly identified. The signal-to-noise ratio of the raw image was decreased to 3.62. This signal-to-noise ratio value is so bad that even the denoised image after 10 iterations of MLEM algorithm was still somewhat blurry. However, the denoised image after 100 iterations of MLEM algorithm has a good quality so that location of the ^{241}Am source was correctly identified and located.

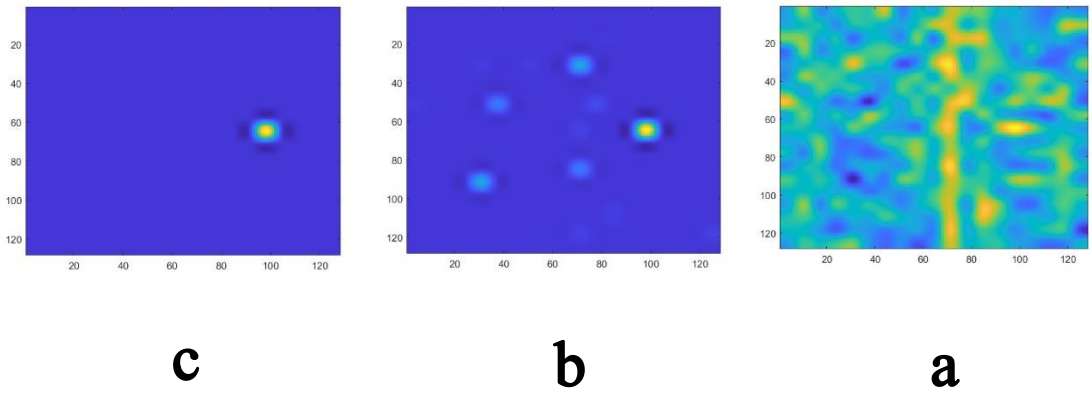

Fig. 5. a) raw image b) denoised image after 10 iterations of the MLEM algorithm c) denoised image after 100 iterations of the MLEM algorithm

Finally, the peak signal-to-noise ratio (SNR) of the captured gamma camera images was evaluated as a function of the ^{241}Am activity (Figure 6). As clear from this figure, a decreasing trend in SNR values was observed with deacreasing ^{241}Am activity. This is because, with the deacresing of the activity of the ^{241}Am source, the flux of photons reaching the gamma camera will decrease, and as a result, the image will not have a good quality.

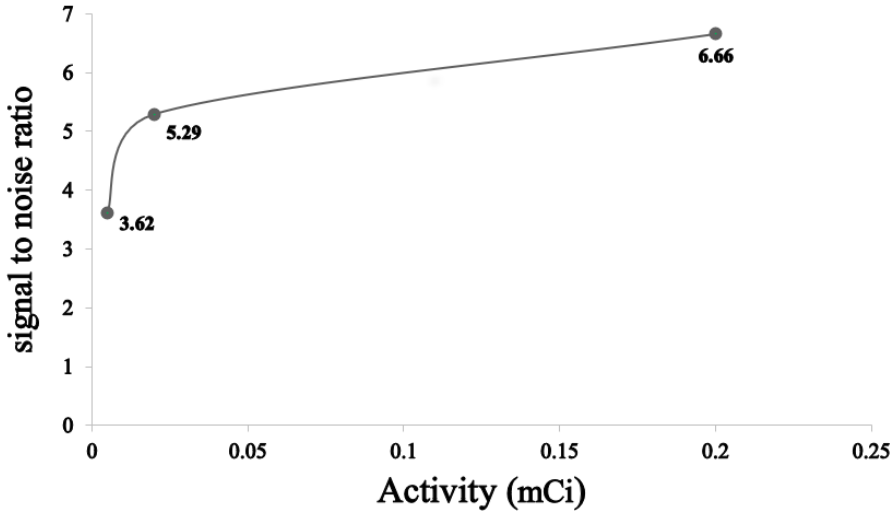

Fig. 6. the peak signal-to-noise ratio (SNR) of the captured gamma camera images as a function of the ^{241}Am activity

Conclusion

In this study, computational simulations using Monte-Carlo Gate software successfully were performed to evaluate the performance of the coded aperture imaging system for a handheld realtime imaging instrument. The proposed system is designed to be a NaI(Tl) detector with dimensions of 27×27×2 cm3 and a rank 19 tungsten musk with hole dimensions of 0.73×0.73 cm2 and thickness of 0.6 cm enlarged with the "mosaic" method (2×2 mosaic structure and 37 mosaic rank) to increase the Fully Coded Field of View (FCFV) which is placed at a distance of 3 cm from the detector. Results showed that the minimum detectable activity (MDA) of the proposed coded aperture for the ^{241}Am surface source at a distance of 10 meters from the system and at an angle of 50 degrees to the line perpendicular to the system along the horizon is equal to 5 μCi. The importance of this research relies on the study of radioactive source localization, especially in security cases such as preventing nuclear terrorism, nuclear disarmament, border monitoring and decontamination; Because often the actual location of the radioactive source is unknown.

References

[1] Hamidreza Shakur, Getting to know the threats of modern warfare in Pertovi area, Imam Hossein University of Officers and Guard Training (AS), 1400: p. 215-190 and 156-154.

[2] Cieslak, M.J., Coded-aperture imaging systems: Past, present and future development e A review., Radiation Measurements. 2016: p. 92 , 59-71.

[3] Tsoulfanidis, N., Measurement and detection of radiation. 2010: CRC press.

[4] Saha, G.B. and G.B. Saha, Fundamentals of nuclear pharmacy. Vol. 6. 2004: Springer.

[5] Wernick, M.N. and J.N. Aarsvold, Emission tomography: the fundamentals of PET and SPECT. 2004: Elsevier.

[6] Fenimore, E.E. and T.M. Cannon, Coded aperture imaging with uniformly redundant arrays. Applied optics, 1978. 17(3): p. 337-347.

[7] Park, S.; Boo, J.; Hammig M.; Jeong, M. "Impact of aperture-thickness on the real-time imaging characteristics of coded-aperture gamma cameras "; NET. 2021, 53, 1266-1276. doi.org/10.1016/j.net.2020.09.012

[8] Meißner, T; Nahm, W; Hesser, J; Löw, N. "Simulation Study on Super-Resolution for Coded Aperture Gamma Imaging"; Med-Ph. 2023. doi.org/10.48550/arXiv.2306.08483

[9] Liu, Y; Shuai, L; Li, D; Liu, S; Wang, Y; Zhou, W; Huang, H; Wang, X. "High-sensitivity stereo coded aperture gamma camera for three-dimensional localization of radioactive hotspots"; AIP Adv. 2022. 12. doi.org/10.1063/5.0096865

[10] He, W ; Wang, Y; Liang, X; Zhou, W; Zhu, Z; Han, H; Zhai, J; Zeng, X; Feng, B; Tang, H; Li, D; Long Wei, Z.Z; Huang, X. "High-performance coded aperture gamma camera based on monolithic GAGG: Ce crystal"; ISO4 Appl. Radiat. Isot. 2021, 92. doi.org/10.1063/5.0035991

[11] Zhu, B; Wang, Z; Gao, T; Chen, Q; Huang, Q; Mao, X; Zhao, C; Tao, M; Qi, P; Zhao, Q; Chaowen Yang, Y.L.R.Z. "A new contrast-to-noise ratio for image quality characterization of a coded-aperture γ camera"; ISO4 Appl. Radiat. Isot. 2021. doi.org/10.1016/j.apradiso.2021.109592

[12] Hashemi, S.M; Hosseinkhani, P; Shakur, H. "Simulation and performance evaluation of coded aperture gamma imager system with wide field of view". Measurement and radiation safety, 2023, 12, 111-120 (Persian in). doi.org/10.22052/rsm.2023.252810.1020

ICNST 2024
International Conference on Nuclear Science and Technology
6- 8 MAY 2024 | Isfahan, Iran

I&C Cables Qualification for Existing NPPs Without Previous EQ Plan Utilizing Cable Specimens (Paper ID: 1532)

Darbandsari A.[1*], Ahmadian S.[1], Haghighatpour H.[1]

[1]Electrical and Instrumentation, TAVANA, Tehran, Iran

Abstract

Instrumentation and control (I&C) cables by transmitting important measurement, control and protection signals such as neutron flux, dose-rate, temperature, pressure, short-circuit and so on to control and decision centers and keeping the integrity between sub-systems play a key role in maintaining the security of nuclear power plants (NPPs). Therefore, ensuring of I&C cables qualification is a vital issue. Because, I&C cables failure can lead to serious events and disruptions in the operation of the NPP and its safety related systems. This paper presents a comprehensive program for the qualification of I&C cables which contains of cable specimens optimal placement (i.e., location, number and length of specimens), periodical functional post-ageing tests (including electrical, mechanical and design basis events (DBE)) for existing NPPs without previous environmental qualification (EQ) plan. In addition, in this paper, several practical condition-based monitoring techniques are introduced, which are used as a supplement to the qualification program, to ensure the qualification of the cables between two consecutive qualification periods (e.g., 5 years).

Keywords: Existing Nuclear power plant, Environmental qualification (EQ), Condition monitoring, Instrumentation and control (I&C) cables, Safety-related systems.

I. ABBREVIATION

I&C	Instrumentation and Control	SCAP	SCC and Cable Ageing Project
NPP	Nuclear Power Plant	EQDB	Equipment Qualification Data Bank
EQ	Environmental Qualification	LOCA	Loss of coolant accident
DBE	Design Basis Event	HELB	High energy line break
CM	Condition Monitoring	MSLB	Main steam line break
XLPE	Cross-linked Polyethylene	TGA	Thermogravimetric Analysis
EPR	Ethylene-Propylene Rubber	CI	Condition Indicator
PVC	Polyvinyl Chloride	EAB	Elongation at Break
EPDM	Ethylene Propylene Diene Monomer	EPRI	Electric Power Research Institute
EPR	Ethylene-Propylene Rubber	NRC	Nuclear Regulatory Commission
PEEK	Polyether Ether Ketone	TID	Total integrated dose

II. Introduction

After the accident at the Fukushima nuclear power plant, safety issues have received more attention [1]. It is necessary that safety-related systems continue to perform their tasks following a DBE. The word “Safety” is related to both radiation risks under normal conditions and radiaton risks as a consequence of accidents [2]. Environmental Qualification (EQ) is a preocedure which demonstrate that an equipment is capable to perform its safety functions in normal and DBE environment throughout their qualified life [3]. NPPs contain of hundreds kilometers of electrical cables including control, instumentation, AC power, DC power and telecommunication. The contribution of each of these cables in a typical NPP [4] is shown in Fig 1. As it can be seen, control and instrumentation cables, account for a significant share of about more than 80% of power plant cables, which shows the high importance of these cables. Major replacement of electrical cables in existing NPPs is both impractical and unaffordable. Thus, the assurance of the health of installed cables is important to have confidence that aged cables will perform when needed.

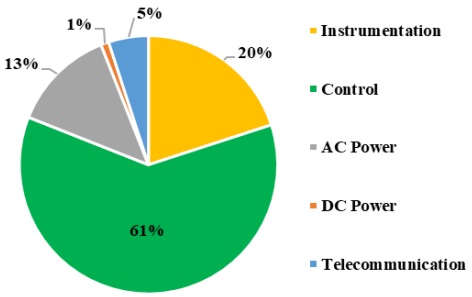

Fig. 1. The share of each type of power plant cables [4]

From the point of reliability the most important part of electrical equipment is the insulation. The most important property of the insulation is the dielectric strength. The insulation system has to satisfy other requirements (physical, chemical, mechanical, electrical etc.) in its lifetime. The most commonly used insulation materials for electrical cables in NPPs are XLPE, EPR, EPDM, PEEK and PVC [5]. More information about cables specifications including type, voltage, total length installed, average service temperatures, average service dose rate, insulation material, jacket material and so on has been presented in [6]. Because, passing through several different operating environments over the length of cable route throughout the NPP, cables are exposed to many stresses, e.g., mechanical stresses, thermal, chemical and physical stresses (moistening, radiations, and different kinds of pollution from air) from the environment. Portions of such a cable may pass through harsh environmental conditions, such as

high temperature, high radiation, high humidity or moisture. Harsh stressors can cause excessive ageing and degradation in the exposed sections of a cable system that could shorten its life and cause unexpected early failures [7]. Due to the stresses in operation, the molecular structure of the insulation material suffers different changes. In most cases the changes of the material structure manifest in the alteration of physical properties.

In general, there are two methods to evaluate the condition of cables in the NPP: the accelerated ageing method and the method of using cables specimens. In the accelerated ageing method, the equivalent ageing time in operating conditions is estimated by Arrhenius equation as below [5]:

$$\frac{t_s}{t_a} = e^{(\frac{E_a}{k})(\frac{1}{T_S}-\frac{1}{T_a})} \qquad (1)$$

Where E_a is the activation energy (eV), k is the Boltzmann's constant ($8.617 \times 10^{-5}\ eV/°K$), t_a is the accelerated ageing time (hr), t_s is the operating time (hr), T_a is the thermal ageing temperature ($°K$) and T_S is the operating temperature ($°K$).

The main drawback of this method is high uncertainty. In fact, the results are not reliable for ageing at operating conditions because of Inverse temperature effect, Dose-rate effect and Diffusion limited oxidation. On the other words, the input parameters of this method, such as the activation energy strongly affect the output [8]. For instance, Fig. 2 shows the calculated qualified life according to activation energy error. As it can be seen, a small error in the assumed activation energy will change the calculated qualified life by several years [9].

Several articles have been written about evaluating cables condition using the accelerated ageing method, for example, in reference [10] the cables of the Wolsung NPP unit 1 were revaluated for extending the lifetime in Korea.

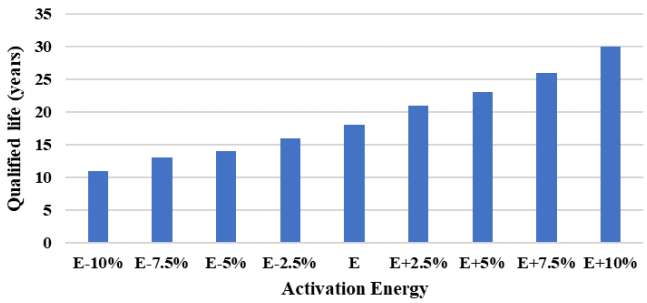

Fig. 2. Activation energy measurement error versus life estimation

On the other hand, the evaluation of cables by the method of using cable specimens has received less attention. In this method, firstly, the critical places are identified in terms of ageing, then the optimal number and length of specimens are determined according to the qualification program defined for an operation period (e.g., 50 years). These samples are installed in designated places under special conditions from the beginning of operation, in order to experience conditions similar to cables in use. Then, in the qualification period, which is generally 5 years or the interval between three consecutives refueling stops [9], they are subjected to various functional tests in order to confirm their qualification for the next qualification period. The advantage of this method is that the results are closer to reality and the calculated qualified life is more accurate. Additionally, the main challenge of cables qualification is the impossibility of disconnection in operating conditions, which can be tackled by using the specimens placement technique.

The NRC recommends that condition monitoring techniques be used to ensure that worn plant cable insulation materials do not pose safety challenges, particularly in post-accident conditions. Among the condition monitoring techniques, especially those that are non-destructive are of interest to the nuclear industry [11]. In general, several methods have been presented in various references to assess the condition of cables, each of which has different advantages and disadvantages. But in the meantime, electrical methods such as insulation resistance voltage, partial discharge, etc. are more popular because most of methods use lower voltage than the nominal voltage, therefore the electrical methods are non-destructive ones. This paper presents a novel qualification method which is based on periodical tests on cable specimens. This method is suggested for old NPPs without a previous qualification plan. In addition, condition-monitoring methods are used as a supplement to proposed method which guarantees the correct performance of the I&C cables between the two consecutive qualification periods.

The rest of this paper is organized as follows. The proposed qualification method is introduced in Section III. Development of the proposed method for existing NPPs without previous EQ plan is explained in Section IV. Finally, the paper is concluded in Section V.

III. Proposed Qualification Method

Cable qualification is to demonstrate that the cable is capable to perform its safety functions in both normal and DBE condition during its qualified life. A Design Basis Event (DBE) is a postulated event

used in the design to establish the acceptable performance requirements of the structures, systems, and components e.g., LOCA, HELB or MSLB. Qualification methods are categorized to type testing, operating experience which is limited use in case of DBE and analysis which is not acceptable alone and can be used as a supplement to other methods [12].

CBQ is a developed version of EQ program which guarantees equipment performance. As shown in Fig. 3, the concept of CBQ is performing CM measurements during qualification stages. Fig. 3 demonstrates that degradation occures during ageing procedure, therefore performance capability decreases gradually. The CM type should be compatible with insulation material. Firstly, a basic CM (CM_0) is measured on a new cable (Stage 1), that will be compared with following measurements of CM. At stage 2, During ageing, CM_{ageing} is measured to show how the condition indicator (CI) changes during ageing. At stage 3, DBE test is done and at this point, The tests are conducted to determine the ability of the cables to function during postulated environmental conditions simulating normal and design basis event/LOCA service conditions expected within the containment area of nuclear power generating station and $CM_{post\text{-}DBE}$ is measured. Finally, at stage 4, The post-accident condition is simulated for equipments required after the DBE, and CM is measured again ($CM_{Post\text{-}DBE\ period}$). The CM value after the post-accident period should pass the acceptance criteria. If the equipment pass the tests, the equipment will be qualified for the next EQ period. Otherwise, the equipment is unqualified and corrective action including repair or replacement should be considered. The capability curve of the cables which are installed in mild environments is show by dotted line in Fig. 3. Cables in mild environments will not experience DBE condition during lifetime and their capability curve as shown does not have any steep slope. In this condition, qualification is not needed and periodical condition monitoring (regular walkdowns) is enough to ensure their health [12].

A. Cable Specimens Requirements

In this section, the requirements related to the cable specimen, including the type, number, length, marking and installation method are described. The types of specimens for testing contain complete cable, insulated wire and insulation materials. For instance, coaxial cables are tested as complete cables to show that there is no undesirable interaction between different parts of a cable and to ensure that wire insulation is able to perform its required functions independent of the jacket material [12].

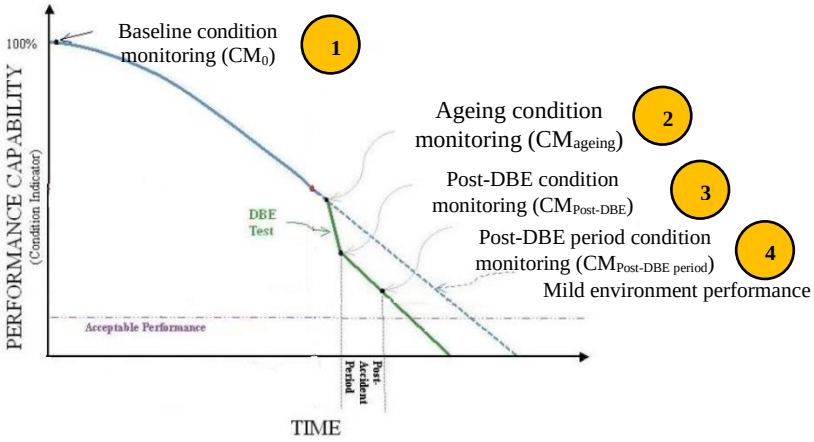

Fig. 3. Condition based-qualification methodology

Regarding the number of specimens, it is extracted from the qualification program. For example, if the lifetime of the power plant is 50 years and we want to repeat the qualification tests every 5 years, we should consider 10+1 samples of each selected cable for qualification. The 10 specimens are utilized for performing functional tests, and one specimen is intended for measuring the basic functional data for the cable. The number and length of cable specimens based on EQ program and economic constraints should be justified. According to IEEE standard minimum length of a cable specimen for DBE testing analysis is 3.05 m [12]. This amount of cable length should be directly exposed to the DBE environment condition. Therefore, it is recomended conservatively to consider longer samples. Apart from the length considered for performing the DBE test, another additional part of the cable length should also be allocated for performing destructive tests such as EAB and electrical tests. For example, a 6m sample can be divided into two parts, 5m for non-destructive tests (electrical) and 1m for destructive tests (mechanical). Other modes are also possible provided EQ requirements are met.

Marking cable samples is very important section of qualification procedure. The main objective of sample marking is to ensure that the test center is able to correctly identify samples throughout the qualification program and correctly refer to them in the qualification documents (i.e. qualification test, performance test report and qualification final report). Samples marking should be in such a way that they are durable and not distorted under the harsh conditions of various tests such as thermal, radiation and immersion [9].

Cable samples inside containment are usually installed in separate trays and stands as shown in Fig. 4. These samples are usually placed in critical places in terms of temperature, radiation and DBE conditions in the early years of the power plant, but subject to the use of the accelerated ageing method

(based on the Arrhenius law) in old power plants, these samples can also be used. By placing the samples in places with more critical conditions (harsher) than the majority of the power plant environment, the cable ageing warning can be received faster and appropriate corrective action can be taken. It is very important that the samples have unlimited access to air to avoid limited oxidation. Also, samples should be identified with the help of metal ID tags so that they do not deteriorate during the life of the power plant (often more than 50 years). Samples should be available in sufficient numbers to perform periodic condition monitoring tests. These samples are evaluated in specific intervals. This interval is usually defined every 5 years after ten years of the life of the power plant, and if significant deterioration is observed, this interval can be shortened.

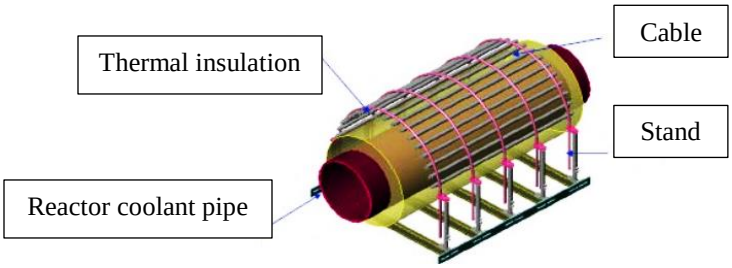

Fig. 4. The stand for specimen in the plant [13]

B. Cable Specimens Optimal Placement

In this section, the optimal placement of cable specimens has been discussed. The different zones of the plant with safety-related cables should be categorized based on environmental conditions including temperature and radiation dose for both normal and accident conditions. In the classification of power plant areas, other parameters such as humidity, vibration, etc., should be included if they are effective. Environmental indicators for evaluating normal operating conditions should preferably be based on the values specified in environmental monitoring. Power plant areas can be classified into different zones according to the table below.

Table 1. Zone classification at NPP [9]

Zone	environmental conditions		
	DBE	Maximum values in normal condition	
		Temperature (°C)	Radiation (Gy)*
I	×	≤40	$\leq 10^2$
II	×	≤50	$\leq 5 \times 10^4$
III		≤50	$\leq 5 \times 10^4$
IV**			

*TID at 50 years.

**Zone with environmental conditions sever than III (e.g. hot spot areas)

After classifying the areas of the power plant, the process of determining the optimal location for the installation of the cable specimens is carried out according to the flowchart Fig. 5.

C. Condition Monitoring

There are a wide range of cable testing inculding passive and active [9]. Passive methods are non-intrusive. For instance, visual and tactile inspection and infrared thermography. On the other hand, Active methods contain hands-on testing, such as mechanical, electrical, and chemical tests. Table 2 presents a compherensive comparison of common cable testing techniques. Mechanical techniques measure properties such as hardness, mass loss, viscoelasticity, or size. Mechanical testing methods mostly are destructive. Also, they can reveal only the condition of cable at the test location. Therefore, defects that may exsit at different points of cable length are not detected and located [9]. From electrical point of view the cable insulation is a lossy dielectric. It can be characterised by Breakdown voltage (dielectric strength), Specific resistance (specific conductivity), Permittivity, Loss factor (Tan δ). In the background, there are two dielectric processes: conduction and polarization. Most methods use lower voltage than the nominal voltage, therefore the electrical methods are non-destructive ones. The dielectric properties can be measured in time or frequency domain. Local tests contain Time domain reflectometry (TDR), Frequency domain reflectometry (FDR) including broadband impedance, JTFDR and LIRA as well as general electrical tests contain Dielectric loss (Tan δ) & permittivity, Insulation resistance and Return voltages. Table 3 shows perefered electrical condition monitoring methods with accpetance criteria in the proposed EQ program.

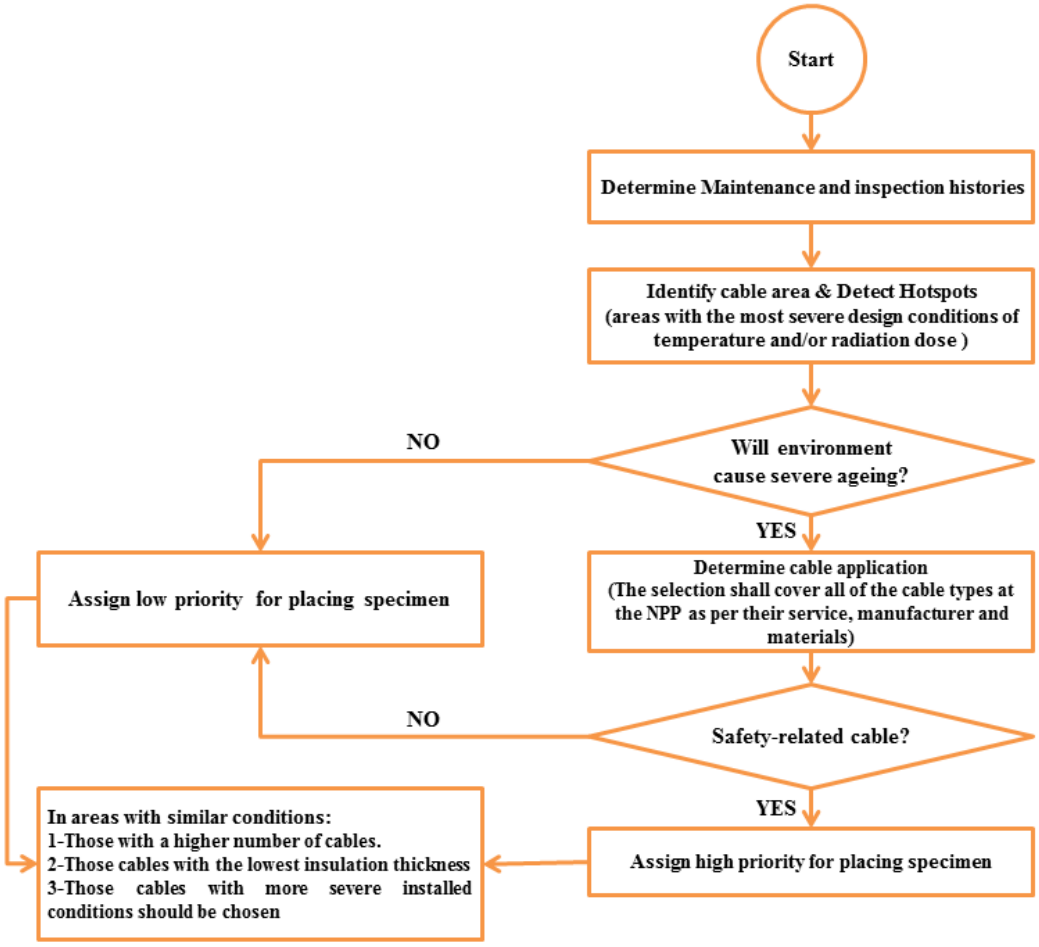

Fig. 5. Procedure of optimal placement cable specimens

IV. Development of The Proposed Method on Npp Without Previous Eq

When there is no previous EQ program for cables, the first step is to collect and find relevant information about the type of cable using available sources such SCAP and EQDB databases [12]. Then, an initial assessment should be done in order to find the significant deterioration of the existing cables in the power plant with the help of visual inspection, environmental monitoring and condition monitoring for the cables in the areas that have been exposed to the highest temperature and dose.

Table 2. Common condition monitoring methods

Cable Testing Technique	Application	Monitored property	Materials applicable
Visual/physical inspection	Detecting local damages such as cracks, color change, contamination, presence of chemicals spray or oils.	Visual	All
Thermography	Determining hot spots	Physical	All
Frequency domain reflectometry (FDR)	FDR and TDR are applicable for identifying any impedance mismatches throughout entire cable length.	Electrical	All
Time domain reflectometry (TDR)			
LCR	Inductance (L), capacitance (C), and resistance (R), are measured and used in addition to TDR and FDR to detect circuit defects such as open circuit, short circuit, humidity intrusion, or any age-related problems.	Electrical	All
Insulation resistance (IR)	IR test is utilized in order to measure the insulation quality of cable and its resistance.	Electrical	All
Reverse time domain reflectometry (RTDR)	Assessment of the quality of shielding around the conductor of a coaxial or triaxial cable.	Electrical	All
Elongation-at-break (EAB)	It expresses the capability of insulation material to resist changes of shape without crack formation.	Mechanical	All
Indenter	Indenter is correlated with Elongation-at-break in order to evaluate insulation condition.	Physical	EPDM, EPR, PVC, CSPE

Table 3. Suggested CM methods for proposed EQ

Cable Testing Technique	Instruction	Acceptance criteria	
		Control	I&C
Insulation resistance (Ω)	Applying 500V DC voltage for at least one minute	>1MΩ	>10 MΩ
Withstand Voltage (kV)	Following IR measurement, the mandrels including the samples will be immersed in room temperature water. While immeresed, the samples are exposed to withstand voltage test for at least 5 minutes.	>1MΩ	>10 MΩ
Leakage current (mA)	The voltage is applied 80V/mil AC and Leakage current is measured.	<5mA	<5mA
DBE	The cables are exposed to tempretaure and pressure profile of LOCA as well as certain chemical spary such as boric acid for certain days while they are energized at nominal voltage and current. Then, IR, withstand voltage and leakage current are measured which should be in acceptance range.		

If degradation is significant, priority is to replace those cables with qualified cables. Also, It is recommended to replace PVC cables to prevent fire (except halogen-free types). If the cables are not significantly aged, an EQ program should be created for the existing cables. For this purpose, it is necessary to use samples of identical cables in terms of materials, which are available in the storage in an un-aged form, or cables that are naturally aged in the environment of the power plant and have been replaced with qualified cables. Accelerated ageing process should be fully implemented for unworn cables coming out of storage that are similar in terms of wear to the cables installed in the power plant. In order to simulate accelerated wear, accurate knowledge of the activation energy is very important.

Some methods of measuring the activation energy are presented in [14]. if there is little information available on cable materials, it is prefered to replace existing cable with qualified cable. The flowchart of the suggested method is shown in Fig. 6.

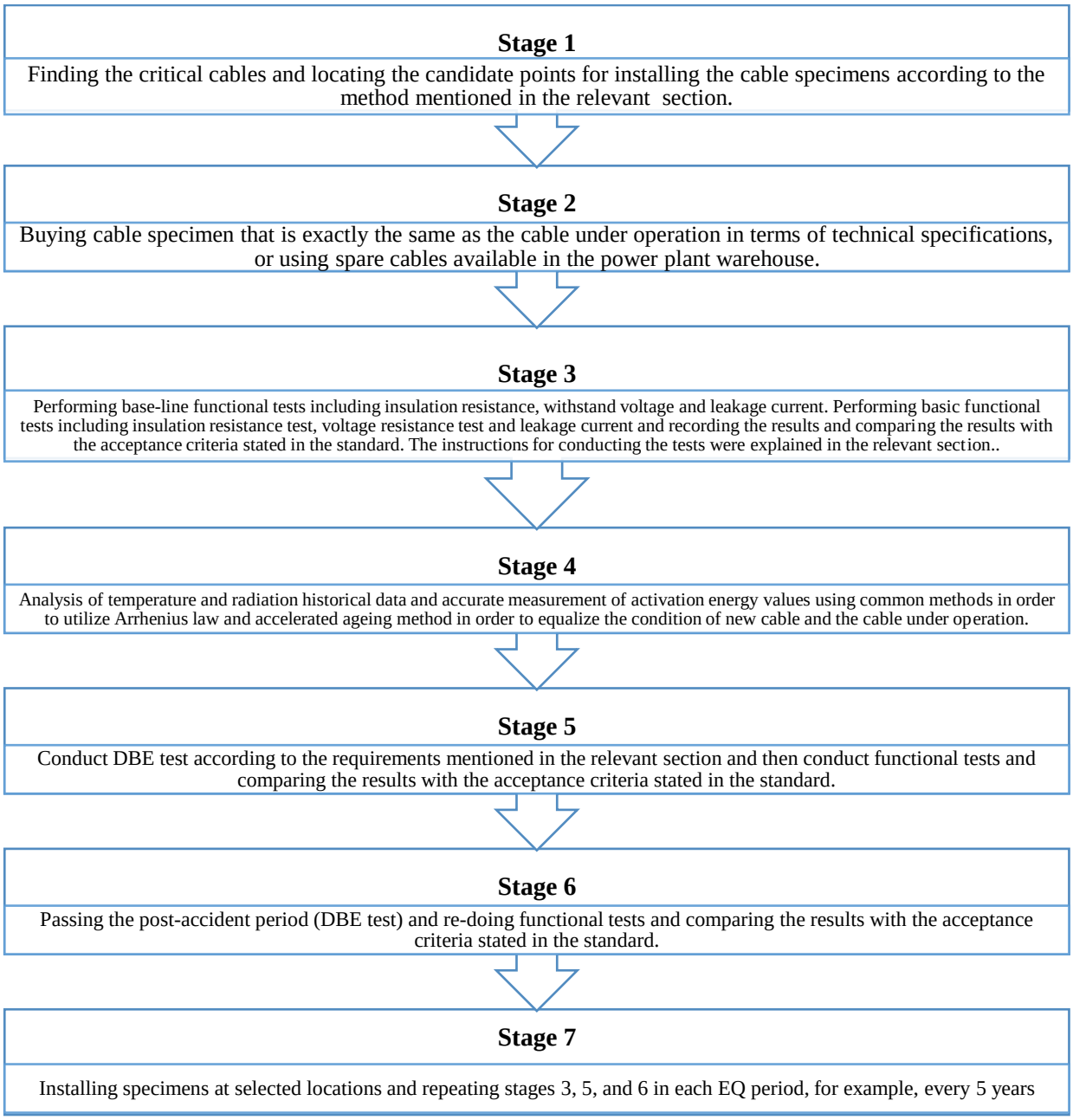

Fig. 6. The stages of proposed EQ method

V. Conclusions and Future works

This paper presents a novel procedure for the qualification of I&C cables. Unlike previous literatures that generally focus on CM techniques and conducting tests, this article firstly presents the qualification procedure by using specimen placement and their requirements, including location, length, number, installation and marking method. Then it introduces condition monitoring tests such as elongation at break, insulation resistance, FDR, TDR, etc. Also, in the introduction of CM tests, an attempt has been made to introduce a set that is technically more practical and can be performed in the field. Finally, this method can be implemented and used for all old NPPs that do not have a previous qualification program in order to extent the operating license or evaluate the current condition of the I&C cables. As the future works, it is suggested to implement the presented procedure practically for a power plant without previous EQ program and report its results.

References

[1] Lam, J.C., Cheung, L.Y., Han, Y. and Wang, S., 2022. China's response to nuclear safety pre-and post-Fukushima: An interdisciplinary analysis. Renewable and Sustainable Energy Reviews, 157, p.112002.

[2] IAEA Safety standard series No.SF-1, Fundamental Safety Principles, 2006.

[3] Guide, R., 2009. 1.211: Qualification of Safety-Related Cables and Field Splices for Nuclear Power Plants. US Nuclear Regulatory Commission.

[4] Liu, Frank. "Nuclear power station cables." The Global Cable Industry: Materials, Markets, Products (2021): 249-289.

[5] Ramteke, P. K., A. K. Ahirwar, N. B. Shrestha, VVS Sanyasi Rao, K. K. Vaze, and A. K. Ghosh. "Thermal ageing predictions of polymeric insulation cables from Arrhenius plot using short-term test values." In 2010 2nd International Conference on Reliability, Safety and Hazard-Risk-Based Technologies and Physics-of-Failure Methods (ICRESH), pp. 325-328. IEEE, 2010.

[6] Report on the first and second terms (2012-2017) of the NEA Cable Ageing Data and Knowledge (CADAK) Project. Available at: https://one.oecd.org/document/NEA/CSNI/R(2018)8/en/pdf

[7] Watson, S. and McDaniel, C., 2014. Electrical Cable Aging and Condition Monitoring Codes and Standards for Nuclear Power Plants: Current Status and Recommendations for Future Development.

[8] Choudhary, Maninder, Muhammad Shafiq, Ivar Kiitam, Amjad Hussain, Ivo Palu, and Paul Taklaja. "A review of aging models for electrical insulation in power cables." *Energies* 15, no. 9 (2022): 3408.

[9] IAEA Nuclear Energy Series, No.Np-T-3.6, Assessing and Managing Cable Ageing in Nuclear Power Plants''.

[10] Lee, S.H., Kim, M.Y., Jang, H.S. and Jeong, C.H., 2012, September. Evaluation of accelerated ageing cables used in nuclear power plant. In 2012 IEEE International Conference on Condition Monitoring and Diagnosis (pp. 681-684). IEEE.

[11] Boguski, J., and G. Przybytniak. "Benefits and drawbacks of selected condition monitoring methods applied to accelerated radiation aged cable." *Polymer Testing* 53 (2016): 197-203.

[12] INSTITUTE OF ELECTRICAL AND ELECTRONICS ENGINEERS, IEEE Standard for Qualifying Class 1E Equipment for Nuclear Power Generating Stations, IEEE Std 323-2003.

[13] SCC and Cable Ageing Project (SCAP) — Final Report, AEN/NEA (2010), www.oecd-nea.org

[14] Gong, Y., Tang, J., Sun, B.N., Yang, Z.G., Shi, X.Q., Liu, X.Q., Xie, Y.C. and Xu, X.L., 2018. Comparative study on different methods for determination of activation energies of nuclear cable materials. Polymer Testing, 70, pp.81-91.

ICNST 2024 International Conference on Nuclear Science and Technology
6- 8 MAY 2024 | Isfahan, Iran

Estimation of gamma dose rate in crane cabin during inspection and loading of spent fuel assemblies into a dual purpose cask. (Paper ID: 1602)

Bavarnegin E*, Abedi E, Keyvani M and Salartash R
[1]*Reactor and nuclear safety research school, NSTRI, Tehran, Iran*

Abstract

When the irradiated fuel assemblies are removed from the reactor core, they are placed in service pool for decreasing the residual heat and radioactivity. After about two years, the spent fuel assemblies can be transported to wet storage pool and after about 10 years they can be stored in dry cask. Loading of spent fuel assemblies into cask is very important in terms of radiation protection. Dual purpose cask (DPC) can be used for both transportation and storage of spent fuel assemblies. Two DPCs have been constructed in TRR that can load 16 spent fuel assemblies. In this study gamma dose rate in the place of operator (crane cabin) during inspection and loading of spent fuel assemblies into cask have been calculated. The cabin is located at a distance of 4.5m from an open door cask. Calculations have been carried out using MCNPX2.7 and ORIGEN2.1 for 55% burn up and 10 years cooling time. Results showed 5 cm lead reduces the gamma dose rate below 10 μSv/h in crane cabin.

Keywords: Dry cask storage, Dual purpose cask, gamma dose rate, spent fuel assemblies

Introduction

When the spent fuel assemblies are removed from the reactor core, they are very hot and radioactive. Because of this, they are usually kept in the reactor service pool for a period of time, where water provides both radiation shielding and cooling. After a certain period of time, they can be transferred to wet storage pool and finally when the heat and radioactivity decreases over time, they are stored in dry cask [1]. Usually, decision on the wet and dry storage time depends on any country strategy for spent fuel management. Many countries use metal or concrete casks for the purpose of dry storage and transportation. Figure1 shows a typical spent fuel storage and transport cask [2].

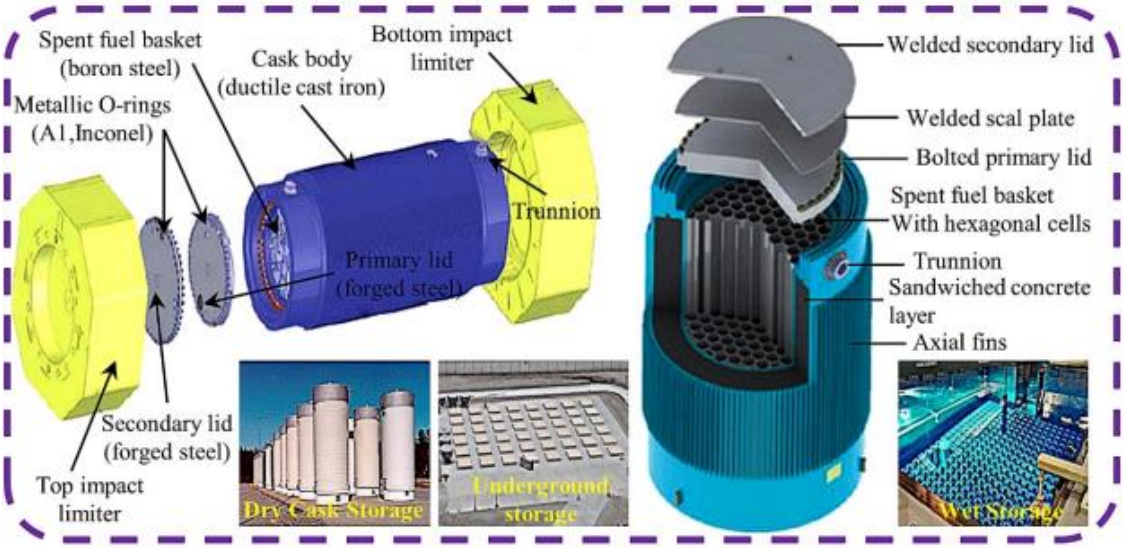

Figure 1: View of a typical spent fuel storage and transport cask [2]

Figure 2 shows a dual-purpose cask that has been designed and constructed in Korea. It can hold 21 fuel assemblies. Cask main body is made of a carbon steel and it has a stainless-steel canister. Outline and cross-sectional view of the Korean DPC is also shown in figure 2 [3].

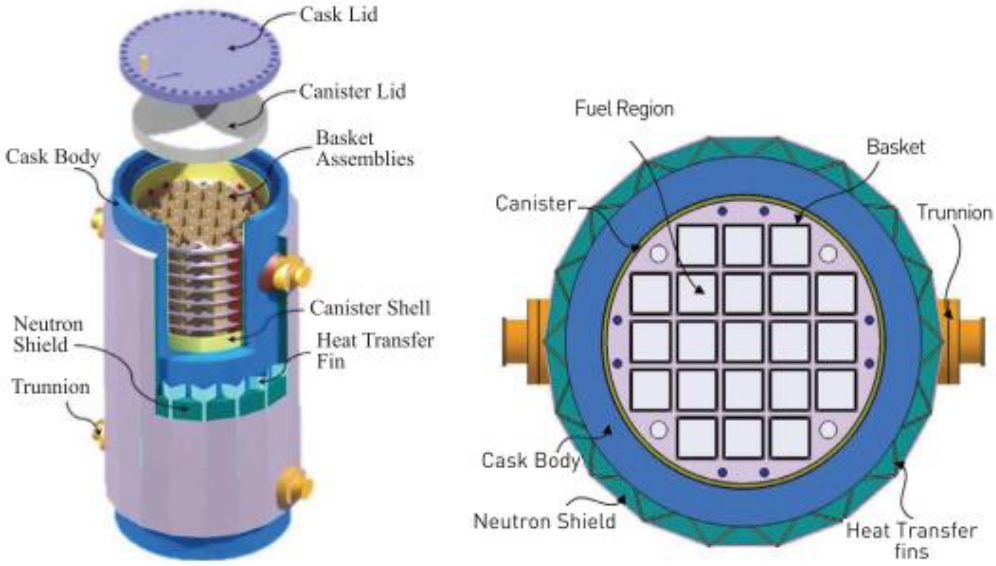

(a) Outline of the metal cask (b) Cross-sectional view of the metal cask

Figure2: Outline and cross-sectional view of the Korean dual-purpose cask

Reviews of some dual-purpose casks are presented in reference [4 &5].

One of the main process in storage of spent fuel assemblies is loading or unloading of the fuel assemblies into the cask under water to move from one place to another. Loading or unloading of spent fuel assemblies into cask is very important in terms of radiation protection and must be done in such a way that only a minimum dose is recieved during practice. In this research, a scenario of transferring fuel into the cask inside the pool is considered and assumed that the cask door is open.The amount of gamma dose rate at the operator's location is estimated.

Material and Methods

In this study, scenario of loading fuel assemblies inside of TRR DPC has been considered and the gamma dose rate has been calculated in crane cabin where the operator monitors the fuels. For this purpose, a dual-purpose cask that has been constructed for storage and transportation of spent fuel assemblies in TRR has been simulated inside a pool using MCNPX code. The Cask includes a canister that has a capacity of 16 fuel assemblies. Figure 3 shows the schematic view of different parts of TRR DPC [6]. The constructed cask is also shown in figure 4. Indeed, in this study the worst possible scenario for loading and unloading of the fuels into cask is considered in such a way that the cask is brought up to the edge of the pool and its door is open and the height of the water inside the cask is up to 10 cm higher than the active length of the fuels. The dimensions of the crane cabin are (2.5 m ×2.3 m ×2.3 m) (L×W×H) and is located at a horizontal and vertical distance of 2.5 m and 3.7 m from the cask, respectively. Figure 5 shows the simulated cask, pool and crane cabin. calculations have been carried out using both ORIGEN [7] and MCNPX code. ORIGEN code is used to calculate gamma emission rate of fuel assemblies for 55% burn up and 10 years cooling time. The gamma source extracted from origen code is used as MCNPX input as the gamma source for dose rate calculations. In these calculations, 5 cm of lead is considered for the floor as well as the 3 sides of the crane cabin. Also, one millimeter of lead is considered for the roof and the back of the crane cabin. It should be noted that the dimensions considered in this study are based on the suggestion of executive group for the construction of this crane cabin in TRR.

Gamma dose rate has been calculated in three positions inside of the crane cabin. Detector positions are shown in figure 5.

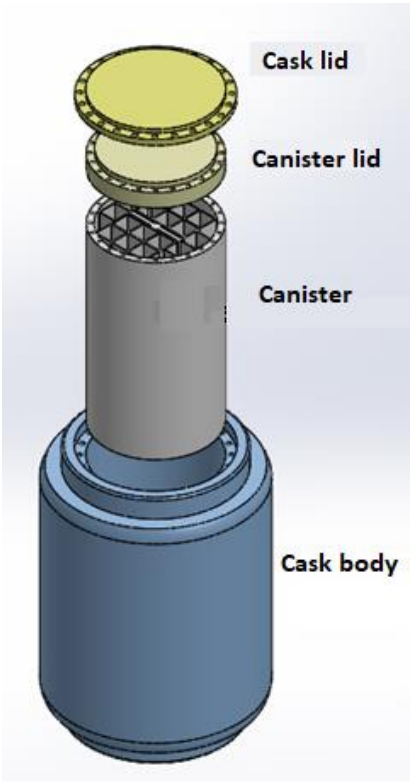

Figure 3: Schematic of TRR DPC [4]

Figure 4: Constructed DPC at TRR [4]

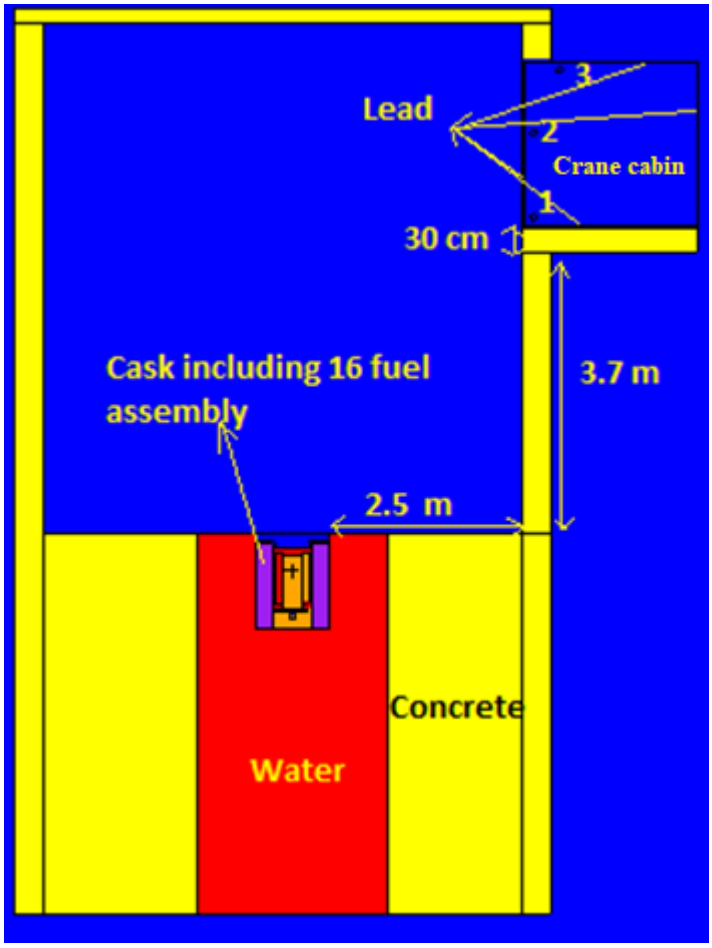

Figure 5: View of simulated cask and Crane cabin

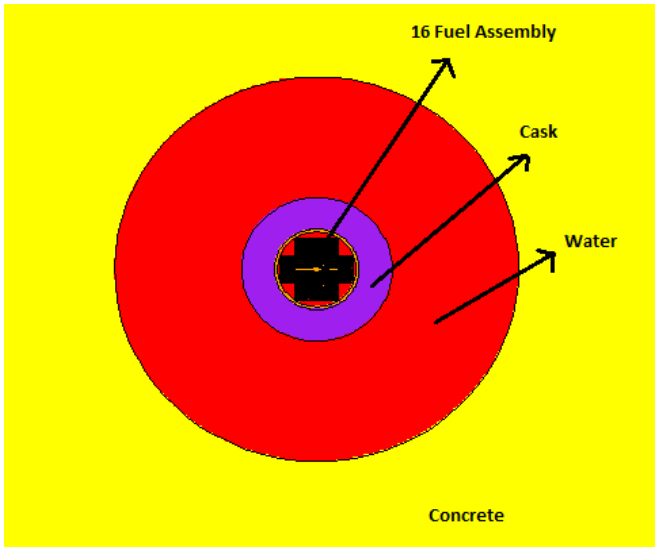

Figure 6: Simulate cask and fuel assemblies

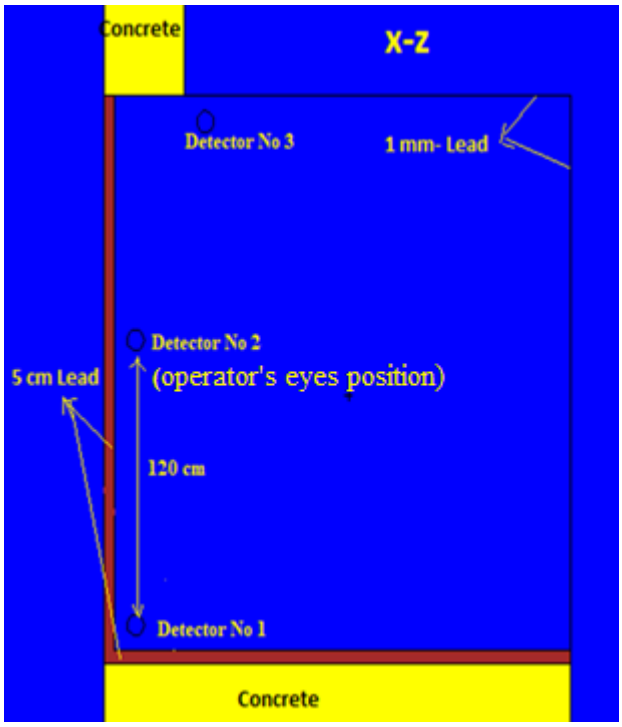

Figure 7: Detector positions in cabin crane

Results and Calculation

In order to calculate the gamma dose rate, gamma spectra of fuel assemblies with 55% burn up were calculated using ORIGEN code. Figure 8 shows the gamma spectra of one spent fuel plate after10 years cooling time.

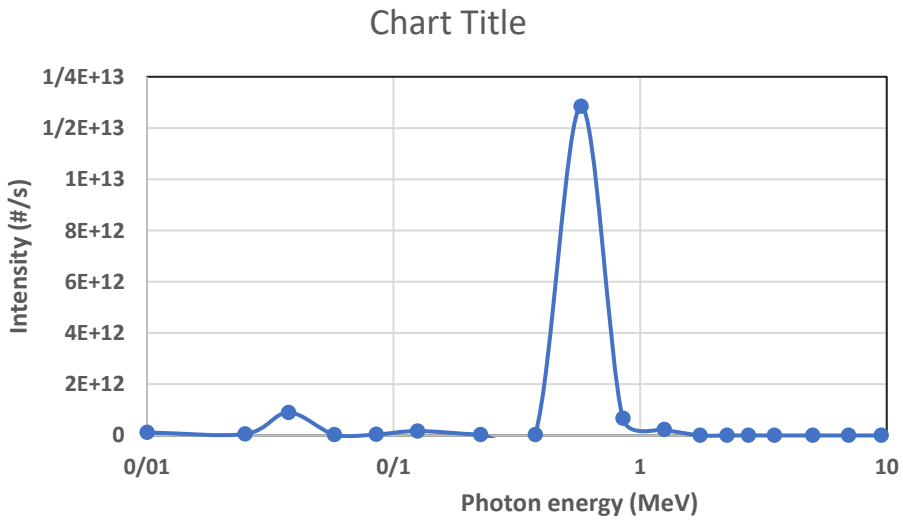

Figure 8: Photon spectra of one fuel plate with 55% burn-up and 10 years cooling time

TRR core is comprised of standard fuel elements (SFE) and control fuel elements (CFE). The SFE consists of 19 fuel plates while the CFE is of the same size and is comprised of 14 fuel plates. In this study extracted gamma spectra was used as gamma source in MCNPX code to calculate the gamma dose rate. Gamma dose rate was calculated using F4 tally with flux to dose conversion factors (DE and DF cards).

Calculated gamma dose rate in 3 different points of crane cabin (as shown in figure7) is presented in table 1.

Table1: gamma dose rate in three different point of crane cabin

Dose rate (µSv/h)		
Detector No 1	Detector No 2 (operator's eyes position)	Detector No 3
30	9	7

Conclusions

In this study, gamma dose rate has been calculated for worse scenario of loading and unloading of cask. It is concluded that for the case where there are 16 fuel assemblies (with 55% burn-up and 10 years cooling time) inside of the cask and the cask door is open and the water level inside of the cask is higher than 10 cm from the fuels active length, gamma dose rate at operator location will be less than 10 µSv/h.

It should be noted that in these calculations, it is assumed that the operator is located at a horizontal and vertical distance of 2.5 m and 3.7 m from the cask respectively. It should be noted that lead bricks can be used in the lower part of the crane where the dose is 30 µSv/h.

References

[1] Fukuda, K., Danker, W., Lee, J. S., Bonne, A., & Crijns, M. J. (2003). IAEA Overview of global spent fuel storage. Storage of spent fuel from Power Reactors, C&S Paper Series, (20).

[2] Qi, Z., Yang, Z., Li, J., Guo, Y., Yang, G., Yu, Y., & Zhang, J. (2022). The advancement of neutron-shielding materials for the transportation and storage of spent nuclear fuel. Materials, 15(9), 3255.

[3] Ko, J.H., Park, J.H., Jung, I.S., Lee, G.U., Baeg, C.Y. and Kim, T.M. (2014). Shielding analysis of dual purpose casks for spent nuclear fuel under normal storage conditions. Nuclear engineering and Technology, 46(4): 547-556.

[4] Garcia, J. (2014). Dual purpose casks in operation. In Workshop on the Development and Application of a Safety Case for Dual Purpose Casks for Spent Nuclear Fuel IAEA headquarter.

[5] Sun, H. and Li, G., 2019, February. International status of the dual purpose cask designed for both transport and storage of spent fuel. In IOP Conference Series: Earth and Environmental Science (Vol. 227, No. 2, p. 022005). IOP Publishing.

[6] Gholamzadeh, Z., Abedi, E., & Mirvakili, S. M. (2021). The effect of the number of spent fuel casks on the dose of the outer part of the hall concrete wall. Radiation Physics and Engineering, 2(3), 1-7.

[7] Croff, A. G. (1980). User's manual for the ORIGEN2 computer code. Technical report, Oak Ridge National Lab.